A Multi-Resolution Foveated Laparoscope

by

Yi Qin

A Dissertation Submitted to the Faculty of the

COLLEGE OF OPTICAL SCIENCES

In Partial Fulfillment of the Requirements

For the Degree of

DOCTOR OF PHILOSOPHY

In the Graduate College

THE UNIVERSITY OF ARIZONA

2015

THE UNIVERSITY OF ARIZONA
GRADUATE COLLEGE

As members of the Dissertation Committee, we certify that we have read the dissertation prepared by Yi Qin, titled “A Multi-Resolution Foveated Laparoscope” and recommend that it be accepted as fulfilling the dissertation requirement for the Degree of Doctor of Philosophy.

____ Date: 11/23/2015
Hong Hua

____ Date: 11/23/2015
Rongguang Liang

____ Date: 11/23/2015
Arthur Gmitro

Final approval and acceptance of this dissertation is contingent upon the candidate’s submission of the final copies of the dissertation to the Graduate College.

I hereby certify that I have read this dissertation prepared under my direction and recommend that it be accepted as fulfilling the dissertation requirement.

____ Date: 11/23/2015
Dissertation Director: Hong Hua

STATEMENT BY AUTHOR

SIGNED: Yi Qin

ACKNOWLEDGEMENTS

I wish to express my most sincere appreciation to my Ph.D. advisor, Professor Hong Hua. It has been my greatest fortune to complete my Ph.D. study in the past 5 years under her supervision. Throughout this journey full of challenges as well as joyfulness, I really appreciate her insights and advices for my study and research. I also want to acknowledge Dr. Mike Nguyen who provided the clinical idea for this dissertation project, Professor Rongguang Liang and Professor Arthur Gmitro for their discussions and suggestions on this dissertation.

I would also like to thank my lab colleagues. Xinda Hu helped me greatly in the art of lens design and inspired me a lot for my research project. Sangyoon Lee helped me with programming and taught me much about the computer vision knowledge. Thanks are also due to Jason Kuhn, Shenghuei Lu, Hekun Huang and Weichuan Gao for various discussions about science, technology, lens design as well as course works.

I would like to acknowledge national institute of health for supporting this research, this project is funded by NIH R21EB013370 and R01EB18921-01

DEDICATION

To my wife Ying Jin for her love and support,

and to my family in China.

TABLE OF CONTENTS

TABLE OF FIGURES 8

ABSTRACT 12

1 INTRODUCTION 14

1.1 Dissertation Contribution 16

1.2 Dissertation Contents and Format 16

2 BACKGROUND AND RELATED WORK 19

2.1 Minimally Invasive Surgery 19

2.1.1 Advantages of MIS 21

2.1.2 Challenge and Limitations of the MIS 22

2.2 Related Technologies 25

3 SYSTEM DESIGN AND ENGINEERING 27

3.1 System Overview 27

3.2 System Specifications 29

3.2.1 Field of view and spatial resolution 30

3.2.2 Magnifications and F/# 31

3.3 First Order Configuration 32

3.4 First-order Parametric Design 37

3.5 Throughput Analysis 42

3.6 Optical System Design 42

3.6.1 Design Challenges 42

3.6.2 Design Procedure 43

3.7 Discussion 45

3.7.1 “Divide and conquer” strategy 45

3.7.2 Assembling and testing consideration 46

4 Prototype Demonstration 48

4.1 Initial Prototype 49

4.1.1 Specifications of a commercial laparoscope 49

4.1.2 Optical system design of the initial prototype 52

4.1.3 Functional test 54

4.2 Customized System Integration and Evaluation 55

4.2.1 Mechanical system design 55

4.2.2 System Assembling Process 57
4.2.3 Image quality verification 58
4.2.4 In-vivo test 63
5 DESIGN AND CHARACTERIZATION OF A CONTINUOUS ZOOM AND AUTOFOCUSING IMAGING PROBE FOR THE MRFL 66
5.1 Design Overview 67
5.2 Tunable lens 69
5.3 Focal error analysis 70
5.4 Optical design and system prototype 72
5.5 Performance evaluation 74
6 CONCLUSION AND FUGURE WORK 76
6.1 Conclusion 76
6.2 Future Work 76
REFERENCES 77
APPENDIX A: Multiresolution foveated laparoscope 82
APPENDIX B: Optical design and system engineering of a multi-resolution foveated laparoscope 86
APPENDIX C: Characterization and in-vivo evaluation of a multi-resolution foveated laparoscope for minimally invasive surgery 98
APPENDIX D: A continuously zoomable multi-resolution foveated laparoscope with auto-focus capability 114

TABLE OF FIGURES

Figure 2.1 Laparoscopic procedure [http://www.edoardorosso.org/] 20

Figure 2.2 Single port access laparoscopy [27] 21

Figure 2.3 Safety issues of laparoscopic surgery [35] 23

Figure 2.4 SPA laparoscopic surgery [36, 37] 24

Figure 3.1 Schematic layout of MRFL in clinical use for MIS applications 28

Figure 3.2 Laparoscope layout 32

Figure 3.3 MRFL layout 32

Figure 3.4 1st configuration of MRFL 33

Figure 3.5 2nd configuration of MRFL 34

Figure 3.6 3rd configuration of MRFL 35

Figure 3.7 4th configuration of MRFL 36

Figure 3.8 Relationship between the objective lens diameter and its focal length 38

Figure 3.9 Diameter of the first-order model of the relay lens as a function of the focal lengths of the objective lens and the half relay group 39

Figure 3.10 Scanning lens diameter as a function of the focal lengths of the scanning lens and the objective lens 40

Figure 3.11 Scan range of the 2D scanning mirror as a function of the focal lengths of the scanning lens and the objective lens 41

Figure 3.12 Flow of the optical design procedure 43

Figure 3.13 Layout of the low-profile MRFL 44

Figure 3.14 MTF of the wide-angle probe 45

Figure 3.15 MTFs of the foveated probe 45

Figure 3.16 Assembling and testing flow of an optical system with multiple relays 47
Figure 4.1 Experiment of measuring the exit pupil diameter and location of the commercial laparoscope 50
Figure 4.2 Exit pupil measurement: (a) image of the exit pupil; (b) calibration target image 50
Figure 4.3 Layout of the direct measurement of the exit pupil diameter.......................... 51
Figure 4.4 Result of the direct measurement of the exit pupil diameter........................... 51
Figure 4.5 FOV measurement of the eyepiece of the laparoscope 52
Figure 4.6 MRFL initial prototype layout... 53
Figure 4.7 Layout and MTFs of the foveated probe 53
Figure 4.8 Layout and MTF of the wide-angle probe.. 54
Figure 4.9 Images captured by the MRFL initial prototype: (a) wide-angle image; (b) high-resolution image of the center field; (c) and (d) high-resolution images of peripheral fields.. 54
Figure 4.10 Laparoscope packaging 55
Figure 4.11 2D scanner gimbal mount.. 56
Figure 4.12 3D model of MRFL... 56
Figure 4.13 MRFL assembling procedure 57
Figure 4.14 Prototypes of MRFL.. 58
Figure 4.15 Images and intensity profiles of the resolution target of the high-magnification probe at 120mm working distance orienting at the center field, (a) in vertical direction; (b) in horizontal direction. 59

Figure 4.16 Images and intensity profiles of the resolution target of the high-magnification probe at 120mm working distance orienting at the corner field, (a) in vertical direction; (b) in horizontal direction. 59

Figure 4.17 Images and intensity profiles of the resolution target of the center field of the wide-angle probe at 120mm working distance, (a) in vertical direction; (b) in horizontal direction. 61

Figure 4.18 Images and intensity profiles of the resolution target of the center field of the wide-angle probe at 120mm working distance, (a) in vertical direction; (b) in horizontal direction. 62

Figure 4.19 MTF measurement.. 63

Figure 4.20 In-vivo animal test 64

Figure 4.21 MRFL in-vivo evaluation with a porcine model at an approximately 120mm working distance from the surgical cite: (a) high-magnification image of the spleen; (b) wide-angle image of the spleen; (c) high-magnification image of the gallbladder; (d) wide-angle image of the gallbladder. The high-magnification and wide-angle images were acquired simultaneously through the MRFL prototype. 65

Figure 5.1 Field coverage of different zoom ratio 67

Figure 5.2 Schematic layout of the zoom probe 68

Figure 5.3 Configurations of the zoom probe: (a) Keplerian type; (b) Galilean type 69

Figure 5.4 Relation between the driving current and optical power of the tunable lens .. 69

Figure 5.5 high-magnification zoom probe layout 73

Figure 5.6 MTF performance of the high-magnification zoom probe.............................. 73

Figure 5.7 3D model of the zoom MRFL 74

Figure 5.8 Images of US1951 resolution target at different zoom ratio: (a) 2×; (b) 2.33×; (c) 2.67×; (d) 3×. 75

Figure 5.9 Images of the gallbladder model at different zoom ratio: (a) 2×; (b) 2.33×; (c) 2.67×; (d) 3× 75

ABSTRACT

Laparoscopic surgery or minimally invasive surgery has great advantages compared with the conventional open surgery, such as reduced pain, shorter recovery time and lower infection rate. It has become a standard clinical procedure for cholecystectomy, appendectomy and splenectomy.

The state-of-the-art laparoscopic technologies suffer from several significant limitations, one of which is the tradeoff of the limited instantaneous field of view (FOV) for high spatial resolution versus the wide FOV for situational awareness but with diminished spatial resolution. Standard laparoscopes lack the ability to acquire both wide-angle and high-resolution images simultaneously through a single scope. During the surgery, a trained assistant is required to manipulate the laparoscope. The practice of frequently maneuvering the laparoscope by a trained assistant can lead to poor or awkward ergonomic scenarios. This type of ergonomic conflicts imposes inherent challenges to laparoscopic procedures, and it is further aggravated with the introduction of single port access (SPA) techniques to laparoscopic surgery. SPA uses one combined surgical port for all instruments instead of using multiple ports in the abdominal wall. The grouping of ports raises a number of challenges, including the tunnel vision due to the in-line arrangement of instruments, poor triangulation of instruments, and the instrument collision due to the close proximity to other surgical devices.

A multi-resolution foveated laparoscope (MRFL) was proposed to address those limitations of the current laparoscopic surgery. The MRFL is able to simultaneously capture a wide-angle view for situational awareness and a high-resolution zoomed-in view for fine details. The high-resolution view can be scanned and registered anywhere

within the wide-angle view, enabled by a 2D optical scanning mechanism. In addition, the high-resolution probe has optical zoom and autofocus capabilities, so that the field coverage can be dynamically varied while keep the same focus distance as the wide-angle probe. Moreover, the MRFL has a large working distance compared with the standard laparoscopes, the wide-angle probe has more than 8× field coverage than a standard laparoscope. On the other hand, the high-resolution probe has 3× spatial resolution than a standard one. These versatile capabilities are anticipated to have significant impacts on the diagnostic, clinical and technical aspects of minimally invasive surgery.

In this dissertation, the development of the multi-resolution foveated laparoscope was discussed in detail. Starting from the refinement of the 1st order specifications, system configurations, and initial prototype demonstration, a customized dual-view MRFL system with fixed optical magnifications was developed and demonstrated. After the in-vivo test of the first generation prototype of the MRFL, further improvement was made on the high-resolution probe by adding an optical zoom and auto-focusing capability. The optical design, implementation and experimental validation of the MRFL prototypes were presented and discussed in detail.

1 INTRODUCTION

Laparoscopy or endoscopy has revolutionized patient care not only in minimally invasive surgery (MIS), but also recently in microscopic imaging for screening and assessment of early-stage diseases [1-4]. Laparoscopy is now one of the most successful means of providing MIS procedures and is routinely performed in several fields such as cholecystectomy, appendectomy, hysterectomy and nephrectomy [5]. It has great advantages to the patient versus an open procedure, including reduced pain and shorter recovery time [6-8].

The state-of-the-art laparoscopic technologies have a number of limitations. One limitation is the trade-off of a limited field of view (FOV) with high spatial resolution versus a wide FOV with diminished resolution [9, 10]. Standard laparoscopes have a fixed optical magnification. Lacking the ability to acquire both wide-angle and high-resolution images simultaneously through a single integrated probe introduces challenges when used in clinical scenarios requiring both close-up zoomed-in views for fine details and wide-angle overviews for orientation and situational awareness during surgical maneuvers. In the current clinical practice, this limitation is addressed by frequently moving the entire laparoscope forward and backward to achieve close-up views for details or wide-angle views for orientation. This practice requires a second trained camera assistant, which introduces ergonomic conflicts, especially with single port access (SPA) [11, 12].

Due to the need for a camera assistant, another limitation relates to the poor ergonomics with hand crossover between the surgeon and the camera assistant, which presents an inherent challenge to laparoscopic procedures [13].

Finally, the recent development of SPA technique has pushed the boundaries of MIS procedures and is expected to play a larger role in the future of laparoscopic surgery [11, 12]. Port-grouping, however, raised a number of problems, including tunnel vision due to the in-line arrangement of instruments, poor triangulation of instruments, requiring crossing of instruments in order to obtain proper retraction, and increased risk of instrument collision due to the close proximity to other surgical devices [14]. As this new technique becomes more widespread, it demands further refinement of laparoscopic instrumentation to address these limitations and optimize surgical task performance. There are already attempts to create cameras that have the lowest possible external profile with HD pictures and automatic focusing. These scopes still require advancing and withdrawing of the lens to obtain magnification, which is described as one of the most frustrating aspects of SPA procedures. It has been suggested that varying lengths of instruments reduces the effect of crowding [11]. A laparoscope with a low profile through an appropriate range of magnification would greatly improve the maneuverability of the other instruments.

In recent decades, a number of laparoscopic technologies have been developed in order to overcome the limitations of the conventional laparoscopic surgery, including robotically assisted laparoscope arm [15, 16]; zoom laparoscopes [17-19]; laparoscopes with varying viewing directions and the dual view endoscope system [20-22]. Except the dual view endoscope system, other technologies still suffer the resolution-FOV tradeoff. The dual view endoscope system is limited by its low optical throughput and fixed two levels of magnifications.

Research in this dissertation is focused on the development of the multi-resolution foveated laparoscope (MRFL) that can capture a wide-angle view and a high-magnification view simultaneously with optical zoom and autofocusing capabilities. The long-term goal is to address those limitations of the current laparoscopes as described above, thus to improve the safety, efficiency and outcome of the minimally invasive surgery.

1.1 Dissertation Contribution

The main contribution of the dissertation is the engineering development of the multi-resolution foveated laparoscope technology. I designed and constructed two prototypes of the MRFL systems, from custom optics, mechanics to software. The first one was built with two fixed levels of magnifications for the wide-angle and high-magnification probe. After the in-vivo test of the first prototype, the second prototype was designed and built according to the surgeon's feedback. The high-magnification probe of the second prototype was redesigned to enable continuous optical zoom and autofocusing capabilities where the field coverage of the probe can vary in real time without any mechanical moving parts. The first-order properties of the optical systems were fully analyzed; the optimization and tolerance techniques for a multiple image relay system were explored. The design and assembly consideration for an optical system with multiple image relays were discussed. Besides, the design and optimization methods of zoom lenses using variable focus elements and off-the-shelf lenses were also developed.

1.2 Dissertation Contents and Format

Following this chapter of introduction, Chapter 2 BACKGROUND AND RELATED WORK summarizes the background, limitations and challenges of the current laparoscopic surgery. Several related technologies aiming to address some of those limitations are reviewed.

Chapter 3 SYSTEM DESIGN AND ENGINEERING presents the detailed system design process and performance analysis, from the first-order optical properties selection to the complete system integration.

Chapter 4 PROTOTYPE DEMONSTRATION presents a detailed performance evaluation of the system prototypes, including the resolution test, MTF test and in-vivo test on a live animal model.

Chapter 5 DESIGN AND CHARACTERIZATION OF A CONTINUOUS ZOOM AND AUTOFOCUSING IMAGING PROBE FOR THE MRFL presents the design method and performance test of the high-magnification optical zoom probe with auto-focusing capability.

Appendix A includes a published peer-reviewed paper [23], introducing the idea and initial prototype of the multi-resolution foveated laparoscope aiming to eliminate the resolution-FOV tradeoff of the state-of-the-art laparoscopes and other related limitations.

Appendix B includes a submitted paper draft. It presents the engineering details of the multi-resolution foveated laparoscope prototype, focusing on the design, optimization, tolerance, stray light, ghost image analysis and system integration.

Appendix C includes a published peer-reviewed paper [24], focusing on the quantitative performance evolution of the multi-resolution foveated laparoscope, and its in-vivo test on an animal model for laparoscopic training.

Appendix D includes a submitted paper draft. It presents the optical design method and performance evaluation of the zoomable high-magnification probe with autofocusing capability.

2 BACKGROUND AND RELATED WORK

Minimally invasive surgery (MIS) or laparoscopic surgery is playing a more and more important role in modern medical surgery. This chapter introduces the background information of the MIS and its advantages over the traditional open surgery. The challenges and the limitations of the current laparoscopic surgery are discussed in details, including the situational awareness issue and ergonomic conflicts. The relevant technologies aiming to overcome these limitations of the conventional laparoscopic surgery are reviewed.

2.1 Minimally Invasive Surgery

Minimally invasive surgery, also known as minimally access surgery, laparoscopic surgery, or keyhole surgery, is a modern surgical technique in which operations in abdomen are performed through small incisions (usually less than 15mm) as opposed to the large incision made in the traditional open surgery. Translated from the Greek, "Laparoscopy" means examination of the abdomen using a scope which is also known as an endoscope [25]. In the traditional open surgery, the surgeon must make a large cut that exposes the organs inside the body to operate on. However, laparoscopy eliminates the requirements for a sizable cut. Instead, the surgeon uses a laparoscope, a low profile telescope-like instrument to provide the interior views of the body. Laparoscopy has been routinely performed in several fields for procedures such as cholecystectomy, appendectomy, hysterectomy, and nephrectomy. It has become the standard approach for several procedures including cholecystectomy (96% of 1.06 million cases performed laparoscopically in 2011 in the USA) and appendectomy (75% of 359,000 cases performed laparoscopically in 2011) [5].

As shown in Figure 2.1, during laparoscopic surgery, the surgeon makes a small cut in the skin, then a trocar is introduced among the muscle fibers. Through the trocar, the laparoscope is inserted into the patient's body. The abdomen is then inflated with carbon dioxide to expand the abdominal walls and permit the surgeon a clear view of the structures inside, as well as provide them with room to work. A laparoscope is equipped with a camera and light source that permit it to transmit images through the optical system to a monitor. The monitor shows a magnified image. By watching the monitor, the surgeon is able to do the process. In addition, other trocars and instruments may be put in according to different procedures. For example, another trocar may be needed for a diagnostic laparoscopy, two more for groin hernia repairs and three more for laparoscopic gallbladder operation. Instruments are introduced through the trocars and the operation is conducted similar to an open surgery.

Figure 2.1 Laparoscopic procedure [http://www.edoardorosso.org/]

In recent years, the single port access (SPA) laparoscopy has been introduced to further reduce the invasiveness of MIS procedures, and may play a larger role in the future of laparoscopic surgery. In a SPA procedure (illustrated in Figure. 2.2), only one incision is made on the patient's body and all the instruments are introduced though one single trocar. It is expected to further reduce the pain and recovery time.

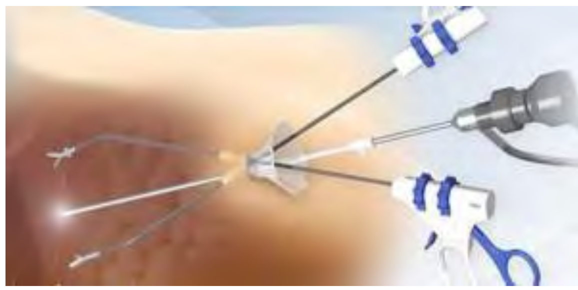

Figure 2.2 Single port access laparoscopy [27]

2.1.1 Advantages of MIS

Compared with the traditional open surgery, MIS has a variety of advantages to the patient [28, 29]. The risk of bleeding during the surgery is reduced because the size of the incision is much smaller than the large incision of an open surgery. This also reduces the likelihood of a blood transfusion being needed to compensate for blood loss.

The smaller incision size also reduces the risk of pain and bleeding after surgery. When a large incision has been made, patients usually require long-term pain relief medication while the stitch-line heals. With laparoscopic surgery, the post-surgical wound is much smaller and the healing process is less painful.

The smaller incision also leads to the formation of a significantly smaller scar after surgery. In cases where the surgical wound is larger, the scar tissue that forms is more likely to become infected as well as being more vulnerable to herniation.

In addition, laparoscopic surgery reduces the exposure of internal organs to possible external contaminates, therefore reduces the risk of post-operative infections.

Last but not the least, the length of hospital stay required is significantly shorter with laparoscopic surgery. Most patients receive a same-day or next-day discharge and can return to their normal daily lives much more quickly than after an open surgery procedure.

2.1.2 Challenge and Limitations of the MIS

Although the laparoscopic surgery has significant advantages over the traditional open surgery, modern laparoscopic surgery confronts several challenges and limitations [29, 30]. The setup of the laparoscopic surgery is very different from that of the open surgery. In an open abdominal operation, for example, the surgeon simultaneously observes his/her hands, the instruments, and the operative field. In laparoscopic surgery, the images of the operating environment are obtained by a laparoscopic camera. The surgeon views his/her operating environment indirectly and performs the surgical tasks bimanually using laparoscopic instruments extended into the patients.

One major limitation of the state-of-the-art laparoscope is the tradeoff of the limited field coverage with high spatial resolution versus large field of view but with a diminished spatial resolution. Standard laparoscopes lack the ability to acquire both wide-angle and high-magnification images simultaneously through a single scope. This limitation introduces challenges when used in clinical scenarios requiring both close-up views for details and wide-angle overviews for orientation and situational awareness during surgical maneuvers. With a standard laparoscope, in order to see fine details of a surgical field, procedures usually performed at a highly zoomed-in view, where the scope is moved in to operate at a short working distance (WD), typically less than 50mm. A highly zoomed-in view leads to the loss of peripheral vision and awareness of potentially dangerous situations occurring outside the immediate focus area of the laparoscope. One example occurs when a non-insulated laparoscopic instrument is in inadvertent and unrecognized contact with an energized instrument resulting in a spread of electric current being applied to unintended structures, a situation known as "direct coupling" [31-33]. Insulation failures in energized instruments themselves can also directly lead to injury to bowl, vascular, and other structures, as indicated in Figure 2.3. These injuries often remain unrecognized if they occur on the part of the surgical instrument that is not within the FOV of the laparoscope. While literature documenting inadvertent injuries in laparoscopic surgery are likely underreported, the Association of Trial Lawyers of America has stated that "during laparoscopic monopolar electrosurgery, most electrosurgical burns are not detected at the time of surgery because they occur outside the surgeon's keyhole field of view", reinforcing the seriousness of this issue [34, 35].

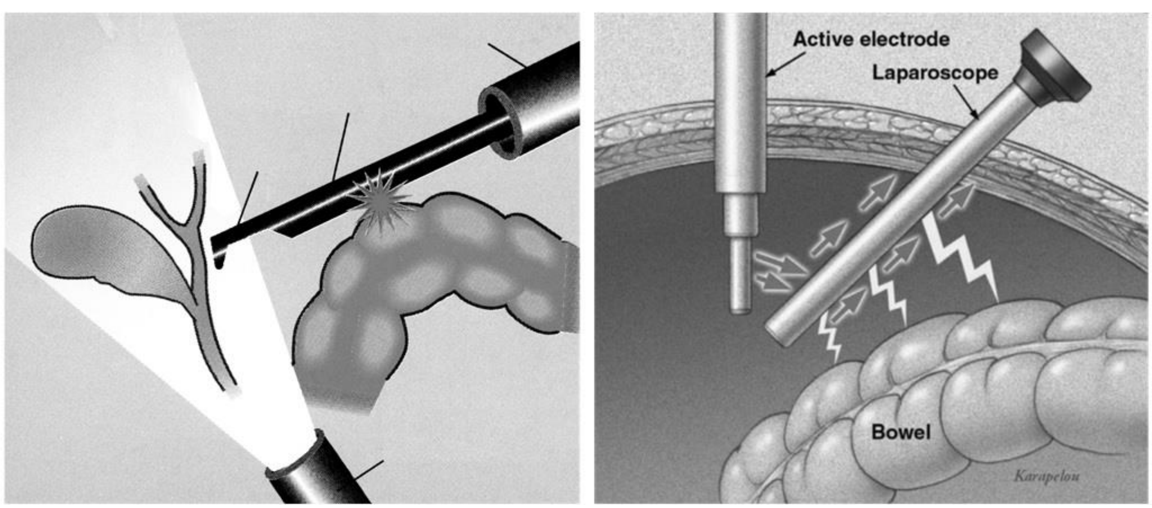

Figure 2.3 Safety issues of laparoscopic surgery [35]

SPA procedures further increase the concerns for inadvertent electrosurgical injuries because the close approximation of instruments in a single port leads to the frequent crossing of instruments out of the surgeons view. As shown in Figure 2.4, a SPA procedure results in a higher potential for injuries from direct coupling of instruments or from unrecognized breaks in instrument insulation causing injury to adjacent tissue [36, 37].

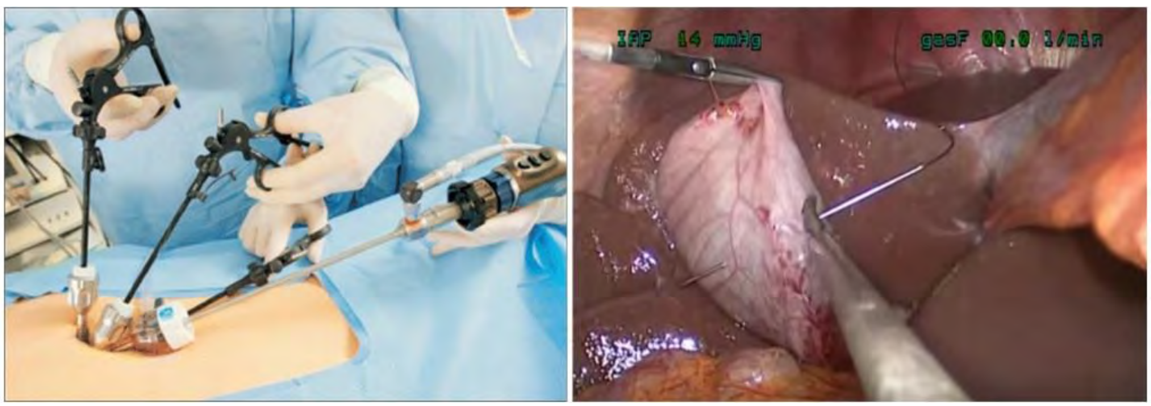

Figure 2.4 SPA laparoscopic surgery [36, 37]

In the current clinical practice, the FOV limitation is addressed by manually moving the entire laparoscope in and out of the camera port to obtain either close-up views for details or wide-angle overviews for orientation. This practice requires a trained assistant for holding and maneuvering the camera. The practice of frequently maneuvering the camera using a trained assistant can introduce ergonomic conflicts with hand cross-over between the surgeon and the assistant holding the camera, which imposes an inherent challenge to laparoscopic procedures [11, 12].

The ergonomic conflicts associated with standard laparoscopy are aggravated with the SPA approach. Port-grouping in SPA procedures raised a number of challenges, including tunnel vision due to the in-line arrangement of instruments, poor triangulation of instruments, requiring crossing of instruments to obtain proper retraction, and increased risk of instrument collision due to the close proximity of the laparoscope to other surgical devices [38].

Another serious problem is the effect of misorientation caused by a mismatch between the line-of-sight of the surgeon and that of the camera controlled by the assistant, because this particular disturbance is larger and cannot be easily overcome. Research has shown that misorientations lead to significant decrease in performance. Moving and reorienting the laparoscope can result in potential confusion about the positions of the internal organs.

2.2 Related Technologies

Aiming to overcome the FOV-resolution tradeoff and the ergonomic limitations of the standard laparoscopy, robotically assisted techniques, such as voice, foot pedal, or head motion-activated cameras, have been developed to eliminate the need of a human camera holder. However, delays in task performance have been reported due to errors in voice recognition or robotic control of camera speed, and also significant practice is required to become efficient with set-up and use [39, 40].

Some latest commercial laparoscopes are equipped with optical zoom camera head with HD pictures and a low external profile, such as the H3 series of Karl Storz [41] and the HD camera head of Stryker [17]. Although it can change the magnification or field coverage effectively, the laparoscope cannot simultaneously capture a wide-angle view and a high-magnification view.

Some research groups have proposed to apply the liquid lens technologies in the laparoscope systems [18, 19], in order to change the magnification or field coverage. However, these systems still suffer the tradeoff between the FOV and spatial resolution.

However, in order to solve the situational awareness issue of the standard laparoscopes, two types of laparoscopes with varying viewing directions have been proposed or commercialized. One of them is the laparoscope with an oblique viewing direction, in which a prism is added in the objective lens to tilt the viewing direction. For this type of laparoscopes, a camera holder is still required to rotate the entire scope to change the viewing direction. The other types can automatically change the viewing direction either by mechanical tilting components [42] or optical method such as rotating prisms [21]. Nevertheless, those optical systems are still limited by the FOV-resolution tradeoff.

The dual-view endoscope prototype demonstrated by Yamauchi et al provides the ability to capture a zoomed-in view and a wide-angle view simultaneously through an image-shifting prim, but the prototype is limited by its low resolution, low light throughput and two fixed level of magnifications [22]. In addition, due to the mechanical shifting component, the entire system is cumbersome, the total weight is 1.5kg.

3 SYSTEM DESIGN AND ENGINEERING

This chapter presents the detailed system design of a multi-resolution foveated laparoscope (MRFL), which has great potential in solving the situational awareness issue and ergonomic conflicts of the current laparoscopic surgery. Starting from the surgical application point of view, a MRFL with dual-view capability is proposed. One view is a wide-angle overview for situational awareness and instrument orientation, the other view is a zoomed-in view with large optical magnification for fine structure details. Then the system requirements such as spatial resolution, optical magnification, and imaging sensor size are specified. Four different types of optical system configurations are discussed and compared. The final configuration is selected based on optical performance, design complexity, manufacturing cost and system ergonomic consideration. The optical system design of the selected configuration is demonstrated including the design challenges and the optimized result. In the end, guidelines for the requirements, design, assembling and testing processes of an optical system with multiple image relays are discussed.

3.1 System Overview

To overcome the situational awareness issue and ergonomic conflicts of the conventional laparoscopic surgery, the MRFL is able to capture a wide-angle overview as well as a high-resolution zoomed-in view simultaneously at a large working distance through a single integrated system. The schematic system layout is shown in Figure. 3.1. In the figure, a low-profile MRFL with an insertion length of 150mm is demonstrated.

The wide-angle probe captures a large overview of the abdominal cavity for orientation and situational awareness with relatively low magnification, while concurrently the high-magnification probe with narrow but adequate FOV obtains images of a sub-region of the wide-angle field at much higher resolution for accurate surgical operation. The instrument therefore provides the ability to survey a large surgical field and to visualize a targeted area with high spatial resolution for surgical treatment. Concurrent access to both imaging scales in real time offers un-compromised context and resolution, which is expected to offer improved situational awareness and therefore better patient safety and surgical outcome.

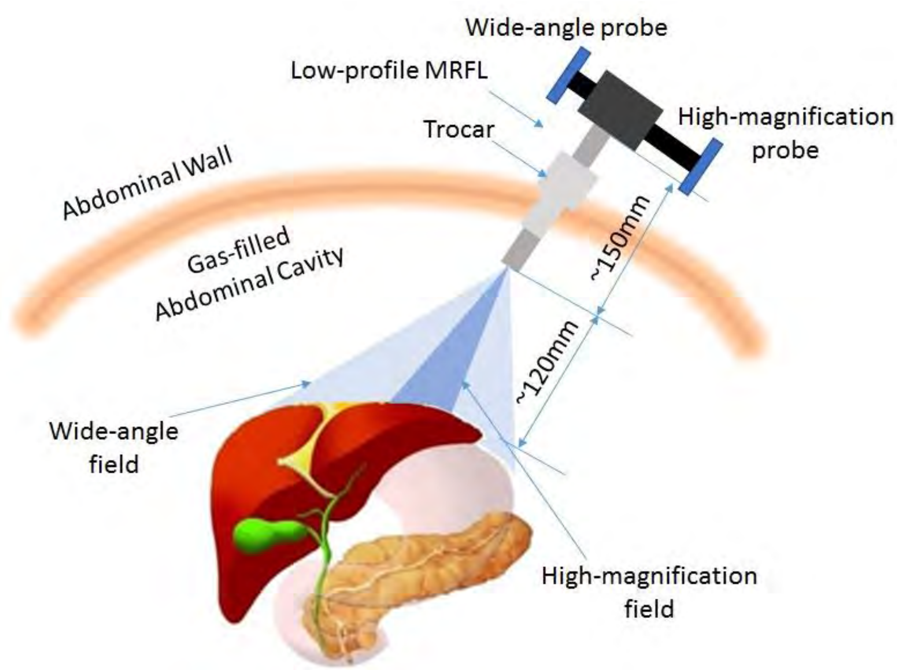

Figure 3.1 Schematic layout of MRFL in clinical use for MIS applications

In addition, a 2D scanning mirror integrated within the system can steer and engage the high-magnification probe to any region of interest (ROI) within the wide-angle field. Therefore, the MRFL system can be secured at a fixed location on the abdominal wall, and different views can be obtained without any physical advancing or withdrawing of the scope. Such arrangement will not only allow MIS procedures to be performed without requiring a dedicated camera assistant or robotic arm, but will also reduce physical interference with other surgical instrument and awkward ergonomic conflicts.

Thirdly, the high-magnification probe provides improved spatial resolution compared a standard laparoscope and enables highly resolvable visualization of tissues and thus enhances intro-operative surgical decision makings. Therefore, it is expected to improve the surgical accuracy, and potentially reduce operation time.

Finally, it is worth noting that the MRFL is optimized to maintain a much longer working distance and low-length profile than those of a standard laparoscope. As illustrated in Figure 3.1, the designed WD of a MRFL is about 120mm or larger, while the typical WD of a standard laparoscope is about 50mm for operation. The length of a low-profile MRFL is about 150mm while a SL has a typical insertion length of more than 350mm. With a longer working distance, the surgical area captured by the MRFL can be effectively increased, and the instrument can be positioned at a further distance from the surgical site to mitigate physical interferences with other surgical instrument in the abdominal cavity. The low-length profile characteristics of the MRFL system further helps to reduce instrument crowding.

In the SPA procedures which suffer from severe instrument crowding and keyhole tunnel vision, these features of an MRFL scope are highly desirable. Since the MRFL is secured at a large distance away from the surgical area and no physical movement is needed, it reduces the interference between the laparoscope and other surgical instruments. In addition, the multi-resolution foveated capability eliminated the keyhole tunnel vision of the standard laparoscope used in the SPA procedure.

3.2 System Specifications

Most of the MRFL specifications were driven by the clinical requirements that need to be met through the research development. This section focuses on how to define the critical system specifications such as FOV, resolution, magnification, light throughput, and first order configuration.

3.2.1 Field of view and spatial resolution

A standard laparoscope usually captures 70° FOV and an optimized working distance of 50mm. The spatial resolution at the optimum working distance is about 2.1lp/mm and the surgical area captured by the camera is about $56 \times 42mm^2$ [10]. Compared with a standard laparoscope, the wide-angle probe of the MRFL captures a 8×~9× surgical field area with a similar spatial resolution (~2lp/mm), the high-magnification probe captures a similar surgical field ($56 \times 42mm^2$) with 3× better spatial resolution (~6lp/mm).

To increase the field coverage, we can either increase the angular FOV or increase the working distance. Since one of the objectives for the MRFL system is to reduce the instruments crowding during the surgery, we choose to increase the working distance while maintaining an 80° angular FOV. In order to increase the spatial resolution of the high-magnification probe, the entrance pupil of the optical system should be increased as well. The maximum spatial resolution in object space is determined by the cutoff frequency denoted in Eq. 3.1

$$f_{cutoff} = \frac{1}{\lambda \times F/\#} \approx \frac{EPD}{\lambda \times WD} \qquad \text{(Eq. 3.1)}$$

At a desired working instance, increasing the entrance pupil diameter (EPD) is required to improve spatial resolution. For the MRFL system, the EPD is set to be 0.8mm, while the EPD of a standard laparoscope is typically about 0.3mm. As a result, the cutoff frequency of the system is 12.12lp/mm. For the required 6lp/mm resolution, a near diffraction limited system can provide reasonable image contrast.

3.2.2 Magnifications and F/#

The magnifications of the two probes in the MRFL system are determined by the ratio between the imaging sensor height and the surgical field height. By considering the optical invariant, the magnifications of the optical system determines the F/# in image space which will affect the choice of imaging sensor. Since a CCD has better signal-to-noise ratio compared with a CMOS sensor at low light level, we selected the CCD sensors for both probes of the MRFL. However, the smallest pixel size for a CCD sensor is about 3.75um, and thus the maximum sampling frequency for a CCD sensor is 140.056lp/mm. As indicated previously, the cutoff frequency in object space determined by the entrance pupil diameter is 12.12lp/mm, therefore if the magnification of the high-resolution probe is larger than 0.0865, the maximum achievable resolution is limited by the optical system, otherwise, the resolution is limited by the pixel sampling. In our prototype, two PointGrey DragonFly II (1280×960) cameras were selected for both probes. The diagonal size of the sensor is 6mm, so the magnification of the high-resolution probe is 0.1055, as shown in Eq. 3.2. Thus the high-magnification probe is limited by the optical system. While the wide-angle probe is limited by the pixel sampling, and its magnification is 0.0298 as shown in Eq. 3.3.

$$m_{high-mag} = \frac{h_{sensor}}{h_{HFOV}} = \frac{3}{120 \times \tan\left(\frac{40^\circ}{3}\right)} = 0.1055 \qquad \text{(Eq. 3.2)}$$

$$m_{wide-angle} = \frac{h_{sensor}}{h_{HFOV}} = \frac{3}{120 \times \tan\left(40^\circ\right)} = 0.0298 \qquad \text{(Eq. 3.3)}$$

Once the magnifications of two imaging probes are finalized, their working F/#s can be calculated by Eq. 3.4. The wide-angle probe is F/4, and the high-magnification probe is

F/15.8. As we can expect, although the wide-angle probe has lower spatial resolvability than the high-magnification probe, due to its low F/#, its image will be sharper than that of the high-magnification probe.

$$F/\#_w = m \times \frac{WD}{EPD} \quad \text{(Eq. 3.4)}$$

3.3 First Order Configuration

A laparoscope is a complicated optical system which consists of an objective lens, multiple relay lenses and an eyepiece for direct eye viewing, as shown in Figure 3.2. For the MRFL, the objective lens and relay lenses are shared by the two imaging probes. In addition, there is an optical 2D scanning system (as shown in Figure 3.3) that can steer the high-magnification probe to any ROI within the wide-angle image, and a beam splitter to split light to different probes.

Figure 3.2 Conventional Laparoscope layout

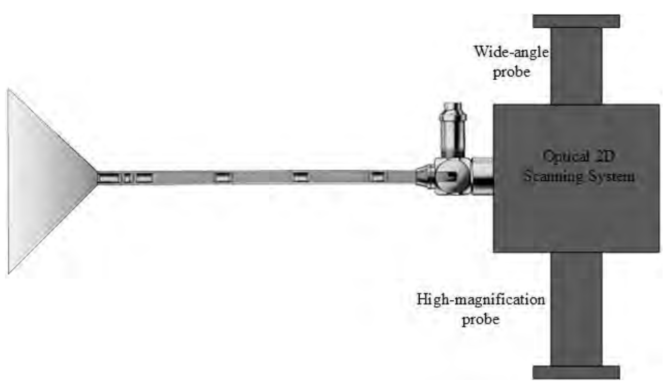

Figure 3.3 MRFL layout

In this section, four different system configurations of the 2D scanning system are discussed and compared by considering the optical design complexity, manufacturing cost, and ergonomic conflicts.

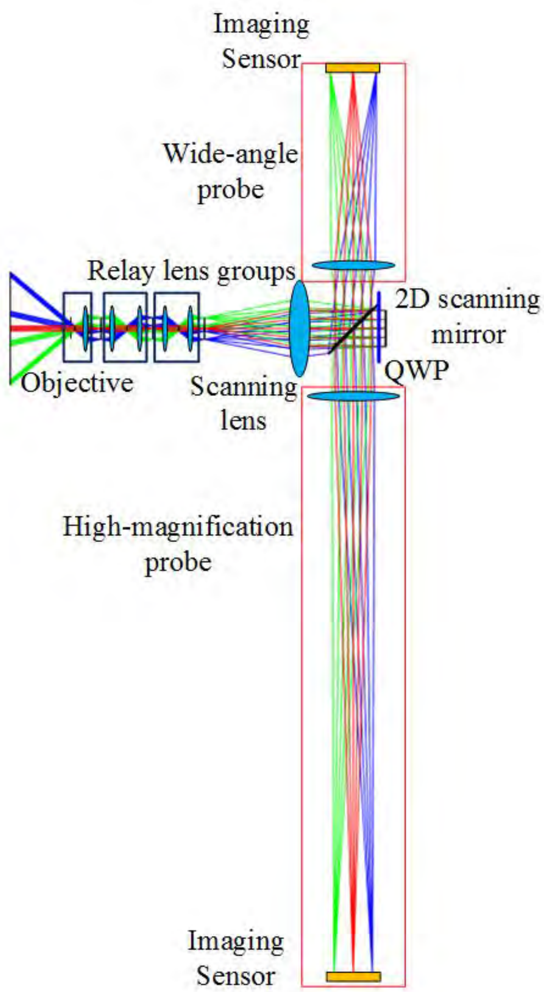

Figure 3.4 1st configuration of MRFL

The 1st configuration is shown in Figure 3.4. The objective lens captures the entire large field, and the relay lenses relay the intermediate image several times to achieve a suitable insertion length. Behind the last intermediate image formed by the relay lenses is the scanning lens which images an intermediate pupil to the 2D scanning mirror. The scanning lens can work as an eyepiece for direct viewing as well. A polarization beam splitter (PBS) and a quarter wave plate (QWP) are utilized for light splitting. The s-polarized light is reflected to the wide-angle probe, while the p-polarized light transmits the PBS. However, after passing the QWP, reflected by the mirror and passing the QWP again, the p-polarized light becomes the s-polarized light. Therefore it is reflected by the PBS and directed into the high-magnification probe.

This configuration is straightforward, the optical design is relatively easy to achieve. As will be discussed later, this is the configuration we choose for the real system design.

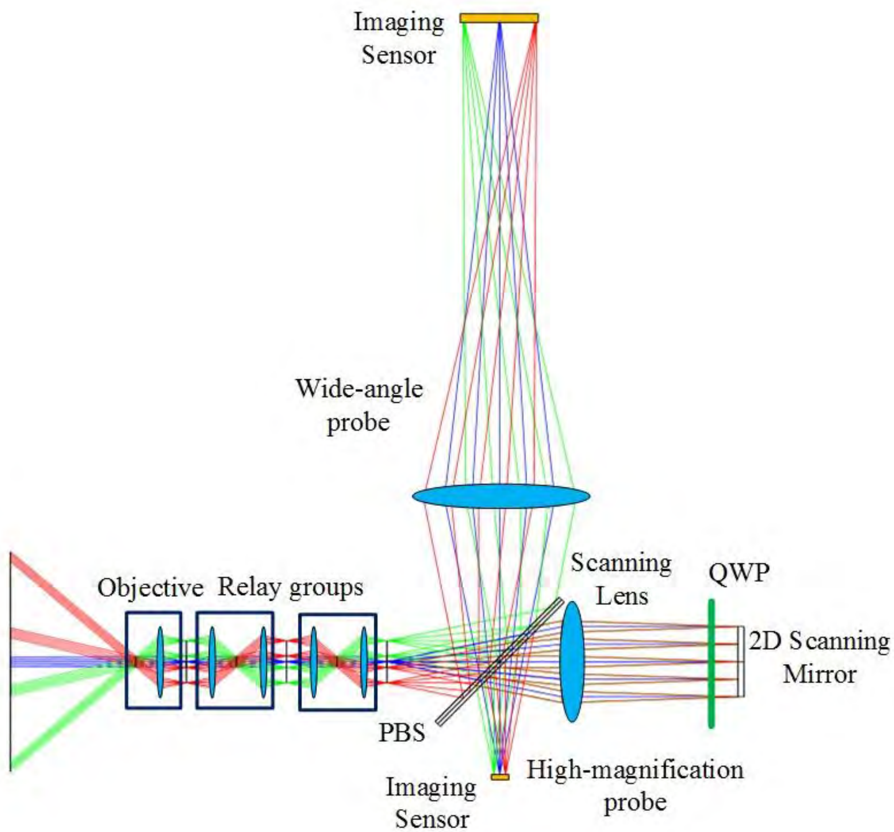

Figure 3.5 2nd configuration of MRFL

Figure 3.5 shows the second configuration of the MRFL, in which the beamsplitting occurs before the scanning lens and the scanning lens is double passed. Therefore, no extra lenses is needed in the high-magnification probe, the high-magnification probe could be quite compact. However, the limitation of this configuration is that the image height of the high-magnification probe is the same as that of the intermediate image of the last relay group, which may not be equal to a standard sensor size.

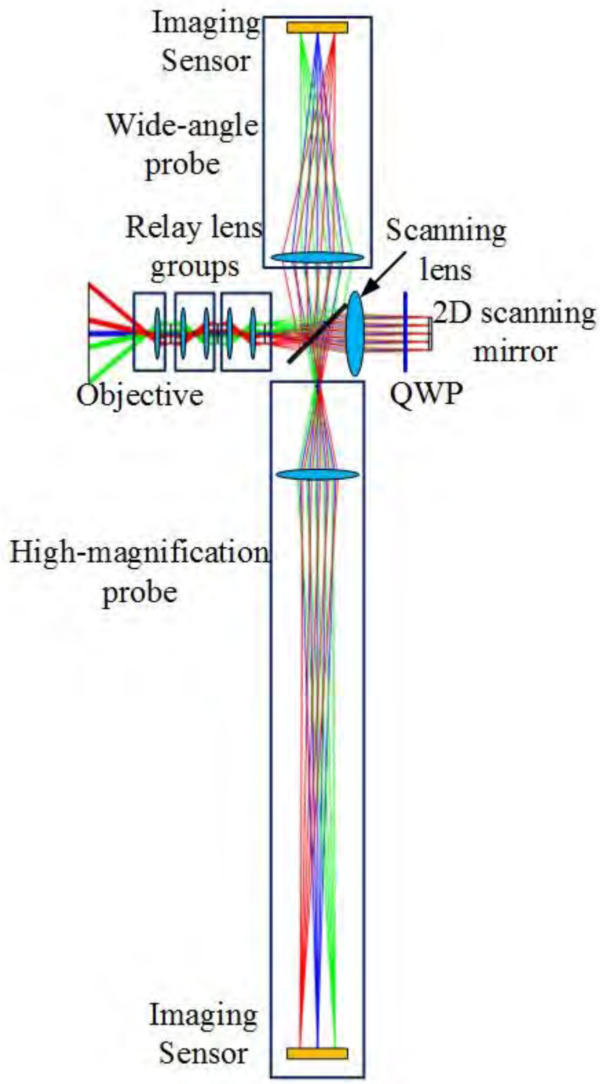

Figure 3.6 3rd configuration of MRFL

To adjust the final image height, a lens group with certain magnification is needed in the high-magnification probe to match the image size to a standard sensor size. Figure 3.6 shows the third configuration, the only difference between the third and the second configurations is that the high magnification probe has a relay lens to magnify the intermediate image relayed by the scanning lens to match the height of the sensor.

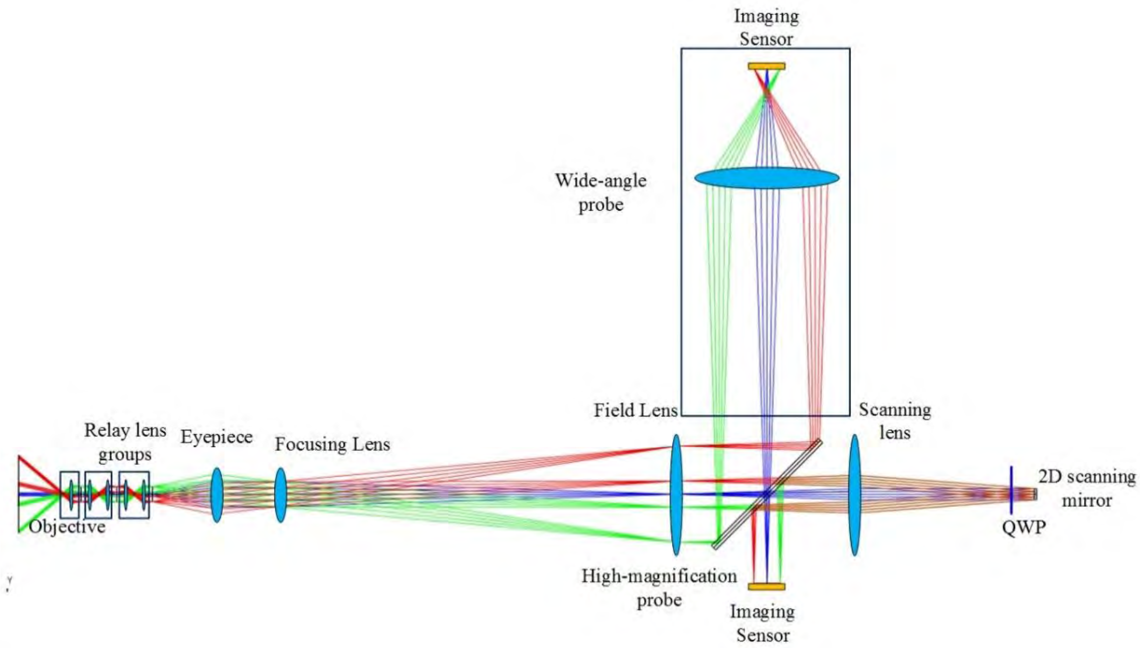

Figure 3.7 4th configuration of MRFL

Another method to achieve a compact high-magnification probe is shown in Figure 3.7. The objective lens group and the multiple relay groups are the same as the previous configurations, but an eyepiece and a focusing lens is inserted in front of the scanning lens to magnify the intermediate image of the last relay group to fit the size of a standard imaging sensor. Therefore no additional lenses are needed in the high-magnification probe. However, the drawback of this configuration is the system is longer than the previous ones due to the additional eyepiece and focusing lens.

Several initial designs were carried out to evaluate the performance and design complexity of each configurations. The first configuration is quite straightforward and the design is less complex than the second and the third one. The second and the third one is difficult to design because the beam splitter is inserted in front of the scanning lens, thus the scanning lens requires a large front focal distance. Since the objective lens and the relay lens groups have low F/#s, the scanning lens also has a low F/#, therefore it is quite difficult to achieve the required performance. Additionally, since the scanning lens is double passed in these two configurations, the aberration balancing is quite different than the first one. The scanning lens design of the fourth configuration is less complex than the second and third ones, because the intermediate image before the scanning lens is magnified and has large F/#. However the scanning system is much longer than others, and it needs more lenses than the first configuration.

By considering all these factors, we choose the first configuration for our customized design. Because for the customized design, less lens elements can reduce the manufacturing cost, and the integrated system should be as compact as possible to reduce the ergonomic conflict during the surgery. Before starting the customized design, an initial bench prototype was built to demonstrate the basic functions of the MRFL by using a commercially available laparoscope, off-the-shelf lenses and cameras which will be demonstrated in the next chapter.

3.4 First-order Parametric Design

In this section, a detailed first-order parametric design is carried out based on the 1st configuration of MRFL as discussed in the previous section. The first-order calculation will guide the design and optimization process of the optical system of the MRFL, such as the focal length and magnification of each sub-system, the lens diameter on the first-order scale, and the selection of the 2D scanning mirror.

The objective lens is shared by the wide-angle probe and the high-magnification probe. It captures the entire surgical field with high spatial resolution. One requirement of the objective lens is the telecentricity in image space. Because the intermediate image is relayed multiple times by the following relay lens groups, the telecentricity would minimize the image quality degradation through multiple image relays.

By using Gaussian optics, the relationship between the intermediate image height and the focal length of the objective lens can be expressed by Eq. 3.5.

$$h_{int-img} = f_{obj} \times \tan(HFOV) \qquad \text{(Eq. 3.5)}$$

The first-order diameter of the objective lens can be calculated by Eq. 3.6. Under the assumption of an 80° full FOV, Figure 3.8 demonstrates the relationship between the focal length of the objective lens and the diameter of the objective lens. As the focal length of the objective lens increases, its diameter increases as well. To meet the requirement of our selected laparoscope packaging, the maximum lens diameter is 5.5mm. Therefore the focal length of the objective lens cannot be larger than 2.8mm.

$$D_{obj} = 2 \times f_{obj} \times \tan(HFOV) + D_{EP} \qquad \text{(Eq. 3.6)}$$

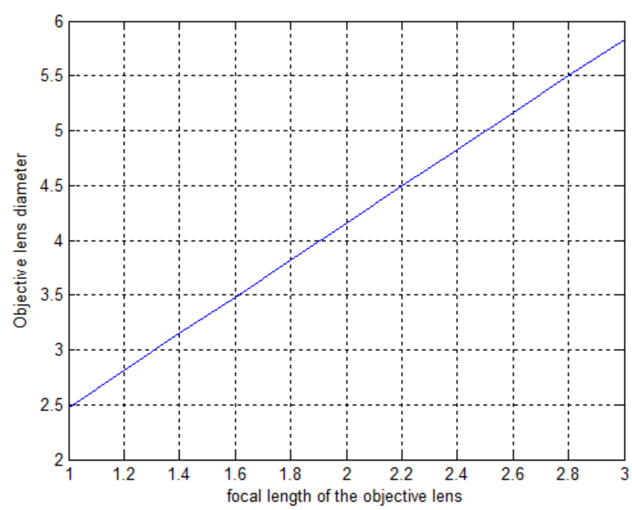

Figure 3.8 Relationship between the objective lens diameter and its focal length

The relay lenses relay the intermediate image multiple times to guarantee enough insertion length of the MRFL for the laparoscopic surgery. The magnification of each relay group is -1. In order to maintain the image quality though multiple relays, the relay lens is required to be telecentric in both object and image spaces. Therefore, the first-order lens diameter can be calculated by Eq. 3.7. Figure 3.9 shows the first-order diameter of the relay lens as a function of the focal length of the objective lens and that of half of the relay lens group.

$$D_{relay} = 2 \times h_{int\text{-}img} + D_{relay-stop} = 2 \times f_{obj} \times \tan\left(HFOV\right) + \frac{f_{half-relay}}{f_{obj}} \times D_{EP} \qquad \text{(Eq. 3.7)}$$

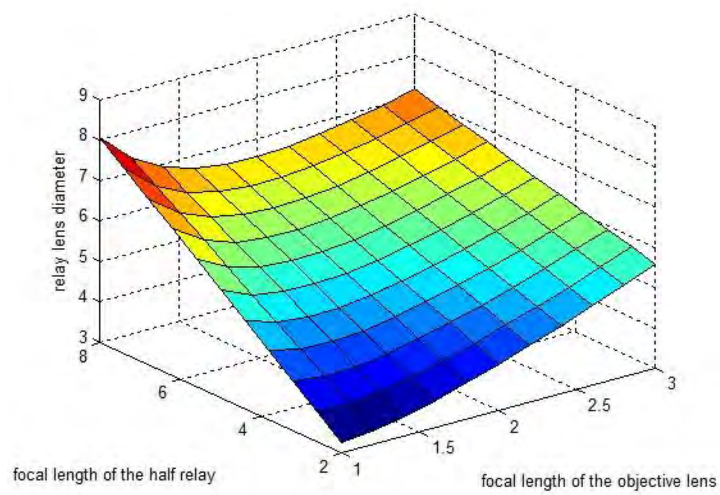

Figure 3.9 Diameter of the first-order model of the relay lens as a function of the focal lengths of the objective lens and the half relay group

The scanning lens relays the pupil to the 2D scanning mirror. The diameter of the relayed pupil or the minimum diameter of the scanning mirror can be calculated by Eq. 3.8. The field angle of the scanning lens can be express by Eq. 3.9. Figure 3.10 shows the scanning mirror diameter as a function of the focal lengths of the objective lens and the scanning lens. Figure 3.11 demonstrates the scanning range of the 2D mirror as a function of the focal lengths of the objective lens and the scanning lens. These figures indicates that there is a tradeoff between the scanning mirror diameter and scanning range. When the scanning mirror has smaller diameter, it requires a large scanning range and vice versa.

$$D_{mirror} = \frac{f_{scan}}{f_{obj}} \times D_{EP} \qquad \text{(Eq. 3.8)}$$

$$\theta = \tan^{-1}\left[\frac{f_{obj}}{f_{scan}} \times \tan(HFOV)\right] \qquad \text{(Eq. 3.9)}$$

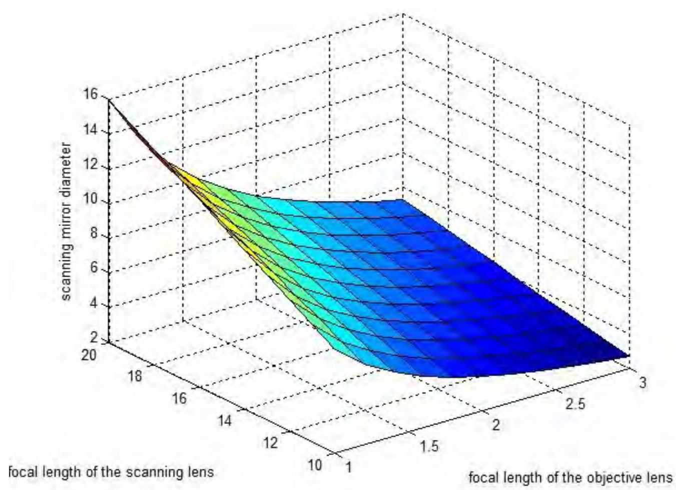

Figure 3.10 Scanning lens diameter as a function of the focal lengths of the scanning lens and the objective lens

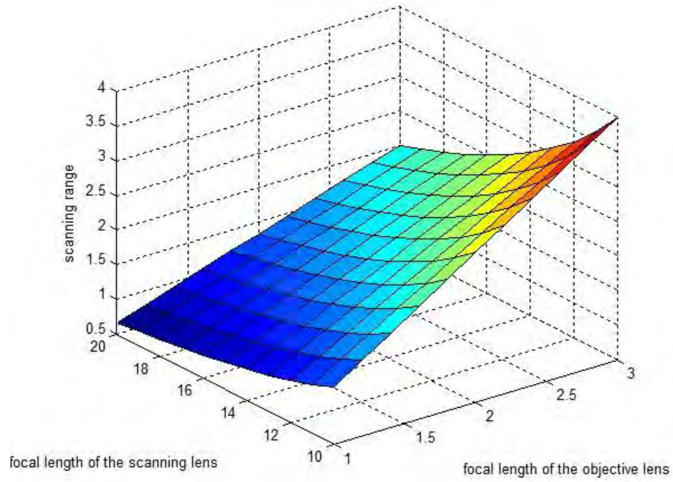

Figure 3.11 Scan range of the 2D scanning mirror as a function of the focal lengths of the scanning lens and the objective lens

The wide-angle probe images the entire field of view to the imaging sensor. Its focal length is expressed by Eq. 3.10.

$$f_{wide-angle} = \frac{h_{sensor}}{h_{int\text{-}img}} \times f_{scan} \quad \text{(Eq. 3.10)}$$

In a similar fashion, the high-magnification probe magnifies a sub field of the entire field of view and relays it to the imaging sensor. Eq. 3.11 demonstrates focal length.

$$f_{high-mag} = \frac{h_{sensor}}{\frac{1}{3} h_{int\text{-}img}} \times f_{scan} \quad \text{(Eq. 3.11)}$$

By considering all these parameters and constraints, we selected the focal length of the objective lens as 2mm, that of the half relay as 4mm and that of the scanning lens as 14mm. Therefore, the diameter of the scanning mirror needs to be larger than 5.6mm and the scanning range is ±1.9°.

3.5 Throughput Analysis

Throughput is an optical invariant that characterizes the light collection capability of an optical system. It is defined as the product of the area of the source and the solid angle that the system's entrance pupil subtends as seen from the source, as indicated by Eq. 3.12.

$$throughput = A\Omega \qquad \text{(Eq. 3.12)}$$

Table 3.1 summarizes the image space throughput comparison between a standard laparoscope and the MRFL. The throughput of a standard laparoscope is 0.086 mm^2 sr, and 0.34 mm^2 sr for the wide-angle probe and 0.04 mm^2 sr for the foveated probe of the MRFL.

	WD (mm)	F/# (obj. lens)	BS ratio	Throughput (mm^2 sr)	
				Foveated	Wide-angle
SL	50	7	N/A	N/A	0.086
MRFL	120	2.5	50/50	0.04	0.34

Table 3.1 Throughput Analysis

3.6 Optical System Design

In this section, the design challenges of the MRFL system are first discussed and then the design procedure is described in detail. In the end, the performance of the optimized MRFL is demonstrated. A more detailed optimization procedure is described in Appendix B.

3.6.1 Design Challenges

The main challenge of the optical system design of the MRFL arises from the large throughput of the system while maintaining the same volume as a conventional laparoscope. Spherical aberration, coma, and astigmatism become quite difficult to correct due to the low F/#s of each sub-systems, because they are proportional 4th power, 3rd power and 2nd power of the entrance pupil diameter respectively. Besides, the image quality should not degrade much as the number of relays increases. However, as the number of relay increases, the even order aberrations accumulate, such as spherical aberration, astigmatism, field curvature and axial chromatic aberration. During the design procedure, we found it was quite difficult and cost-inefficient to design the system by just using conventional refractive glass lenses. So we apply a refractive-diffractive hybrid plastic lens by single point diamond turning to correct those aberrations.

3.6.2 Design Procedure

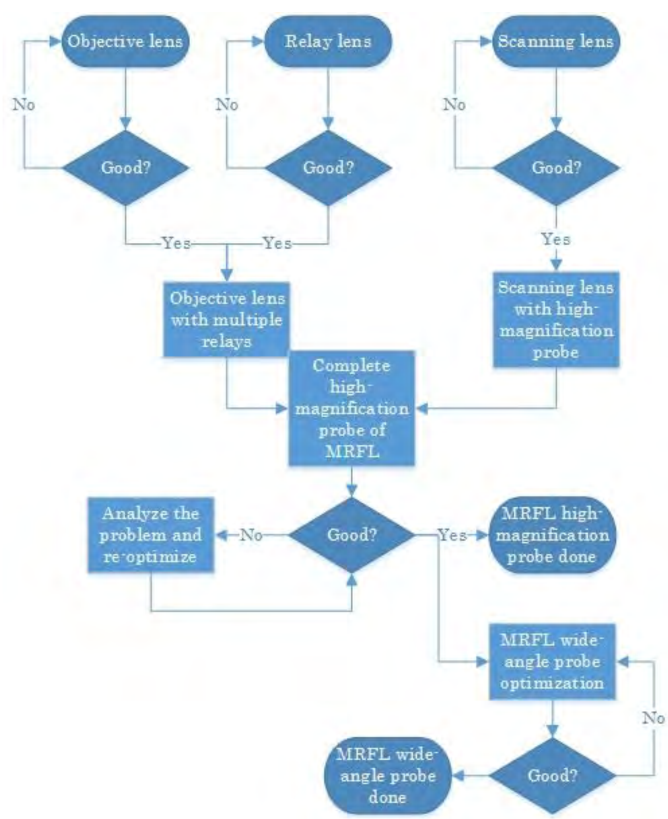

Figure 3.12 Flow of the optical design procedure

The MRFL consists of an objective lens group, multiple relay lens groups, a scanning lens group, a high-magnification probe and a wide-angle probe. The design strategy we chose is to design each sub-system first, then combine them together for further optimization. A detailed design flow is shown in Figure 3.12. In addition, when designing each sub-system, we can intentionally overcorrect some aberrations, so that they can compensate when combining other sub-systems. For example, the field curvature and astigmatism of the objective lens could be overcorrected to compensate the accumulated field curvature and astigmatism of the multiple relay lenses.

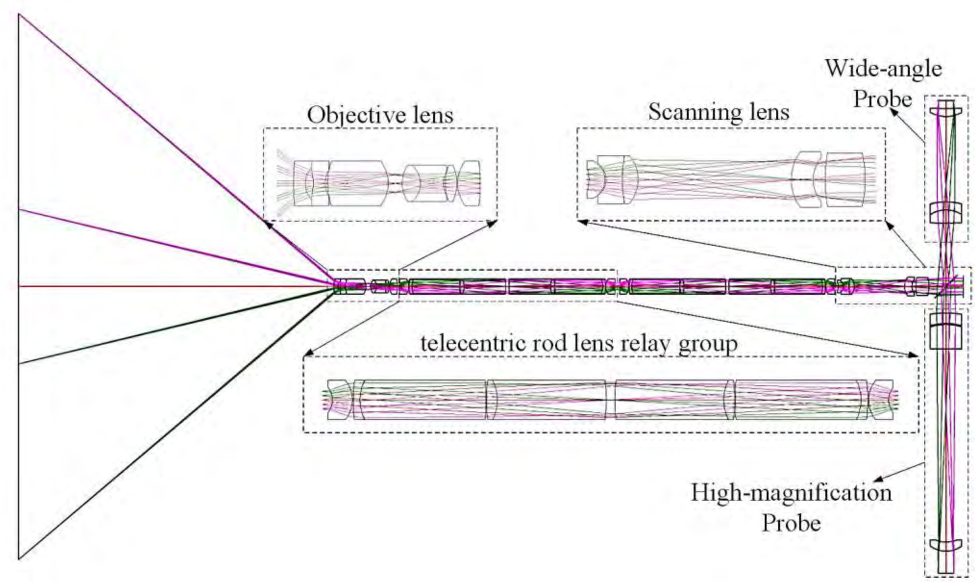

Figure 3.13 Layout of the low-profile MRFL

The optimized optical system of the MRFL is shown in Figure 3.13. Figure 3.14 shows the MTF of the wide angle probe. Figure 3.15 demonstrates the MTF performance of the high-magnification probe aiming at the central FOV and the peripheral FOV. The MTF indicates the high-magnification probe is near diffraction limited; and at the required 60lp/mm frequency, the image contrast is better than 0.1.

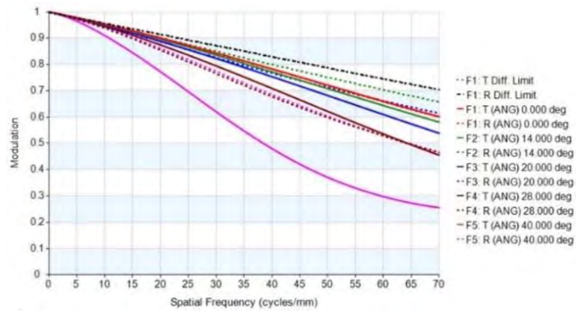

Figure 3.14 MTF of the wide-angle probe

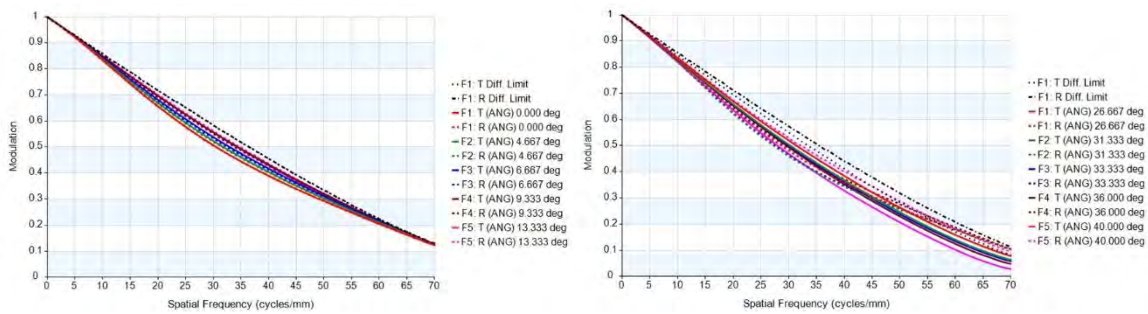

Figure 3.15 MTFs of the foveated probe

3.7 Discussion

In this section, based on the design of the MRFL, we will discuss the generalized design, assembling and testing strategy of an optical system with multiple image relays.

3.7.1 "Divide and conquer" strategy

During the design of the MRLF, we adopted a "divide and conquer" design strategy as illustrated in Figure 3.12, which enabled us to carry out the optimization of the key lens groups in parallel before integrating them. This method is suitable for designing an optical system with multiple image relays. In the initial design phase, each sub-optical system is optimized separately, therefore it allows us to find the best solutions to the sub-systems by applying our knowledge and experience with those well-known lens forms, rather than directly venturing into a complex system.

In the process of optimizing the individual sub-systems, the key constraints must be satisfied in order to meet the optical and mechanical requirements of the integrated system. For example, in the MRFL system design, the lens diameter constraint and telecentricity requirement of the objective lens and relay lenses should be met during the optimization of sub-system. Otherwise, these key constraints will be quite difficult to optimizing during the system integration.

3.7.2 Assembling and testing consideration

By adopting the "divide and conquer" design method, the system assembly and testing procedures become straightforward, since each sub-system has good performance before system integration. Although in the final design stage, all the sub-systems are optimized together for better aberration balancing, the performance of each sub-system does not vary significantly.

For an optical system with multiple image relays, each sub-system could be assembled and tested separately before integration. The residual wavefront aberrations of each sub-system can be read out from the optical design software such as Code V and Zemax. An interferometer could be used to measure the actual wavefront aberrations of each assembled sub-system. Each assembled system is adjusted and fine-tuned until the wavefront errors meet the error budgets. During the system integration, one only needs to adjust those predefined compensators to fine-tune the performance of the integrated system. In the last step, the wavefront error, spatial resolution and MTF are measured to verify the integrated system meets the design requirements. The detailed flow of the assembling and testing procedure is summarized in Figure 3.16.

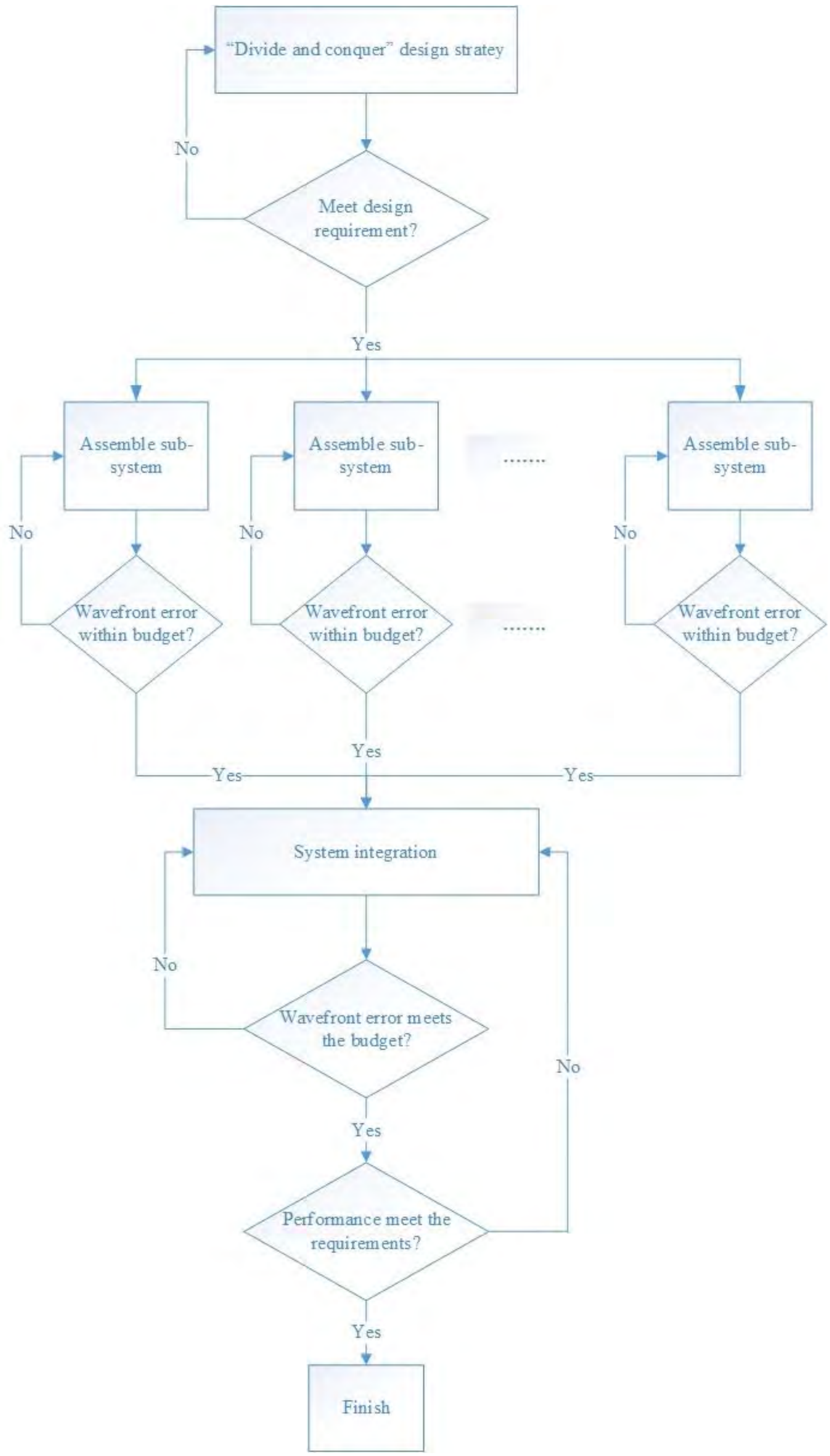

Figure 3.16 Assembling and testing flow of an optical system with multiple relays

4 Prototype Demonstration

Three generations of the MRFL were designed and implemented as part of this research effort. The first generation prototype was a preliminary, proof-of-concept system built with a commercially available laparoscope and off-the-shelf optical and opto-mechanical components. Building it helped me to improve my system design technique and to validate, or correct various design decisions from the optical system to the mechanical constructions. The image quality of the first prototype is limited by the commercial laparoscope which has a small entrance pupil diameter and small working distance. However, it successfully demonstrated the multi-resolution foveated capability.

The second generation prototype is a substantial improvement over the first preliminary implementation. The entire system is a customized design with much larger entrance pupil diameter and working distance while maintaining a standard 10mm laparoscope packaging. Two prototypes were designed and assembled, one is a normal length profile system which has an insertion length about 300mm, thus it could be adapted to the current standard MIS procedure; the other one is a low-length profile system as we proposed in Chapter 2, which has an insertion length of 150mm and has great potential to reduce the instruments conflicts. The second generation prototype was evaluated in a laparoscopic training session to demonstrate its capabilities. In addition, feedback was collected from the surgeon for further refinement of the MRFL.

The third generation prototype adds the optical zoom and autofocusing capability to the high-magnification probe. Therefore, the field coverage or the optical magnification of the zoomed-in view can vary while keeping the same focus distance as the wide-angle probe. In addition there are no mechanical moving components in the zoom probe. Two variable focus elements (VFEs) are implemented to achieve the zooming and autofocusing functions. The detailed design procedure and prototype of the zoom probe will be demonstrated in Chapter 5.

4.1 Initial Prototype

An initial prototype system was designed and built using a commercially available laparoscope and off-the-shelf-lenses, to demonstrate the multi-resolution foveated function of the proposed system. As mentioned in Chapter 3, the 4th system configuration was selected for this initial prototype. The optical properties of the commercial laparoscope were measured first. Then the scanning system and the two imaging probes were designed and optimized with off-the-shelf lenses.

4.1.1 Specifications of a commercial laparoscope

The specifications the manufacturer provides are field of view of the objective lens which is 70 degrees and 0 degree viewing direction. In order to design the following foveated imager, the exit pupil diameter and location had to be characterized, since it should match the entrance pupil of the following optical system. In addition, the field of view of the eyepiece should also be measured in order to choose proper focal lengths and magnifications of the two imaging probes.

A good quality lens was used to measure the exit pupil diameter and location, and to estimate the field of view of the eyepiece of the commercial laparoscope, as shown in Figure 4.1. The lens focal length of that lens is measured by the nodal slide. The result shows that it has an effective focal length of 30mm, a front focal distance of -21.8mm and a back focal distance of -21.8mm. The steps of the experiment are (1) Image the exit pupil of the laparoscope sharply on the detector; (2) Measure the distance L1 between the last surface of the laparoscope and the front surface of the lens; (3) Measure the diameter (D’) of the image of the exit pupil by reading the pixel number of the image; (4) Fix the lens and the imaging sensor, replace the laparoscope by a bar target. Move the target along the rail until it is clearly imaged on the detector. The position of the bar target is the position of the exit pupil of the laparoscope; (5) Measure the distance (L2) between the bar target and the front surface of the lens; (6) Measure the width of each bar of the bar target image (W’), similar to step (3); (7) The physical width of each bar (W) is 0.698mm; (8) The magnification is m = -W’/W; (9) The diameter of the exit pupil is D = D’/|m|; (10) The location of the exit pupil is at a distance (L1-L2) behind the last surface of the laparoscope.

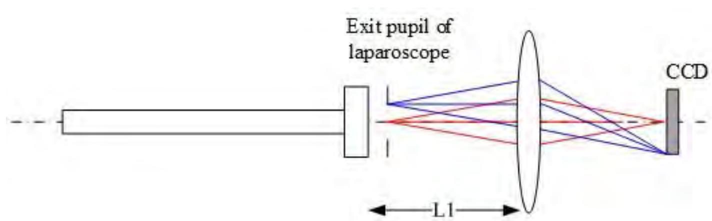

Figure 4.1 Experiment of measuring the exit pupil diameter and location of the commercial laparoscope

The images of the exit pupil and the bar target are shown in Figure 4.2. The measured exit pupil diameter is 1.78mm, and its location is 2mm behind the last surface of the laparoscope.

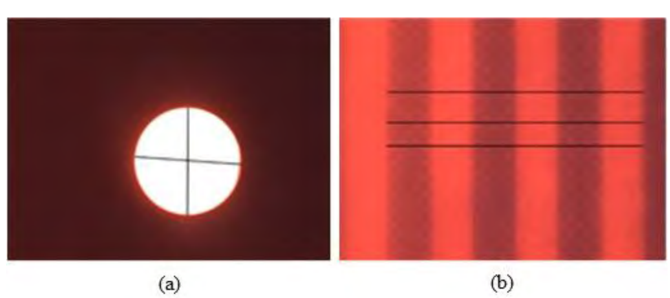

Figure 4.2 Exit pupil measurement: (a) image of the exit pupil; (b) calibration target image

Another method to measure the diameter of the exit pupil is shown in Figure 4.3. Since the exit pupil is behind the last surface of the laparoscope, a CCD sensor is directed placed at the location of the exit pupil.

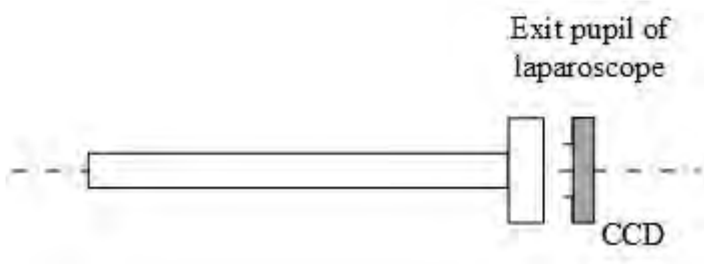

Figure 4.3 Layout of the direct measurement of the exit pupil diameter

The diameter of the exit pupil is measured in Matlab by a circle fitting function, as illustrated in Figure 4.4. The fitted data indicate the pupil radius is 238.967 pixels. Each pixel is 3.75um, therefore the diameter of the exit pupil is 1.7923mm. This result also validates the first method.

Figure 4.4 Result of the direct measurement of the exit pupil diameter

Another important parameter is the angular field of view of the eyepiece of the laparoscope. An experiment was set up as shown in figure 4.5. Two high-quality 28mm lenses were used. One of them formed an intermediate image, and the other one relay that intermediate image onto the sensor. Similar to the measurement of the exit pupil of the laparoscope, a bar target was used to calculate the magnification of the second lens. The measured field angle of the eyepiece is +/-7.06°.

Figure 4.5 FOV measurement of the eyepiece of the laparoscope

In summary, the key parameters of the commercial laparoscope is listed in Table 4.1.

FOV of the objective lens	70°
Exit pupil location	2.3mm behind the last surface
Exit pupil diameter	1.79mm
FOV of the eyepiece	+/- 7.06°

Table 4.1 Specifications of a commercial laparoscope

4.1.2 Optical system design of the initial prototype

The initial prototype using the Karl Storz laparoscope was designed based on the optical properties measured above. They system layout is shown in Figure 4.6. In this prototype, the FOV of the wide-angle probe is 2× that of the high-magnification probe. All the lenses are off-the-shelf lenses, and the cameras used in the initial prototype were PointGrey DragonFly (640×480 pixels) with a color pixel size of 15um.

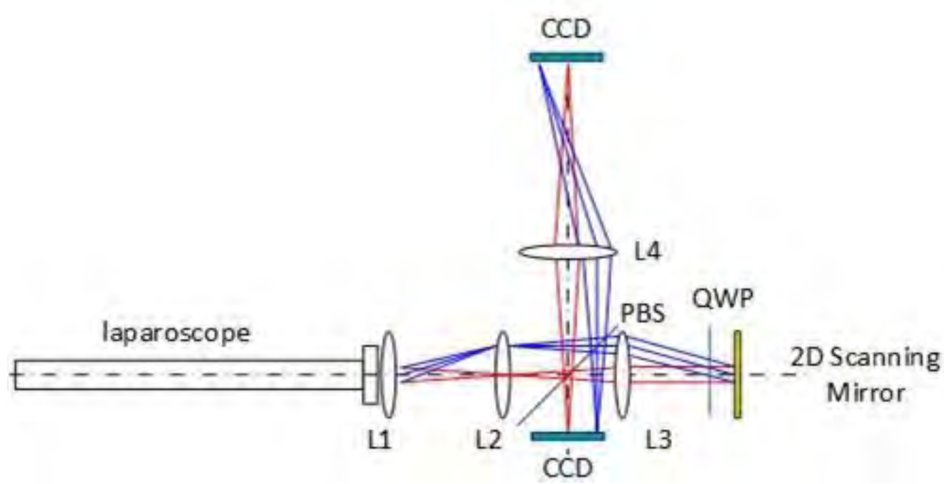

Figure 4.6 MRFL initial prototype layout

The layout and MTF performance of the high-magnification probe are shown in Figure 4.7. The layout and MTF performance of the wide-angle probe are shown in Figure 4.8. The imaging sensor has a cutoff frequency of 33.33lp/mm. The high-magnification probe has a contrast larger than 0.1 at 40lp/mm. Although the image contrast of the peripheral field of the wide-angle probe is slightly lower, it still met our prototyping requirement, since the wide-angle probe is for instrument orientation and situational awareness.

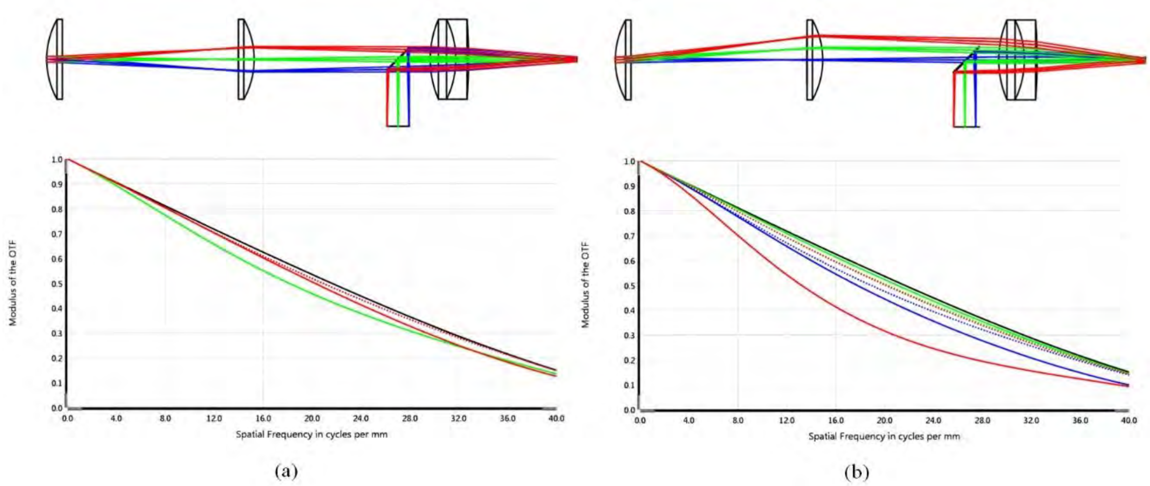

Figure 4.7 Layout and MTFs of the foveated probe

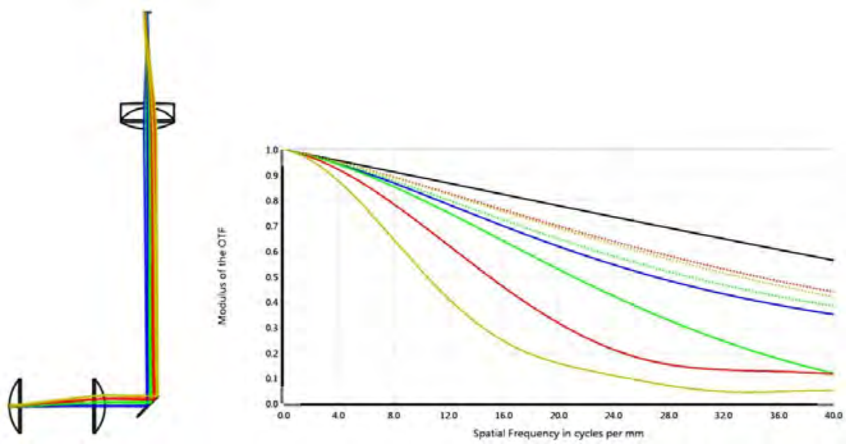

Figure 4.8 Layout and MTF of the wide-angle probe

4.1.3 Functional test

Figure 4.9 shows the images captured by the initial prototype. Figure 4.9 (a) is the image captured by the wide-angle probe; Figure 4.9 (b) shows the high-magnification image oriented at the center FOV; Figure 4.9 (c) and (d) are the high-magnification images oriented at the peripheral FOV.

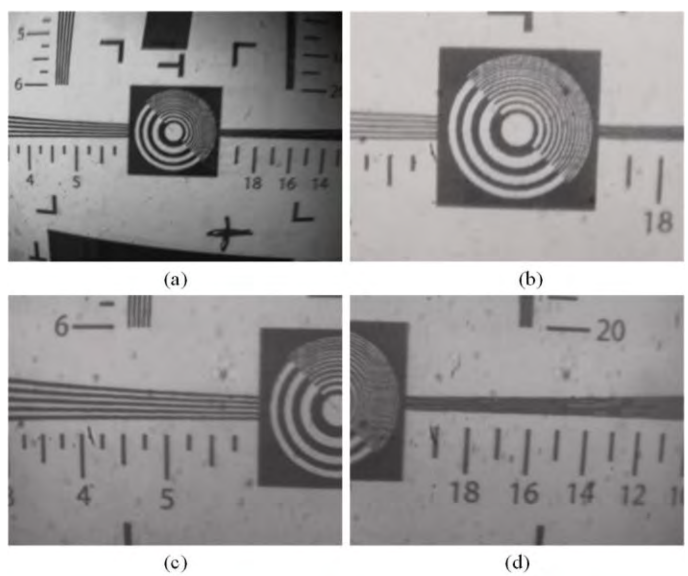

Figure 4.9 Images captured by the MRFL initial prototype: (a) wide-angle image; (b) high-resolution image of the center field; (c) and (d) high-resolution images of peripheral fields

4.2 Customized System Integration and Evaluation

As the initial prototype demonstrated the multi-resolution foveation capability successfully, a customized system was designed (Appendix B). The detailed performance evaluation is presented in APPENDIX C. In this section, I will discuss the mechanical design and the system assembling process, and go over the image quality test result and the in-vivo test in the laparoscopic training lab.

4.2.1 Mechanical system design

A standard laparoscope packaging from Precision Optics Cooperation (www.poci.com) was selected for the MRFL, as shown in Figure 4.10. The outer diameter of the laparoscope tube has a diameter of 10mm. The optical elements are assembled in an inner tube which will be inserted into the outer tube. The objective lens and multiple relay lens groups were assembled in that standard packaging.

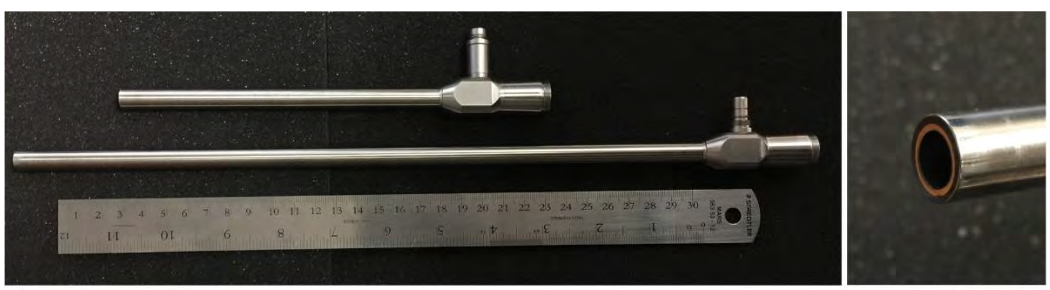

(a) (b)

Figure 4.10 Laparoscope packaging

The scanning mirror is a high precision mirror mounted on a 2D scanning gimbal mount (T-OMG series, Zaber). The tilting range is +/- 7°. The resolution for the azimuth axis is 2.014μrad (0.000115378°) and that of the elevation axis is 1.007μrad (0.000057689°). The speed resolution is 0.00054deg/s for the azimuth axis and 0.00027deg/s for the elevation axis.

Figure 4.11 2D scanner gimbal mount

The mechanical mountings were designed in Solidworks and manufactured by a professional machine shop. Appendix C: (Section xx) shows the mechanical design of the MRFL. All the components of the MRFL including the optical components, 2D scanner, mechanical housing were modeled in Solidworks for clearance verification as well as visualization, shown in Figure 4.12.

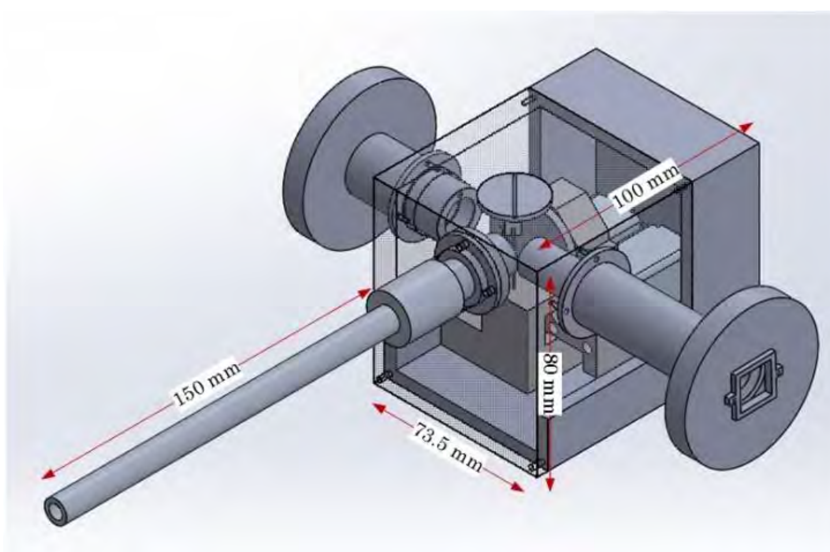

Figure 4.12 3D model of MRFL

4.2.2 System Assembling Process

The assembly of the MRFL was divided into two parts. The first part is the assembly of the objective lens and the relay lenses; the second part is the assembly of the scanning lens, the 2D scanning mirror and the two imaging probes. As mentioned before, the objective lens and the multiple relay groups were assembled in the inner tube of the standard laparoscope packaging. The rest of the MRFL were assembled in a customized designed mechanical housing.

When assembling the objective lens and the relay lenses, the optical elements were aligned on a V-groove firstly as shown in Figure 4.13, and carefully pushed into the inner tube using a high-precision gauge. The rest of the MRFL was assembled in a mechanical housing, the complete MRFL prototypes are shown in Figure 4.14.

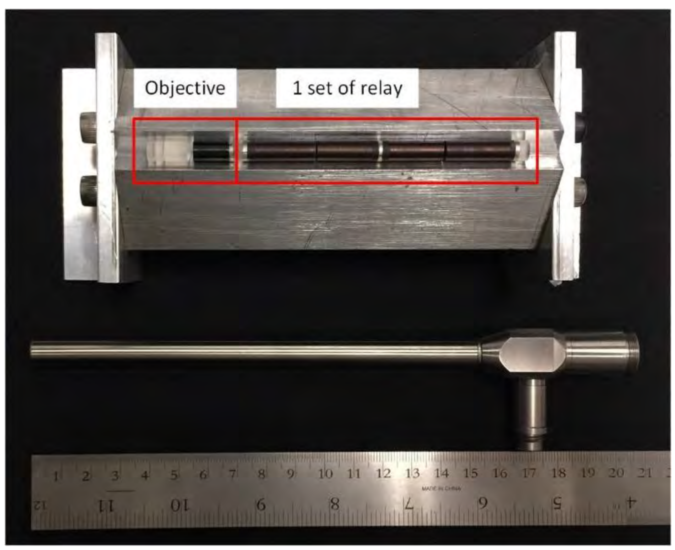

Figure 4.13 MRFL assembling procedure

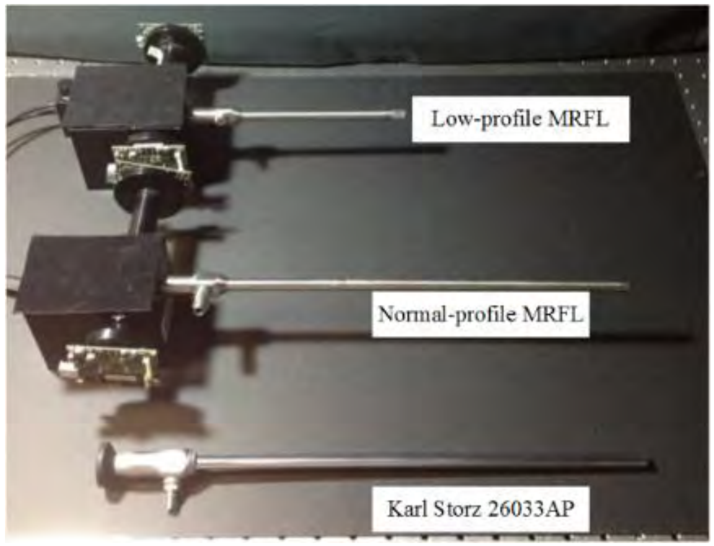

Figure 4.14 Prototypes of MRFL

4.2.3 Image quality verification

The image quality was verified to ensure the performance of the as-built MRFL. Appendix C describes the quantitative image quality test. In summary, the USAF 1951 resolution target was used to characterize the spatial resolution of both imaging probes, and the slanted edge method was used to test the MTF of the high-magnification probe.

Figure 4.15 (a) shows the captured image of the resolution target with the high-magnification probe at 120mm working distance at the center field, along with the intensity profiles of three horizontal target bars in Group 2 (element 4 through 6). Figure 4.15 (b) shows the intensity profiles of three horizontal bars in Group 2 (element 2 through 4). It demonstrates that when the high-magnification probe is at the center field, the group 2 element 5 bar (6.35 lp/mm or 78.74um) can be resolved in the vertical direction, and the group 2 element 4 bar (5.66 lp/mm or 88.34um) is resolvable in the horizontal direction.

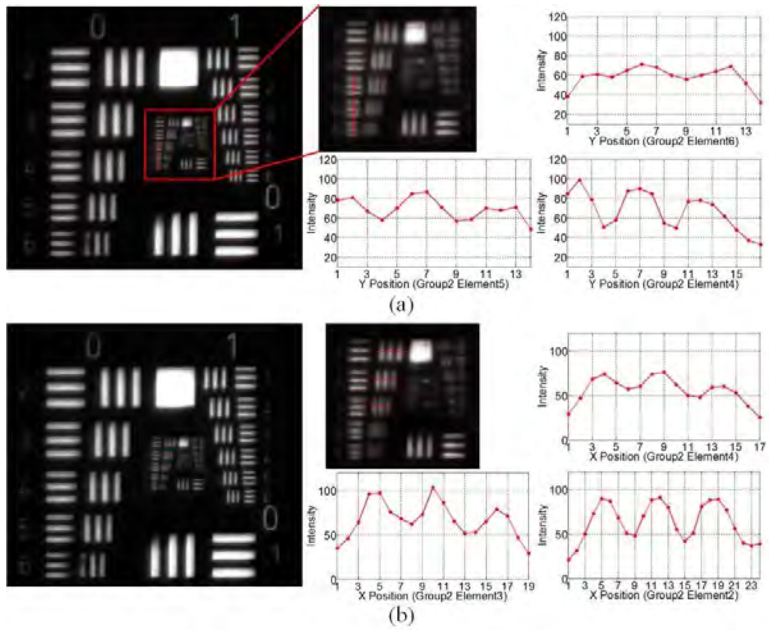

Figure 4.15 Images and intensity profiles of the resolution target of the high-magnification probe at 120mm working distance orienting at the center field, (a) in vertical direction; (b) in horizontal direction.

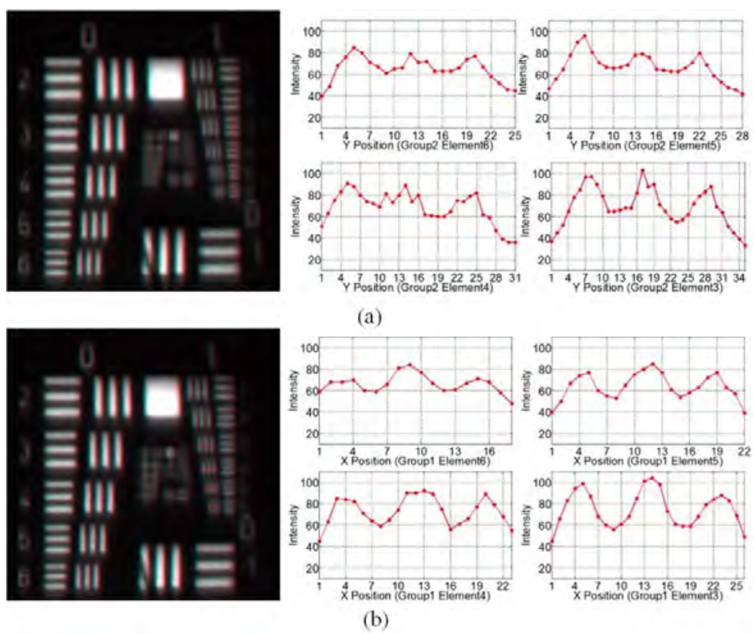

Figure 4.16 Images and intensity profiles of the resolution target of the high-magnification probe at 120mm working distance orienting at the corner field, (a) in vertical direction; (b) in horizontal direction.

Figure 16 (a) and (b) demonstrate the captured image and intensity profiles of the resolution target with the high-magnification probe at 120mm working distance at the corner field in the vertical and horizontal directions, respectively. It demonstrates that the high-magnification probe is able to resolve the group 1 element 6 bar (3.56 lp/mm or 140.45um) in both directions when it orients at the corner field.

Compared with the resolution of the high-magnification probe orienting at the center field, the resolution is lower when it orients at the corner field. One reason is that the MRFL is designed for a flat field, when the high-magnification probe orients at the corner field, the actual working distance is equivalent to 134mm, substantially larger than 120mm, and thus the spatial resolution is expected to decrease. Another reason is the distortion of the optical system, which is a magnification error related to field position. Alike a typical wide-field of view imaging system, the corner field of the MRFL is subject to a substantial amount of barrel distortion (15% at diagonal 80 degrees). Consequently, the actual magnification of the corner field is smaller than the center field, which leads to a lower spatial resolution.

Figure 4.17 shows the resolution of the center field of the wide-angle probe at 120mm working distances. In the center field, the group 1 element 4 bar can be resolved, which corresponds to a spatial frequency of 2.83lp/mm or a limiting resolution of 176um.

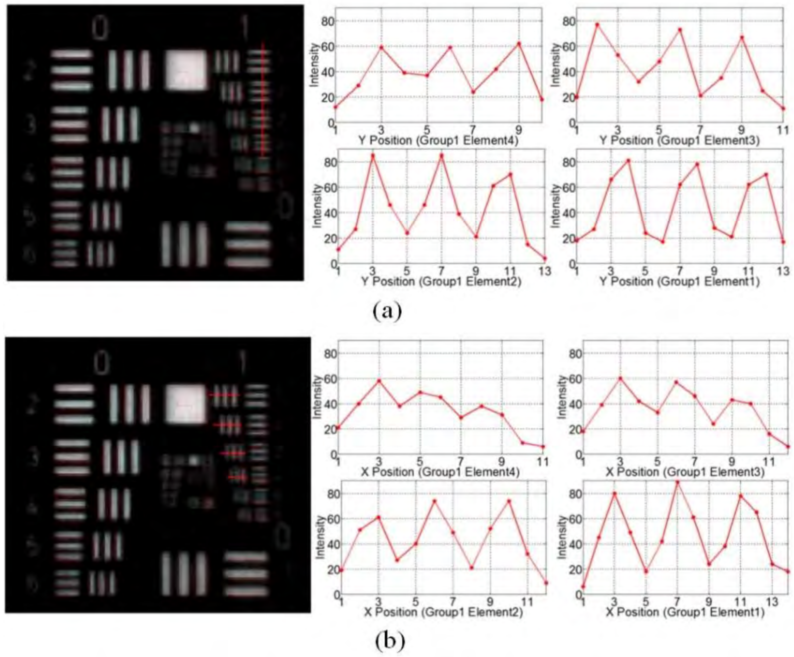

Figure 4.17 Images and intensity profiles of the resolution target of the center field of the wide-angle probe at 120mm working distance, (a) in vertical direction; (b) in horizontal direction.

Figure 4.18 demonstrates the resolution of the corner field of the wide-angle probe at 120mm working distance. It is shown that the group 0 element 5 can be resolved, which corresponds to a spatial frequency of 1.59lp/mm or a limiting resolution of 314um.

Comparing Figure 4.17 and Figure 4.18, it can be found that in the corner field, a certain amount of distortion and lateral color are observable. These aberrations degrade the performance of the corner field. However, it is still acceptable since the wide-angle probe is used for orientation and situational awareness, the performance is not as critical as that of the high-magnification probe.

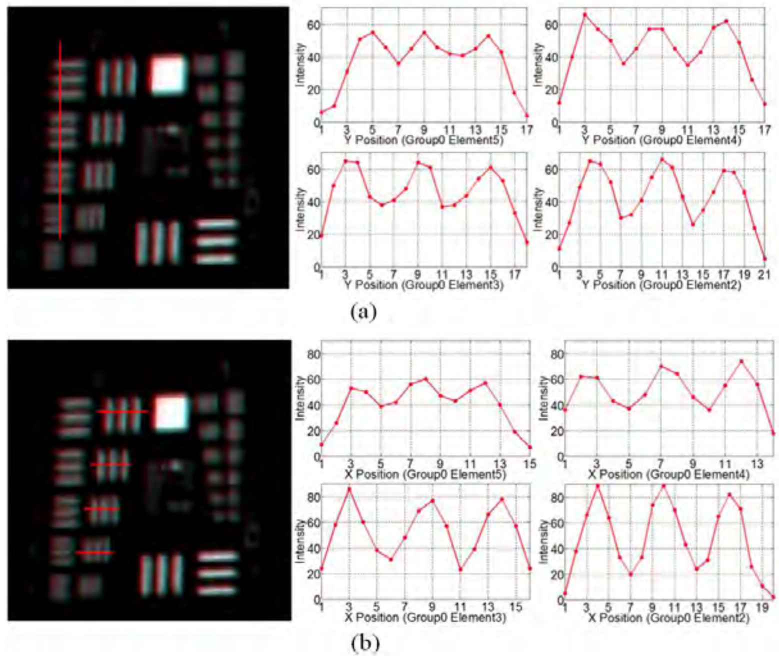

Figure 4.18 Images and intensity profiles of the resolution target of the center field of the wide-angle probe at 120mm working distance, (a) in vertical direction; (b) in horizontal direction.

To further verify the optical performance of the high-magnification probe, we adopted the slanted edge method to measure the MTF of the high-magnification probe at the center field [Imatest LLC]. The MTF measurements in both horizontal and vertical directions were carried out. As shown in Figure 4.19, the dashed black line is the diffraction limited MTF, the red curve is the MTF of the designed high-magnification probe, the solid blue curve is the measured MTF in horizontal direction, and the dashed blue curve is the MTF in vertical direction. In the horizontal direction, about 10% MTF drop was observed across the measured spatial frequency range (up to 70lps/mm), while in the vertical direction, about 20% MTF drop was observed. These performance drops may be attributed to lens manufacturing errors and system assembling errors.

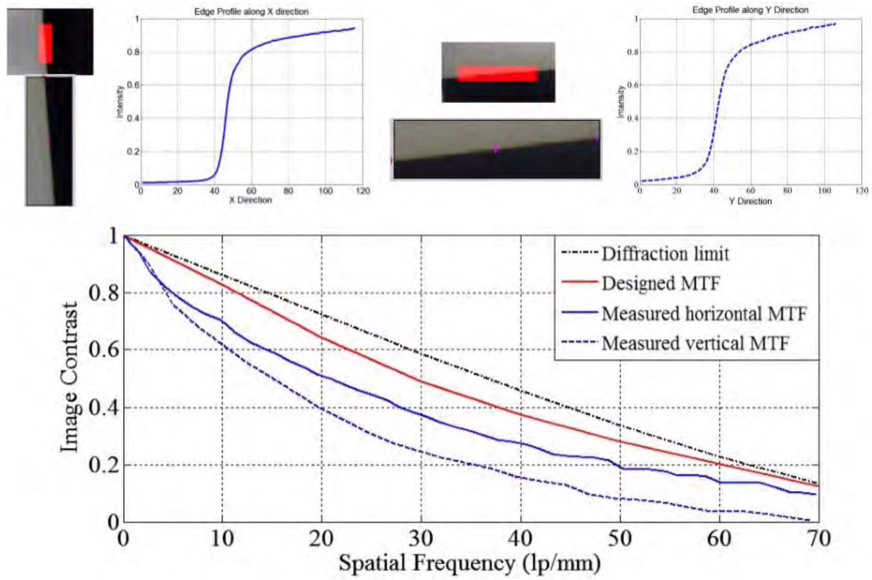

Figure 4.19 MTF measurement

4.2.4 In-vivo test

The MRFL prototypes were evaluated on a live pig model at the live animal lab in the Keck School of Medicine, University of Southern California. The pig was placed under general anesthesia with its abdomen inflated with a CO_2. Three incisions were made on the abdominal wall of the pig with three standard trocars for laparoscopic procedures. During the test, one of the trocars was utilized for positioning a MRFL prototype while a standard laparoscope for comparison or a laparoscopic grabber or scissor may be inserted through the other trocars. Figure 4.20 demonstrated the setup with a normal-length MRFL prototype inserted through the bottom trocar. The images shown in Figure 4.21 and Figure 4.22 were captured with this setup where only about half of the normal-length tube was inserted into the trocar to ensure a working distance round 120mm.

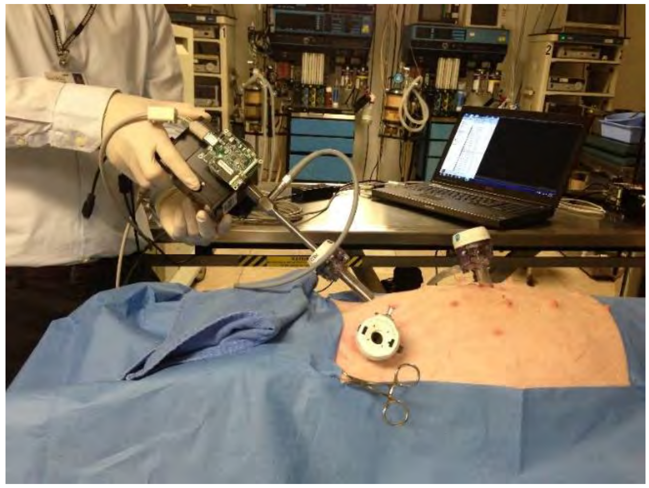

Figure 4.20 In-vivo animal test

Figure 4.21 (a) and (b) demonstrate the high-magnification image and wide-angle image of the spleen captured simultaneously by the two imaging probes of the MRFL prototype, where the splenectomy was performed. Figure 4.21 (c) and (d) demonstrate images of the gallbladder for cholecystectomy. The cyan-boxes in Figure 4.21 (b) and (d) marks the corresponding regions of interest captured the high-magnification foveated probe. The surgical areas displayed in Figure 4.21 (a) and (c) by the high-magnification probe are similar to those by the standard laparoscope used for comparison. These pictures further demonstrate that the high-magnification probe's capability of capturing the adequate fine structures of the spleen and the gallbladder for surgical procedures. Figure 4.21 (b) and (d) demonstrate the surgical fields of the wide-angle probe which are substantially larger than those of the standard laparoscope in comparison. The wide-angle views can guide the manipulation of other instruments without collision. In addition, Figure 4.21 (d) shows the position of a standard laparoscope used for comparison, which suggest that the working distance of the standard laparoscope is much smaller than that of the MRFL. In order to get the close-up view similar to that by the high-magnification probe of the MRFL system or wide-angle view similar to that by the wide-angle probe, the standard laparoscope needs to move forward or withdraw backward from the surgical site.

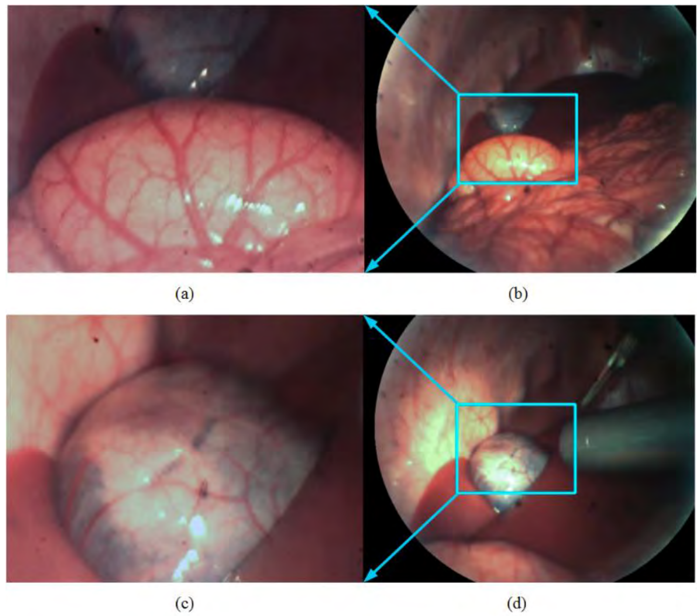

Figure 4.21 MRFL in-vivo evaluation with a porcine model at an approximately 120mm working distance from the surgical cite: (a) high-magnification image of the spleen; (b) wide-angle image of the spleen; (c) high-magnification image of the gallbladder; (d) wide-angle image of the gallbladder. The high-magnification and wide-angle images were acquired simultaneously through the MRFL prototype.

5 DESIGN AND CHARACTERIZATION OF A CONTINUOUS ZOOM AND AUTOFOCUSING IMAGING PROBE FOR THE MRFL

The multi-resolution foveated laparoscope successfully demonstrated its capability of providing the surgeon high-resolution images and situational awareness during the minimally invasive surgery. Although the foveated probe was found to offer an adequate magnification for viewing surgical details, the existing MRFL prototype is limited to two fixed levels of magnifications. The fixed level of magnification without turning to a manual maneuver of the instrument presents limitations. A fine adjustment of optical magnification is highly desired for the foveated probe to obtain high-resolution views with a desired field coverage. For instance, since the optical magnification of the foveated probe of the existing MRFL prototype is 3× that of a standard laparoscope, it is sufficient to perform MIS such as cholecystectomy and appendectomy. However, for surgeries like liver resection and colon resection, larger field coverage may help the surgeon to perform the operation more efficiently.

In this chapter, a high-magnification probe with continuous zooming (2× ~ 3×) and auto-focusing capabilities is presented. The wide-angle probe of the MRFL remains the same as the existing prototype; the foveated zoom probe is able to adjust its optical magnification and keep focused on the same object without any mechanically moving part. This is achieved by utilizing two electronically controlled tunable lenses. The optical approach and the design challenges of the high-magnification zoom probe are presented. Then the optimized design and the prototype are demonstrated. In the end, the spatial resolution performance of the prototype is evaluated and an initial experiment imaging a bladder model is presented to show the field coverage change of the high-magnification zoom probe at different zoom ratio.

5.1 Design Overview

The objective of the zoom probe is to change the magnification of the foveated probe without affecting the wide-angle view and keep the same the focusing distance in the object space for different zoom positions. This requirement imposes a major challenge because varying the optical power for zoom inevitably causes a change of object-image conjugate planes; which results in a change of focusing distance in the object space or a change of the detector plane position in the image space. If not appropriately compensated, varying the optical power of the foveated probe alone may cause severe mismatch of focused object between the wide-angle and foveated probes and cause image blurring during zooming.

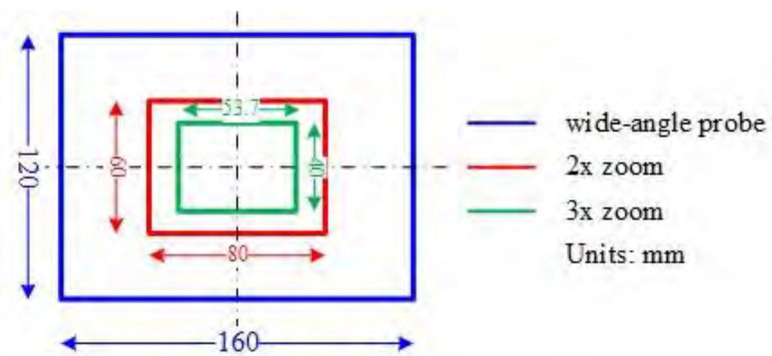

Figure 5.1 Field coverage of different zoom ratio

In the customized MRFL prototypes, the magnification of the foveated probe is 3× of that of the wide-angle probe. As suggested by the surgeon with whom we are collaborating, the foveated probe could be more efficient in practical use if the magnification of the foveated probe could vary from 2× to 3×. The field coverage of different zoom ratios is illustrated in Figure 5.1. At 2× zoom ratio, the field coverage of the foveated probe is about 2.2 times of that of 3× zoom ratio.

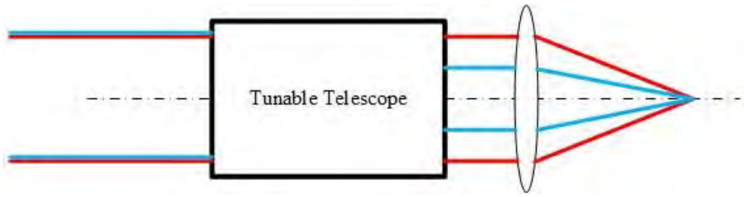

Figure 5.2 Schematic layout of the zoom probe

The schematic layout of the zoom probe with continuous zooming and auto-focusing capabilities is shown in Figure 5.2. It consists of a tunable telescope and a lens group with fixed focal length. The tunable telescope has two variable focal elements (VFEs), therefore its magnification can change by properly adjusting the optical power of the VFEs.

In a conventional zoom lens, at least two lenses need to mechanically move in order to change the zoom ratio and maintain the same focal position. By adopting the configuration shown in Figure 5.2, no mechanically moving components are needed. Two electrically controlled VFEs can change the zoom ratio and keep the focal position in real time.

The tunable telescope can be either a Keplerian type or a Galilean type, as shown in Figure 5.3. The Keplerian type consists of two positive tunable lens groups; and the Galilean type tunable telescope has a positive tunable lens group and a negative tunable lens group. The equivalent focal length of the zoom probe is calculated by Eq. (5.1), where f_{TL1} and f_{TL2} are the focal lengths of the first and second tunable lens group separately; and f_{img} is the focal length of the imaging lens.

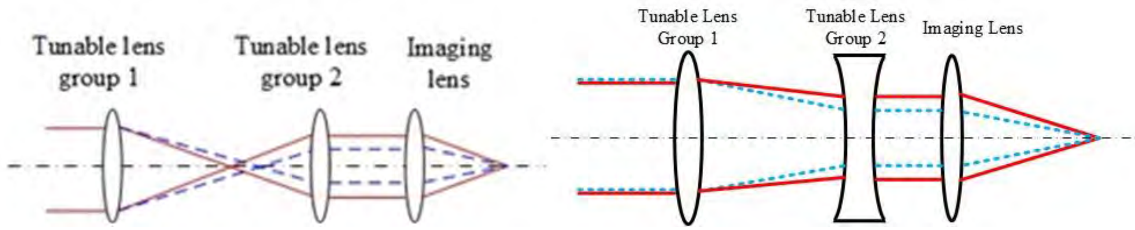

Figure 5.3 Configurations of the zoom probe: (a) Keplerian type; (b) Galilean type

$$f_{zoom} = \frac{1}{\left|m_{telescope}\right|} \times f_{img} = \left|\frac{f_{TL1}}{f_{TL2}}\right| \times f_{img} \qquad \text{(Eq. 5.1)}$$

5.2 Tunable lens

The tunable lenses we selected are Optotune EL-10-30-LD, because this is the only commercially available tunable lens that has a large enough clear aperture. The focal range is from 40mm to 120mm (8.3diopters ~ 22.22diopters). It is controlled by a 12-bit driver with 0.1mA accuracy. Figure 5.4 shows the relation between the driving current and the focal power.

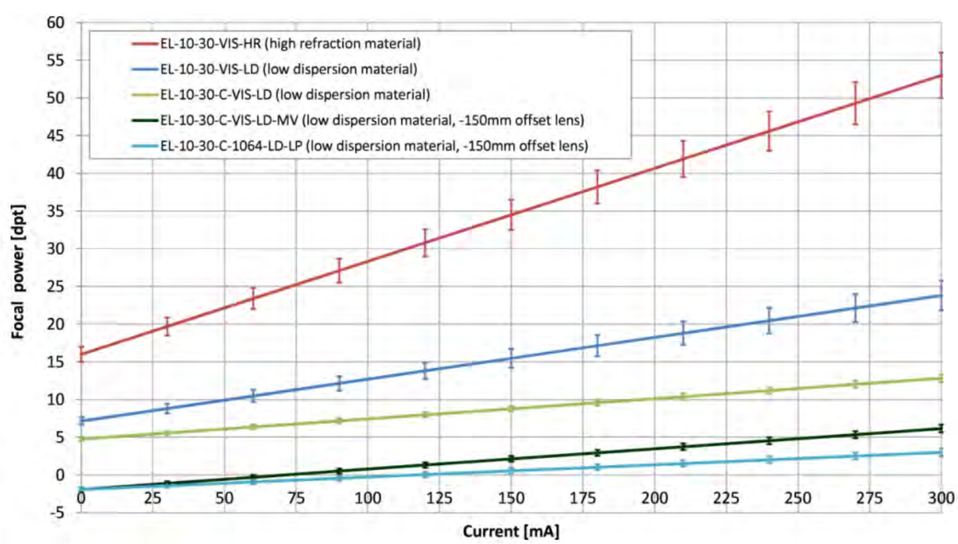

Figure 5.4 Relation between the driving current and optical power of the tunable lens

As indicated in Figure 5.4, the optical power of the tunable lens is a linear function of the driving current. Eq. (5.2) shows the accuracy of the optical power.

$$\Delta\phi = \frac{22.22 - 8.3}{4096} = 0.0034\,diopters \qquad \text{(Eq. 5.2)}$$

In terms of the accuracy of the focal length, Eq. (5.3) shows that the maximum focal error is 49um and the minimum focal error is 6.9um.

$$\begin{aligned} \Delta f &= -\frac{\Delta\phi}{\phi^2} \\ \Delta f_{\max} &= \frac{0.0034}{8.3^2} = 47um \\ \Delta f_{\min} &= \frac{0.0034}{22.22^2} = 6.9um \end{aligned} \qquad \text{(Eq. 5.3)}$$

5.3 Focal error analysis

Since each tunable lens has a finite focal accuracy, it may cause image blurring during zooming. However, if the focal error is smaller than the depth of focus of the zoom probe, that error can be ignored.

The objective lens is F/2.5, which corresponds to a numerical aperture of NA 0.2. Therefore the NA on the foveated camera is calculated by Eq. (5.4). Since f_{zoom} varies from 60mm to 90mm, NA varies from 0.0311 to 0.0467

$$NA = \frac{0.2}{f_{zoom}/f_{scan}} = \frac{0.2}{f_{zoom}/14} \qquad \text{(Eq. 5.4)}$$

The depth of focus of the zoom probe can be calculated by Eq. (5.5), where B' is the pixel size. Therefore the minimum depth of focus of the zoom probe is ±80um.

$$DOF \approx \pm\frac{B'}{2NA} \qquad \text{(Eq. 5.5)}$$

Assume the first tunable lens has a focal length error of $\Delta f_1 = 0.049mm$, which is the maximum focal error; and the second tunable lens has a focal length error of $\Delta f_2 = -0.049mm$, which has the same amplitude as Δf_1, but with opposite sign. On the second tunable lens, use the Newtonian Equation to calculate the image distance. Since now the object is 0.098mm left to the front focal point of the second tunable lens, the image distance can be calculated by Eq. (5.6).

$$z_1' = \frac{F_2^2}{2\Delta f} \qquad \text{(Eq. 5.6)}$$

Ideally, the final image is at the back focal plane of the fixed lens. However, when there is focusing error of the tunable lenses, the final image position will shift. Assuming the distance between the second tunable lens and the imaging lens is *t*. We use the Newtonian Equation, as shown in Eq. (5.7) to calculate the final image position, where F is the focal length of the imaging lens.

$$\left\{\frac{F_2^2}{2\Delta f} - \left[t_{img} - F - \left(F_2 - \Delta f\right)\right]\right\} \times z' = F^2 \qquad \text{(Eq. 5.7)}$$

Since,

$$\frac{F_2^2}{2\Delta f} \gg t_{img} - F - \left(F_2 - \Delta f\right) \qquad \text{(Eq. 5.8)}$$

We can make an approximation to get Eq. (5.9).

$$\frac{F_2^2}{2\Delta f} \times z' = F^2 \qquad \text{(Eq. 5.9)}$$

Therefore,

$$\begin{aligned} z' &= \frac{F^2}{F_2^2} \times 2\Delta f < DOF = 0.08mm \\ \frac{F}{F_2} &< \sqrt{\frac{0.08}{2 \times 0.049}} = 0.9035 \end{aligned} \qquad \text{(Eq. 5.10)}$$

By a similar analysis, we can conclude that for the Galilean type tunable telescope, as long as Eq. (5.11) is met, the focal error from the tunable lenses can be ignored.

$$\left|\frac{F}{F_2}\right| < 0.9035 \qquad \text{(Eq. 5.11)}$$

5.4 Optical design and system prototype

For the optical system design of the zoom probe, I also adopted the “divide and conquer” strategy described in Chapter 3. In the initial design phase, the zoom probe was optimized separately. When the performance and the key constraints were satisfied, it was integrated with the MRFL.

As mentioned in the previous section, the tunable telescope can be either a Keplerian type or a Galilean type. In the initial design phase, both types can achieve good starting point. However, when integrating with the MRFL, only the Keplerian type worked well. It was difficult for the Galilean type to meet the constraints of the clear apertures of the tunable lenses. The reason is that the Galilean type telescope is not a pupil-forming telescope, and the pupil aberrations arising from the MRFL would be very difficult to correct over a zoom range. Conversely, the Keplerian type forms an intermediate pupil, thus it is easier for the Keplerian type to meet the clear aperture constraints and provide a uniform performance over the different zoom range.

The MRFL with the optimized zoom probe is shown in Figure 5.5. As discussed in the previous sections, two tunable lens groups form a Keplerian telescope which is capable of continuous zooming and autofocusing. Besides the tunable lenses, all other lenses in the zoom probe are off-the-shelf lenses from Edmund Optics and Ross Optical. In The first tunable group, the plano-convex lens is used to reduce the beam size, because the clear aperture of the tunable lens is 10mm in diameter. The plano-concave lens adds the adequate optical power to the first tunable group and corrects the spherical aberration to some extent. In the second tunable group, a doublet with a strong middle surface is applied near the relayed pupil location, in order to correct the chromatic aberration and sphero-chromatism. In the imaging lens group, a plano-concave lens and a plano-convex lens were used to correct the field curvature and astigmatism.

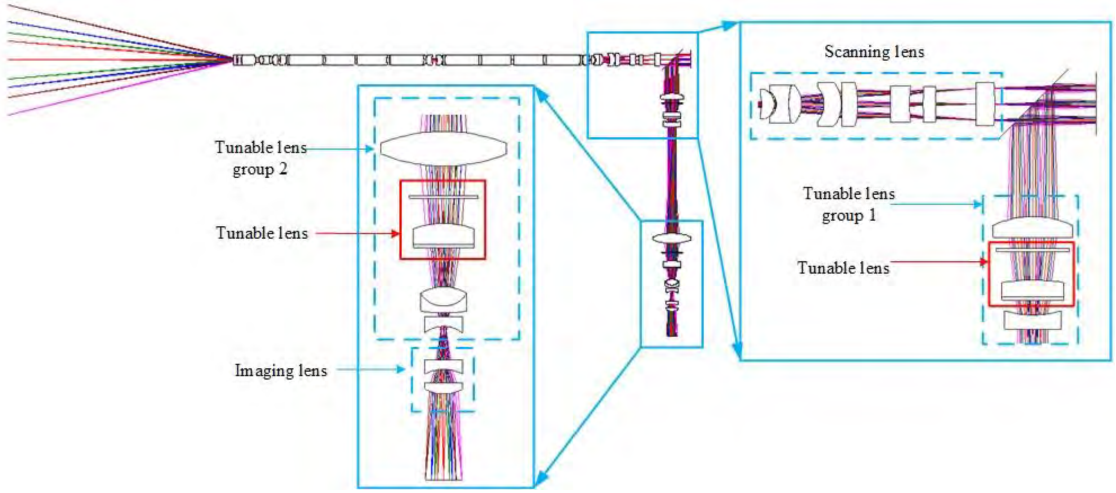

Figure 5.5 high-magnification zoom probe layout

The MTF performance of the zoom probe is demonstrated in Figure 5.6, where Figure 5.6(a) shows the MTF of the center FOV of 3× zoom, Figure 5.6(b) summarizes the MTF across the zoom and scan range. Each line is the average MTF of a specific zoom and scan value. As indicated by the figure, all the fields and zooms have a similar near-diffraction limited performance.

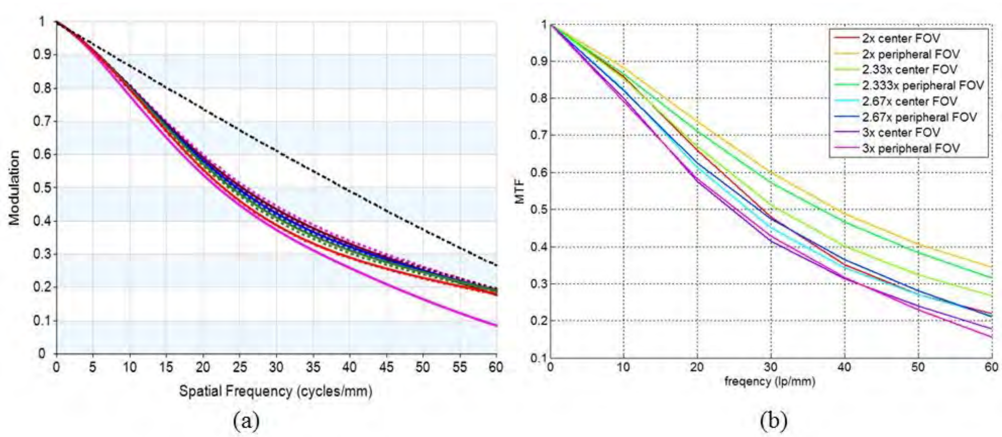

Figure 5.6 MTF performance of the high-magnification zoom probe

The 3D model of the zoom MRFL is shown in Figure 5.7. The zoom probe is mounted by the cage system from Edmund Optics, and all the lens mounts are 3D printed by QuickParts using stereolithography. The lenses are UV cured with the 3D printed lens mounts. The total cost of the zoom probe is less than $1500, because all the components including the optics are off-the-shelf-components. For comparison, we quoted another design with all customized lenses, and it cost about $10,000 and the delivery time was more than 1 month. In the next section, the performance of the zoom probe will be demonstrated. Moreover it also demonstrates the capability of off-the-shelf lenses to build high quality optical system.

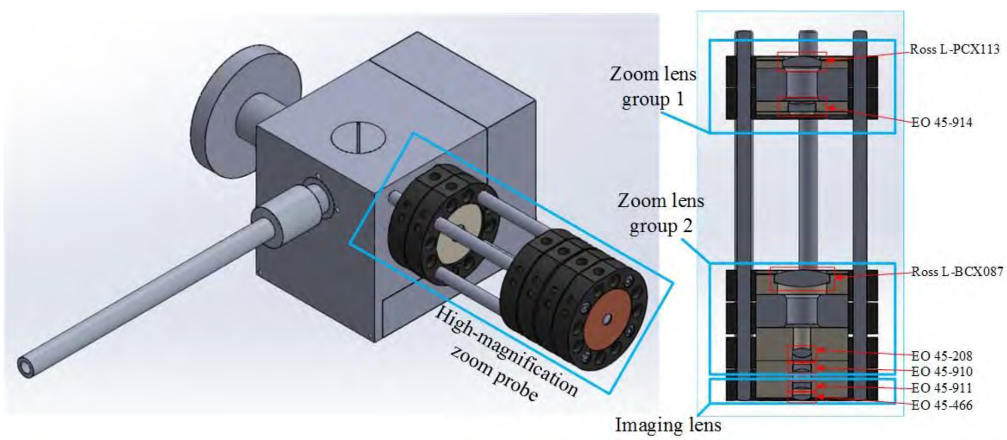

Figure 5.7 3D model of the zoom MRFL

5.5 Performance evaluation

A US1951 resolution target was used to test the resolution of the zoom probe. The resolution target is located at the optimized 120mm working distance. Figure 5.8 demonstrates the resolution of the zoom probe of different zoom ratios. From Figure 5.8(a) to (d), the zoom ratio changes from 2x to 3x. As shown in the figures, the best resolvable bar images vary from element 3 group 2 (5.04lp/mm) to element 2 group 3 (8.98lp/mm), at the corresponding zoom ratio from 2× to 3×.

Figure 5.9 demonstrates the field of view change of different zoom ratios. A bladder model is used as the object, and is placed at 120mm working distance. Figure 5.9(a) to (d) shows the different field coverage of different zoom ratios from 2× to 3×. To be noted, as the field coverage changes when varying the optical magnification of the zoom probe, the bladder model is always in focus.

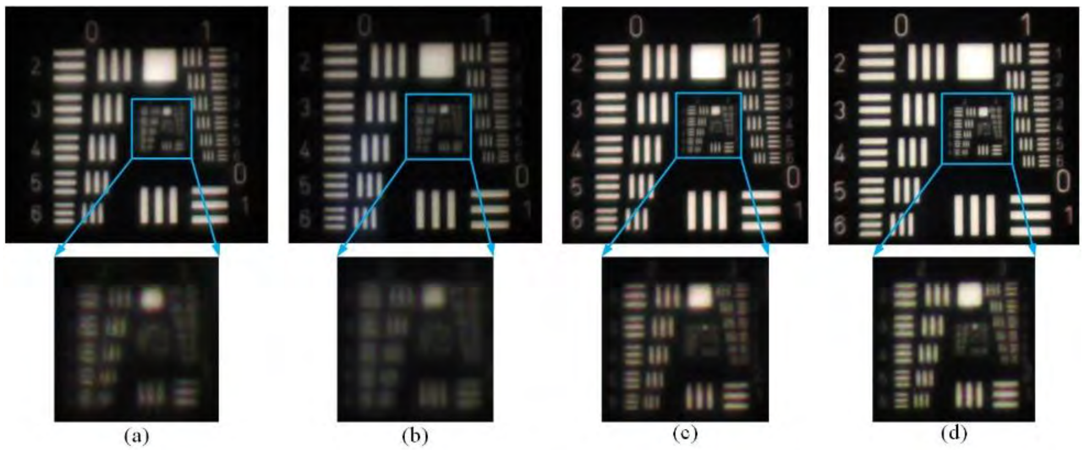

Figure 5.8 Images of US1951 resolution target at different zoom ratio: (a) 2×; (b) 2.33×; (c) 2.67×; (d) 3×.

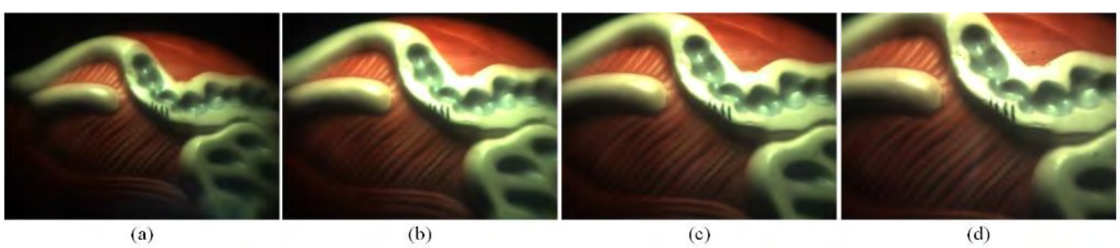

Figure 5.9 Images of the gallbladder model at different zoom ratio: (a) 2×; (b) 2.33×; (c) 2.67×; (d) 3×

6 CONCLUSION AND FUGURE WORK

6.1 Conclusion

In this dissertation, a multi-resolution foveated laparoscope was proposed to address the limitations of the current laparoscopes, such as situational awareness issue, FOV-resolution tradeoff, instruments conflict and ergonomic conflict. It has great potential in improving the safety and efficiency of the laparoscopic surgery.

High performance MRFL prototypes were designed and constructed, which is suitable for in-vivo testing in laparoscopic training lab. A high-resolution imaging probe with optical zoom and auto-focusing capabilities were designed and constructed, after collecting feedbacks of the first in-vivo test from the surgeon.

6.2 Future Work

Future work on the multi-resolution foveated laparoscope may include the followings:

(1) Design a compact and robust mechanical housing to integrate the zoom foveated probe to the mutli-resolution foveated laparoscope.

(2) Develop a calibration procedure to calibrate the distortion and scanning mirror accuracy, as well as the magnification error of the zoom foveated probe.

(3) Develop and compare the efficiency of different display modes for the laparoscopic training lab.

REFERENCES

1. A. Cuschieri (1991), “Minimal access surgery and the future of interventional laparoscopy,” Am J Surg 161: 404–407.
2. Nelson, L.J. (2007) “Cystoscopes Push Imaging Boundaries”. Advanced Imaging.
3. Hyun-Joon Shin, Mark C. Pierce, Daesung Lee, Hyejun Ra, Olav Solgaard, and Rebecca Richards-Kortum, “Fiber-optic confocal microscope using a MEMS scanner and miniature objective lens,” Opt. Express 15, 9113-9122 (2007)
4. A. S. Haka, K. E. Shafer-Peltier, M. Fitzmaurice, J. Crowe, R. R.Dasari, and M. S. Feld, “Diagnosing breast cancer by using Raman spectroscopy,” Proc. Natl. Acad. Sci. U.S.A. 102, 12371–12376 2005.
5. J. Heemskerk, R. Zandbergen, J. G. Maessen, J. W. M. Greve, and N. D. Bouvy, “Advantages of advanced laparoscopic systems,” Surg. Endosc. 20(5), 730–733 (2006).
6. Beger HG, Schwarz A, Bergmann U. Progress in gastrointestinal tract surgery: the impact of gastrointestinal endoscopy.Surg Endosc 2003;17:342-50.
7. So JB, Chiong EC, Chiong E, Cheah WK, Lomanto D, Goh P, Kum CK. Laparoscopic appendectomy for perforated appendicitis. World J Surg 2002;26:1485-8.
8. Rassweiler J, Seemann O, Schulze M, Teber D, Hatzinger M, Frede T. Laparoscopic versus open radical prostatectomy: a comparative study at a single institution. J Urol 2003;169:1689-93.
9. Heemskerk J. Zandbergen R. Maessen JG. Greve JW. Bouvy ND, “Advantages of advanced laparoscopic systems,” Surgical Endoscopy. 20(5):730-3, May 2006.

10. Pierre SA. et al. “High definition laparoscopy: objective assessment of performance characteristics and comparison with standard laparoscopy,” Journal of Endourology. 23(3):523-8, Mar 2009.

11. Canes D. Desai MM. Aron M. Haber GP. Goel RK. Stein RJ. Kaouk JH. Gill IS. “Transumbilical singleport surgery: evolution and current status,” European Urology. 54(5):1020-9, Nov. 2008.

12. A. Gumbs, L. Milone, and P. Sinha, “Totally transumbilical laparoscopic cholecystectomy,” J. Gastriointest Surg., 13:533-534, 2009.

13. Rassweiler J. Safi KC. Subotic S. Teber D. Frede T., “Robotics and telesurgery--an update on their position in laparoscopic radical prostatectomy,” Minimally Invasive Therapy & Allied Technologies: 14(2):109-22, 2005

14. P. Swain, R. Austin, K. Bally, and R. Trusty, “Development and testing of a tethered, independent camera for NOTES and single-site laparoscopic procedures,” Surg. Endosc, Feb. 2010.

15. W. Yulu, and K. Laby, “Automated endoscope system for optimal positioning,” Robotics and Computer-Integrated Manufacturing, 13(2):188, June 1997.

16. http://www.freehandsurgeon.com/

17. https://www.stryker.com/

18. F. S. Tsai, D. Johnson, C. S. Francis, S. H. Cho, W. Qiao, A. Arianpour, Y. Mintz, S. Horgan, M. Talamini, and Y. H. Lo, “Fluidic lens laparoscopic zoom camera for minimally invasive surgery,” J. Biomed. Opt. 15(3), 030504 (2010).

19. S. Lee, M. Choi, E. Lee, K. D. Jung, J. H. Chang, and W. Kim, “Zoom lens design using liquid lens for laparoscope,” Opt. Express 21(2), 1751–1761 (2013).

20. B. S. Terry, Z. C. Mills, J. A. Schoen, and M. E. Rentschler, “Single-port-access surgery with a novel magnet camera system,” IEEE Trans. Biomed. Eng. 59(4), 1187–1193 (2012).

21. B. Tamadazte, G. Fiard, J. Long, P. Cinguin, and S. Voros, “Enhanced vision system for laparoscopic surgery,” in proceeding of IEEE conference on Engineering in Medicine and Biology Society (Osaka, Japan, 2013), pp. 5702–5705.

22. Y. Yamauchi, J. Yamashita, Y. Fukui, K. Yokoyama, T. Sekiya, E. Ito, M. Kanai, T. Fukuyo, D. Hashimoto, and H. Iseki, “A dual-view endoscope with image shift,” in proceedings of Computer assisted radiology and surgery (Paris, France, 2002), pp. 183–187.

23. Y. Qin, H. Hua, and M. Nguyen, “Multiresolution foveated laparoscope with high resolvability,” Opt. Lett. 38(13), 2191–2193 (2013).

24. Yi Qin, Hong Hua, and Mike Nguyen, "Characterization and in-vivo evaluation of a multi-resolution foveated laparoscope for minimally invasive surgery," Biomed. Opt. Express 5, 2548-2562 (2014).

25. http://www.laparoscopyhospital.com/

26. http://kolachalamsurgery.com/office-visit/laparoscopic-procedure

27. http://www.weightlosscenterar.com/bariatric-procedures/single-incision-laparoscopic-surgery.php

28. Vic Valanovich, “Laparoscopic vs open surgery: a preliminary comparison of quality-of-life outcomes,” Surg Endosc. 2000 Jan;14(1):16-21.

29. Patrick J. O'Regan and Dawn L. Anderson, "Laparoscopy in General Surgery The pros and cons of endoscopic surgery," Can Fam Physician. 1992 Jul; 38: 1661–1665.

30. H. Xin, J.S. Zelek, H. Carnahan, "Laparoscopic surgery, perceptual limitations and force: A review," First Canadian Student Conference on Biomedical Computing; Kingston, Ontario, Canada. 2006. No. 144.

31. Andrew I. Brill, Joseph R. Feste, Trudy L. Hamilton, Antonios P. Tsarouhas, Scott R. Berglund, Joseph B. Petelin, and Paul G. Perantinides, "Patient Safety During Laparoscopic Monopolar Electrosurgery - Principles and Guidelines," Journal of the Society of Laparoendoscopic Surgeons, 1998 Jul-Sep; 2(3): 221–225.

32. Fuchshuber, Pascal et al. "Ensuring Safety in the Operating Room – The 'Fundamental Use of Surgical Energy' (FUSE) Program." International anesthesiology clinics 51.4 (2013): 65–80. PMC. Web. 16 Nov. 2015.

33. Mark A. Talamini, "Fundamental use of surgical energy (FUSE)," Surgical Endoscopy September 2013, Volume 27, Issue 9, pp 3055-3055.

34. Miranda CS, Carvajal AR. Complications of Operative Gynecological Laparoscopy. JSLS : Journal of the Society of Laparoendoscopic Surgeons. 2003;7(1):53-58.

35. Alkatout, Ibrahim et al. "Principles and Safety Measures of Electrosurgery in Laparoscopy." JSLS : Journal of the Society of Laparoendoscopic Surgeons 16.1 (2012): 130–139. PMC. Web. 16 Nov. 2015.

36. Jon I Einarsson, Tiffany R Jackson, "Single-incision laparoscopic myomectomy," Journal of Minimal Access Surgery, Vol. 7, No. 1, January-March, 2011, pp. 83-86.

37. Solomon D, Shariff AH, Silasi DA, Duffy AJ, Bell RL, Roberts KE, "Transvaginal cholecystectomy versus single-incision laparoscopic cholecystectomy versus four-port laparoscopic cholecystectomy: a prospective cohort study," Surg Endosc. 2012 Oct;26(10):2823-7. Epub 2012 May 2.

38. Chamberlain RS, Sakpal SV, "A comprehensive review of single-incision laparoscopic surgery (SILS) and natural orifice transluminal endoscopic surgery (NOTES) techniques for cholecystectomy," J Gastrointest Surg. 2009 Sep;13(9):1733-40. doi: 10.1007/s11605-009-0902-y. Epub 2009 May 2.

39. Wagner AA. Varkarakis IM. Link RE. Sullivan W. Su LM "Comparison of surgical performance during laparoscopic radical prostatectomy of two robotic camera holders, EndoAssist and AESOP: a pilot study". Urology. 68(1):70-4, Jul. 2006

40. Comparative study of human and robotic camera control in laparoscopic biliary and colon surgery. Proske JM. Dagher I. Franco D. Journal of Laparoendoscopic & Advanced Surgical Techniques. Part A. 14(6):345-8, 2004 Dec.

41. www.karlstorz.com

42. http://medical.olympusamerica.com/

APPENDIX A: Multiresolution foveated laparoscope

Yi Qin, Hong Hua and Mike Nguyen

This paper was published in Optics Letters, vol. 38, no.13, pp. 2191-2193, 2013

Multiresolution foveated laparoscope with high resolvability

Yi Qin,[1] Hong Hua,[1,*] and Mike Nguyen[2]

[1]3D Visualization and Imaging Systems Laboratory, College of Optical Sciences, University of Arizona, 1630 East University Boulevard, Tucson, Arizona 85721, USA

[2]Department of Surgery, University of Arizona, 1501 N. Campbell Ave., Tucson, Arizona 85724, USA

*Corresponding author: hhua@optics.arizona.edu

Received March 11, 2013; accepted May 8, 2013;
posted May 21, 2013 (Doc. ID 186712); published June 19, 2013

A key limitation of the state-of-the-art laparoscopes for minimally invasive surgery is the tradeoff between the field of view and spatial resolution in a single-view camera system. As such, surgical procedures are usually performed at a zoomed-in view, which limits the surgeon's ability to see much outside the immediate focus of interest and causes a situational awareness challenge. We proposed a multiresolution foveated laparoscope (MRFL) aiming to address this limitation. The MRFL is able to simultaneously capture wide-angle overview and high-resolution images in real time; it can scan and engage the high-resolution images to any subregion of the entire surgical field in analogy to the fovea of human eye. The MRFL is able to render equivalently 10 million pixel resolution with a low data bandwidth requirement. The system has a large working distance (WD) from 80 to 180 mm. The spatial resolvability is about 45 μm in the object space at an 80 mm WD, while the resolvability of a conventional laparoscope is about 250 μm at a typically 50 mm surgical distance.

OCIS codes: (170.2150) Endoscopic imaging; (170.3880) Medical and biological imaging; (170.3890) Medical optics instrumentation; (220.0220) Optical design and fabrication.
http://dx.doi.org/10.1364/OL.38.002191

Laparoscopes have been widely adopted for many clinical applications, especially in minimally invasive surgery (MIS). The state-of-the-art laparoscopic technologies, however, have several limitations [1]. First of all, the major limitation is a tradeoff between the spatial resolution and the field of view (FOV) [2]. With the state-of-the-art laparoscopes, to see fine details of a narrow surgical field, surgical procedures are usually performed at a zoomed-in view, where the laparoscope is used at a short working distance (WD), typically less than 50 mm. A highly zoomed-in view leads to the loss of peripheral vision and awareness of situations occurring outside the immediate focus area of the laparoscope, which may cause fatal problems in some extreme cases such as unawareness of excessive bleeding. This limitation is clinically addressed by manually moving the entire laparoscope in and out of the camera port to obtain either close-up views or wide-angle overviews. A trained assistant is required for maneuvering the camera.

Second, the practice of frequently maneuvering the camera by a trained assistant introduces ergonomic conflicts between the surgeon and the assistant. Robotically assisted systems have been developed to eliminate the need for a human camera holder. However, delays in task performance are reported due to errors in voice recognition or robotic control of camera speed, and also significant practice is required to become efficient with setup and use [3]. The ergonomic conflict is aggravated with the increasingly popular single port access (SPA) technique. Port-grouping in SPA procedures raises a number of problems. One of the most significant aspects is the limited spacing. It has been suggested that varying the magnification of the laparoscope and making it a low profile can reduce the effect of crowding [4].

Several technologies have been developed and applied to laparoscopes to alleviate the FOV-resolution tradeoff. For instance, digital zoom is a common technique adopted for effectively changing the FOV coverage, but it does not improve the optical resolution. The foveated lens design technique [5] extends the FOV by introducing a large amount of distortion to the peripheral field, which leads to much lower spatial resolvability of the peripheral field than that of the central field. The fluidic lens laparoscopic zoom camera [6] has a small volume and a long WD and can vary its FOV. It may effectively reduce the effect of ergonomic conflicts, but it is not able to simultaneously capture wide-angle and zoomed-in views. The dual-view endoscope system [7] offers the ability to capture both wide-angle and zoomed-in views simultaneously, but the system is limited by the low resolution and low light throughput.

We proposed a multiresolution foveated laparoscope (MRFL), which has the potential to make MIS procedures more efficient and safer. The conceptual system layout is shown in Fig. 1. The MRFL is able to simultaneously acquire both wide-angle overview and high-resolution zoomed-in images of a surgical area integrated through shared objective and relay lenses. A dual-view MRFL prototype was designed and implemented, of which the wide-angle probe captures an 80° FOV for situational awareness and the high-resolution probe covers a 26° FOV of interest with as high as 45 μm resolution in the object space for accurate procedures. The high-resolution probe can be engaged at any subfield of the entire surgical

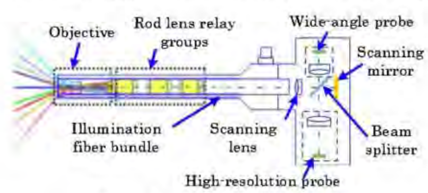

Fig. 1. Conceptual system layout.

0146-9592/13/132191-03$15.00/0

field in real time by using a 2D scanner. The MRFL prototype system equivalently yields a resolution of more than 10 million pixels with two HD image sensors. The optical system was designed so that a standard 10 mm diameter package was adapted for housing the objective and relay groups along with illumination fibers, which facilitates the rapid adoption of the developed technology for clinical use. Additionally, the prototype system was optimized for a long WD from 80 to 180 mm. It was further designed to achieve flexible length profiles, a normal profile for a standard multiport procedure, and a low profile for SPA procedures, by allowing a reconfigurable number of relay groups. Benefiting from the long WD, a low-profile MRFL system can be mounted at a fixed pose through a camera port and can potentially reduce the conflicts with other surgical instruments and reduce the need for additional incisions and thus cut down on scarring and healing time.

The optical layout of the MRFL system is shown in Fig. 2. It consists of a shared $f/2.5$ objective lens group, multiple shared relay lens groups, a scanning lens group, a wide-angle imaging probe, and a high-resolution foveated imaging probe. To fit the standard 10 mm diameter package, the diameters of the objective lens and the rod lens relay groups need to be less than 5.7 mm. The objective lens captures the entire 80° FOV with a diffraction-limited performance. It was designed to be telecentric in image space. The relay lens groups were designed to be telecentric in both object and image space, and each relay group works at a magnification of −1. The telecentricity of the objective and relay groups enables a flexible number of relay lens groups of limited diameter to be concatenated, without noticeable degradation of image quality, to create laparoscopes of different length profiles. To reduce fabrication cost, each of the relay groups was designed to be identical, and the left and right portions within each relay group are symmetric.

The scanning lens group works like an eyepiece with a 2D scanning mirror placed at the exit pupil. A polarizing beam splitter (PBS) along with a quarter-wave plate is inserted between the scanning lens and the mirror for splitting the light paths for the wide-angle and high-resolution probes. The PBS directs the s-polarized light into the wide-angle imaging probe and p-polarized light into the high-resolution imaging probe. Although a PBS and a quarter-wave plate were used to improve the light efficiency, compared to a standard single-view laparoscope, only half of the collected light goes into the high-resolution probe, and the other half goes into the wide-angle probe. The anticipated light-splitting effect

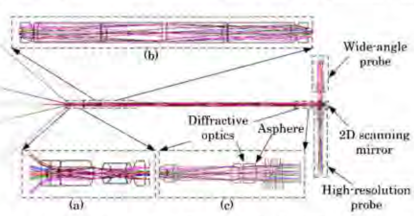

Fig. 2. System layout of MRFL: (a) objective lens group, (b) one relay lens group, and (c) scanning lens group.

was compensated for by the fact that the F/2.5 objective lens has twice as much light collection capability as a standard F/4 objective lens. Moreover, the lower F-number objective lens provides better resolution.

The optical system design of the MRFL system was quite challenging due to the limited lens diameter, large FOV, telecentric requirements, and low F number. The objective lens was designed to have a focal length, f_{obj}, of 2 mm and have diffraction-limited performance with 17% distortion. The length of each relay group is 80 mm. Each group has a symmetric configuration to take advantage of the fact that the odd-order aberrations such as distortion, coma, and lateral chromatic aberration are canceled out. Each group was well optimized with diffraction-limited performance so that the image quality will not degrade much when the number of relay groups increases.

The scanning lens group requires a long exit pupil distance (EPD) to accommodate for the PBS and wave plate. The focal length of the scanning lens, f_{scan}, is 14 mm, while the EPD is 16 mm. However, one problem is that as the number of relay groups increases, the spherical aberration and the longitudinal chromatic aberrations accumulate. In order to correct those accumulated aberrations through multiple relay groups, we apply a diamond-turned plastic hybrid lens in the scanning lens group. One surface of the plastic lens has a diffractive optical element (DOE), and the other surface is aspheric. The DOE has the opposite dispersion compared to the refractive lens, so that the longitudinal chromatic aberrations can be balanced. The aspheric surface corrects the higher-order aberrations. The plastic lens was placed near the intermediate pupil to effectively balance those accumulated aberrations.

Both the wide-angle and high-resolution imaging probes use simple optics. The wide-angle probe consists of a doublet and a field lens, and the high-resolution probe has two singlets and a field lens. The focal length of the wide-angle imaging probe is 30 mm, while that of the high-resolution imaging probe, $f_{high\text{-}res}$, is 90 mm.

By controlling the tilting angle of the scanning mirror, the high-resolution probe can be engaged to any subfield of the entire surgical area. Assuming the high-resolution probe is aiming at $\theta°$ in the entire FOV, the tilting angle of the scanning mirror, $\beta°$, is given by

$$\beta = 0.5 \times (f_{obj}/f_{scan}) \times \theta. \qquad (1)$$

In our prototype design, the maximum tilting angle required is 1.9° to cover the full FOV. A motorized gimbal mirror mount (Zaber T-OMG Series) was used, which has a tilting range of ±7°, a maximum speed of 7°/s, and a minimal scanning step of 0.0001°. The mirror enables the ability to scan across the entire surgical field in less than 0.4 s and to fix the position of the high-resolution probe with an accuracy of 0.097 mm.

The MRFL was optimized at the WD of 120 mm with a depth of field from 80 to 180 mm. The corresponding surgical field is about 80 mm × 60 mm at an 80 mm WD and 240 mm × 180 mm at 180 mm distance, respectively. For the high-resolution probe, of which the FOV is 1/3 of that of the wide-angle probe, the visual surgical

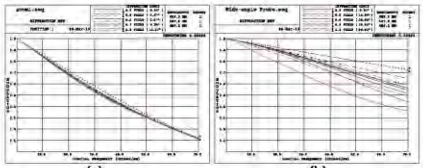

(a) (b)

Fig. 3. (a) MTF of high-resolution probe when $\beta = 0°$ and (b) MTF of wide-angle probe.

field is 27 mm × 20 mm at an 80 mm WD and 80 mm × 60 mm at a 180 mm WD.

In the prototype we used 1/3" color CCD sensors (PointGrey DragonFly2 DR2-13S2C-CS) for both imaging probes. The pixel resolution of the sensors is 1280 × 960, and the color pixel size is 7.5 μm × 7.5 μm. The spatial resolvability of the high-resolution probe is given by

$$D = 7.5um/(m_{\text{high-res}} \times m_{\text{obj}}). \quad (2)$$

where m_{obj} and $m_{\text{high-res}}$ are the magnifications of the objective lens and the high-resolution imaging probe, respectively. At a giving WD, L, they are calculated by $m_{\text{obj}} = -f_{\text{obj}}/L$ and $m_{\text{high-res}}/f_{\text{scan}}$, respectively. The spatial resolvability of the high-resolution probe is 46.67, 70, and 105 μm, corresponding to a spatial frequency of 10.7, 7.1, and 4.8 lps/mm, at a WD of 80, 120, and 180 mm, respectively.

The MTF curves of the wide-angle and the high-resolution imaging probes at 120 mm WD are shown in Fig 3. For both imaging probes, the image contrast is larger than 0.15 at 66 lp/mm, which corresponds to the cutoff frequency of the image sensors in the image space. The high-resolution probe has the same diffraction-limited performance when $\beta = 1.9°$.

Figure 4(a) shows the system prototype. The normal profile package has four relay groups, and the low-profile package has two relay groups. Figure 4(b) shows an image captured by the wide-angle probe with an abdominal cavity model placed at a 120 mm WD. The size of the model is 160 mm × 120 mm. Figure 5 shows a preliminary test result captured by the high-resolution probe with a US1951 resolution target placed at an 80 mm WD. Group 3 element 3 can be resolved, which corresponds to 10.10 lps/mm in object space (bar width 49.5 μm). A display interface is designed so that the high-resolution image can be embedded into the wide-angle image, in analog to the fovea of the human eye.

The MRFL system has superb optical quality and field coverage compared with a conventional laparoscope. Assuming a typical 70° FOV and 50 mm WD, the corresponding visible area of a conventional laparoscope is only 56 mm × 42 mm with a spatial resolvability of about 2 lps/mm in the object space. With the MRFL at an 80 mm WD, the surgical area by the wide-angle probe is about two times that of the conventional one. More prominently, the resolvability of the high-resolution probe is more than 10 lps/mm in the object space, which is five times that of the conventional one. With the MRFL at an 180 mm WD, the area covered by the wide-angle probe is more than 18 times that of the conventional laparoscope, while the area covered by the high-resolution scope is twice that of the conventional one. The resolvability of the high-resolution probe in the object space is 4 lps/mm, which is twice as good as that of the conventional one

(a) (b)

Fig. 4. (a) MRFL prototype and (b) wide-angle image of an abdominal cavity 120 mm away from the MRFL.

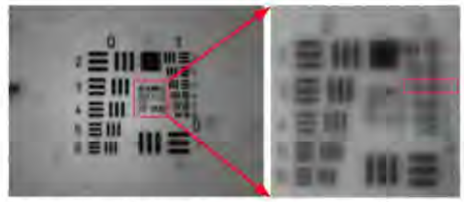

Fig. 5. High-resolution image at 80 mm WD.

In conclusion, we developed an MRFL that can provide both wide-angle and high-resolution images of a surgical area. With this foveated and multiresolution capability, this device is anticipated to provide surgeons good situational awareness and better resolution during laparoscopic surgeries; thus it can help provide better and safer surgeries for patients. The device is able to equivalently render 10 million pixel resolution (9 × 1280 × 960) by using only two HD (1280 × 960) cameras. Compared to the use of a superresolution camera, the MRFL system can save much bandwidth and have a faster frame rate, which is required in laparoscopic surgery. Moreover, the MRFL can reduce the space limitation in SPA procedures. The system will be tested under animal models.

This work is funded by National Institutes of Health Grant Award R21EB013370.

References

1. S. Pierre, M. Ferrandino, W. Simmons, C. Fernandez, P. Zhong, D. Albala, and G. Preminger, J. Endourol. **23**, 523 (2009).
2. J. Heemskerk, R. Zandbergen, J. Maessen, J. Greve, and N. D. Bouvy, Surg. Endosc. **20**, 730 (2006).
3. A. Wagner, I. Varkarakis, R. Link, W. Sullivan, and L. Su, Urology **68**, 70 (2006).
4. D. Canes, M. Desai, M. Aron, G. Haber, R. Goel, R. Stein, J. Kaouk, and I. Gill, Eur. Urol. **54**, 1020 (2008).
5. H. Nathan and S. T. Tomasz, J. Biomed. Opt. **17**, 021104 (2012).
6. F. Tsai, D. Johnson, C. Francis, S. Cho, W. Qiao, A. Arianpour, Y. Mintz, S. Horgan, M. Talamini, and Y. Lo, J. Biomed. Opt. **15**, 030504 (2010).
7. T. Sekiya, E. Ito, M. Kanai, and M. Matsumoto, Proc. SPIE **6080**, 60800E (2006).

APPENDIX B: Optical design and system engineering of a multi-resolution foveated laparoscope

Yi Qin and Hong Hua

This paper will be submitted to Applied Optics for review.

Optical design and system engineering of a multi-resolution foveated laparoscope

Yi Qin, Hong Hua*

3D Visualization and Imaging System Lab, College of Optical Sciences, University of Arizona, 1630 E University Blvd., Tucson, AZ, USA, 85721

**Email: hhua@optics.arizona.edu*

The tradeoff between the spatial resolution and field of view is one major limiting factor for the-state-of-the-art laparoscopes. In order to address this limitation, we demonstrated a multi-resolution foveated laparoscope (MRFL) which is capable of simultaneously capturing both a wide-angle overview for situational awareness and a high-resolution zoomed-in view for accurate surgical operation. In this paper we focus on presenting the optical design and system engineering process for developing the MRFL prototype. More specifically, the first order specifications and properties of the optical system are discussed, followed by a detail discussion on the optical design strategy and procedures of each sub system. The optical performance of the final system, including diffraction efficiency, tolerance analysis, stray light and ghost image, is fully analyzed. Finally, the prototype assembly process and the final prototype are demonstrated.

OCIS codes: *(080.2740) Geometric optical design; (170.2150) Endoscopic imaging; (170.3880) Medical and biological imaging; (220.1000) Aberration compensation; (220.0220) Optical design and fabrication.*

1. Introduction

Laparoscopes, which provide surgeons with the vision of the surgical field inside a human body, have been playing important roles in modern minimally invasive surgeries (MIS). The performance and quality of the laparoscope directly affect the surgical outcome. The state-of-the-art laparoscope suffers a number of major limitations, one of which is the tradeoff of the limited instantaneous field of view (FOV) for high spatial resolution versus the wide FOV but diminished resolution [1]. It is unable to acquire both the high-resolution and the wide-angle images simultaneously. This limitation raises a series of problems such as situational awareness issue, ergonomic conflict, instruments collision [2, 3]. Although the zoom camera head [www.stryker.com] and other new laparoscope technologies [4, 5] have been developed to improve the laparoscopic surgery by changing the optical magnification or viewing directions, they still cannot capture both a wide angle view and a high resolution view simultaneously.

Aiming to address those limitations, we proposed a multi-resolution foveated laparoscope (MRFL), which is able to capture a wide-angle overview as well as a high-magnification zoomed-in view simultaneously [6]. The characterization and in-vivo evaluation of the MRFL prototype has been demonstrated [7]. In summary, an MRFL has two imaging probes, a high-magnification probe and a wide-angle probe, integrated in a compact system. Fig. 1 shows the optical layout of an MRFL prototype with a short length profile. In the front end, the two imaging probes share the objective lens, multiple relay lens groups and the scanning lenses. The objective lens captures an 80° FOV at a nominal 120mm working distance (WD); then the intermediate image is relayed by multiple identical rod relay lens groups to enable flexible length profile (e.g. 2 groups of relay lenses create a low-profile scope with an insertion length about 150mm). The scanning lens group works like an eyepiece and collimates the intermediate image for further imaging. At the far end next to the scanning lens group, a polarizing beamsplitter (PBS) splits the optical path into two polarization states: the reflected s-polarized light for the wide-angle probe and the transmitted p-polarized light for the high-magnification probe. In the transmission path, a two-axis scanning mirror is placed at the pupil conjugate position to steer the imaging field of the high-magnification probe toward a region of interest. A quarter wave plate (QWP) is inserted in front of the scanning mirror with its axis at 45° with respect to the tangential plane. The transmitted p-polarized light becomes s-polarized light after double passing the QWP and reflected by the mirror, and is directed toward the high-magnification probe.

The insertion length of the MRFL is proportional to the number of relay groups. Two prototypes with different insertion lengths were designed and built. The standard length profile MRFL has about 300mm insertion length, which is similar to that of a standard laparoscope, with 4 rod relay groups for a standard multi-port laparoscopic procedure, The short length profile MRFL has an insertion length of 150mm, which can help reduce the conflicts with other surgical instruments and the need for additional incisions, with 2 rod relay groups.

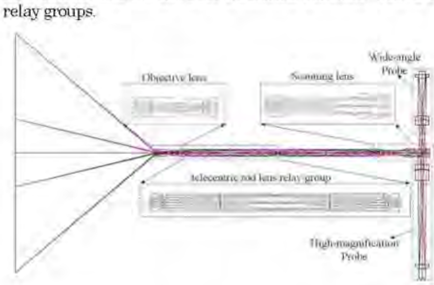

Fig. 1 System layout of a MRFL with low length profile

Compared with a standard laparoscope, the dual-view MRFL has a larger working distance (~120mm) than a standard one (~50mm), which enables the wide-angle probe to capture an 8× larger surgical area. In addition, by designing an optical system with a much larger throughput, the high-magnification probe captures a similar surgical area to a standard laparoscope but with 3× better spatial resolution. Therefore the MRFL can afford the surgeon with a clear vision from the high-magnification probe with finer details, and an overview from the wide-angle probe for situational awareness and preventing misoperation.

While our previous work [6, 7] focused on demonstration of the MRFL system capabilities and its potential clinical applications, this paper will concentrate on the detailed optical design procedure and system engineering challenges, from developing the first-order system specifications and analysis to the optical design strategies and optical system tolerance analysis. The rest of the paper is organized as follows. Section 2 will detail the process of developing the first-order system specifications and properties primarily driven by the clinical applications and choices of key components. Based on these system requirements, Section 3 will present the detailed design strategy and optimization procedure for each sub-optical system including the objective lens group, the relay lens group, the scanning lens group, the wide-angle probe and the high-magnification probe. Section 4 will analyze the key performances of the resulted optical system, including the diffraction analysis of a diffractive optical element used in the design, the tolerance analysis, the stray light and ghost image analysis. The last section will demonstrate the mechanical design and the prototype of the MRFL system.

2. First-Order System Properties and Specifications

Most of the MRFL system specifications were driven by the clinical objectives and requirements to be met through this research development and this section will focus on articulating how the critical system specifications, including FOV, resolution, magnification, light throughput, as well as the optical allocations, were developed through analytical understanding of the clinical requirements.

A standard laparoscope usually has a FOV of 70° and an optimized working distance (WD) of 50mm. At its optimized WD, the visible surgical area is approximately 56×42mm², with a spatial resolution of 2.1 line pairs per millimeter (lp/mm) [8]. The ultimate goal of the MRFL development is to provide the ability to survey a large surgical field for improved situational awareness and to visualize a targeted area in high spatial resolvability for surgical treatment, without having to maneuver the instrument in and out as with a standard laparoscope. More specifically, compared to a standard laparoscope, the wide-angle probe of the MRFL aims to achieve a similar spatial resolution but covers an 8×~9× larger surgical area; and the high-magnification probe aims to provide a 3× better spatial resolution and a similar surgical area. Based on these clinical requirements, the overall system is specified to have a working distance of 120mm, an angular FOV of 80° for the wide-angle probe, and a 26° FOV for the high-magnification probe, which is about 1/3 of the wide-angle FOV. As a result, the wide-angle probe captures a surgical area of 160×120mm², while the high-magnification probe captures a surgical area of 53×40mm² which is similar to a standard laparoscope.

The resolution of a laparoscope is determined by two factors, one is the ratio between the entrance pupil diameter and the working distance (WD) of the objective lens, and the other is the pixel size of the imaging sensor. In order to achieve a 3× better spatial resolution (at least 6lp/mm in the objective space) for the high-magnification probe than a standard laparoscope, the entrance pupil diameter (EPD) of the objective lens is set to be 0.8mm. The cutoff frequency in the object space can be calculated by Eq. (1)

$$f_{cutoff} = \frac{1}{\lambda \times F/\#} = \frac{EPD}{\lambda \times WD} = \frac{0.8mm}{0.55um \times 120mm} = 12.12lp/mm \tag{1}$$

With the cutoff frequency of 12lp/mm in the object space, we anticipate high image contrast at the desired resolution of 6lp/mm. It is worth noting that the EPD of a standard laparoscope is less than 0.3mm, which suggests that the MRFL with a 0.8mm EPD has 7× more light collection capability than a standard laparoscope. Such a large throughput will make the optical system design quite challenging.

In the prototype, two 1/3" imaging sensors (Pointgrey DragonFly II 1280×960 pixels) are used for both imaging probes. The diagonal size of the sensor is 6mm with a pixel size of 3.75um, which yields a sampling frequency of 133.3lp/mm in the image space. Based on the combination of system and sensor specifications, the transvers magnification, the image-space working F/#, and the image-space cutoff frequency of the high-magnification probe are calculated according to Eqs. (2), (3), and (4). The resulting image-space cut-off frequency of 114.9 lp/mm is slightly lower than that of the sensor actual sampling frequency, which suggest that the high-magnification probe is limited by the optical system rather than sampling. In order to achieve the desired 6lp/mm resolution in object space, the optical system will be optimized and evaluated for the performance of 60lp/mm in the image space for the rest of sections.

$$\left| m_{high-mag} \right| = \frac{h_{sensor}}{WD \times \tan(HFOV/3)} = \frac{6/2}{120 \times \left(\tan 40^{\circ}/3\right)} = 0.1055 \tag{2}$$

$$F/\#_{w} = WD/\mathrm{EPD} \times \left| m_{high-mag} \right| = 120/0.8 \times 0.1055 = F/15.82 \tag{3}$$

$$f_{cutoff} = \frac{1}{\lambda F/\#_{w}} = 114.9lp/mm \tag{4}$$

The focal length and numerical aperture (NA) of the objective lens is another important parameter to determine at the early design stage. In the MRFL system design, these parameters are strictly constrained by the maximally allowable lens diameter in order to meet the requirement for a standard 10mm diameter package for housing the objective and relay lens groups as well as the illumination fibers. We adopted a standard laparoscope packaging from Precision Optical Cooperation which dictates the maximum lens diameter to be 5.6mm. In addition, the objective lens is required to be telecentric in the image space, thus the image quality won't degrade after multiple relay groups. By considering all these constraints, the focal length of the objective lens is specified to be 2mm, resulting in an image-space NA of 0.2. Using first-order optics, the diameter of the objective lens group is 4.16mm, which meets the lens diameter requirement and be fit into the laparoscope tube.

The objective lens group is followed by multiple sets of identical relay lens groups. Most patented relay lens for laparoscope has a numerical aperture (NA) of 0.1 and a total length less than 45mm [9, 10]. In the MRFL system design, in order to reduce the total cost as well assembly challenges, we aimed to push the length of each relay group to be larger than 80mm so that only 2 sets of relays are needed for the low profile MRFL and 4 sets of relays for the standard profile MRFL. Since the relay lens is used to relay the intermediate image formed by the objective lens, its object height should match the image height of the objective lens; its entrance pupil should match the exit pupil of the objective lens, and its NA should also match the 0.2 NA of the objective lens. Such a substantially larger NA and longer profile length than relays used in standard laparoscopes add another level of challenge to the overall optical system design.

Following the relay lenses is the scanning lens group which not only serves the function of a common eyepiece used in standard laparoscope but also relays the pupil onto the 2D scanning mirror for the high-magnification imaging probe. Due to the insertion of a PBS between the scanning lens and the mirror, a large pupil clearance is required. After a preliminary trade study to balance the requirements for space, performance, and overall compactness, a 14mm focal length was selected for the scanning lens group.

Finally, the focal lengths of the wide-angle and high-magnification imaging lenses are determined according to the specifications of the overall system as well as the objective, relay and scanning lens groups. As a result, the focal length of the wide-angle probe is set to be 30mm, while the focal length of the high-magnification probe is set to be 90mm to achieve 3× magnification over the wide-angle probe. Table 1 summarizes the first order properties and the specifications of the MRFL.

Table 1 Specifications of the MRFL

MRFL	
FOV	80°
Working distance	120mm
Wide-angle probe	
Field coverage	160×120mm^2
Spatial resolution	2lp/mm
Working F/#	F/5.3
High-magnification probe	
Field coverage	53×40mm^2
Spatial resolution	6lp/mm
Working F/#	F/15.8

3. Design strategy and optimization procedure

As discussed in the previous sections, the optical design of the MRFL system consists of 5 mutually-dependent sub-systems, including the objective lens group, the telecentric rod relay lens groups, scanning lens groups, high-resolution imaging probe, and the wide-angle imaging probe. A successful optical design of such a complex optical system requires taking into account a wide range of system design constraints and performance requirements. In this section, we mainly focus on our optical design and optimization strategies and the key design procedures.

3.1 Design strategy

Although the optical design of each sub-optical system is well known, the optical design of the MRFL system is a challenging task due to its large throughput, limited lens diameter and the complex interaction among the sub-systems.

Overall, we adopted a "divide and conquer" design strategy illustrated in Fig.2. This strategy enabled us to carry out the optimization of the key lens groups in the MRFL system, including the objective, relay and scanning lenses, in parallel before they were ready to be integrated At the initial design phase, the shared objective lens, relay lens and the scanning lens were designed and optimized separately, which allowed us to find best solutions to the sub-systems by applying our knowledge and experiences with these well-known lens forms, rather than directly venturing into a complex system . Once good designs were found for these sub-systems, the objective lens and the multiple groups of relay lenses were combined for further optimization. In the meanwhile, a well-corrected scanning lens was combined and optimized together with the imaging lens group for the high-magnification probe. Following a good design for a combined objective-relay group, the objective lens, multiple groups of relay lenses, scanning lens and high-magnification probe were integrated and optimized all together. In the last step, by fixing the designs of the objective, relay and scanning lenses, the imaging lens for the wide-angle probe was optimized.

In the process of optimizing the individual sub-systems, aside from accounting for the various performance requirements, we identified the key constraints that must be satisfied in order to meet the optical and mechanical requirements of the integrated system. For instance, strict telecentricity requirement was enforced for the designs of the objective lens as well as the relay lens, which help to ensure minimum amount of image quality degradation when the objective and multiple groups of relay lens were combined.

Choosing a proper starting point for each sub-system is a critical consideration. It can not only achieve better performance, but also reduce the optimization cycles. The objective lens group requires large FOV and large entrance pupil, therefore we selected an inverse telephoto lens type.

For the relay lens group, we chose a symmetric configuration, with each half being a Petzval lens type. Since the magnification of each relay group is -1, a symmetric lens can naturally correct odd order aberrations such as coma and distortion. In addition, Petzval lens type can achieve a good performance for a large numerical aperture and also correct field curvature [10]. The field curvature should be correct at each intermediate images, because the field curvature accumulates as the number of relays increases.

The scanning lens is similar to an eyepiece but with a much larger pupil clearance for the insertion of a PBS and other components. In order to correct the higher order aberrations and axial chromatic aberration accumulated from the multiple relay lenses, an aspheric refractive-diffractive plastic lens is applied in the scanning lens group.

The high-magnification imaging probe and the wide-angle imaging probe are relatively simple compared to the other lens groups. Although the high-magnification probe needs a diffraction limited performance, it only captures 1/9 of the entire surgical area. The wide-angle probe, capturing the entire surgical field, does not require a diffraction limited performance as the sampling frequency of the sensor is much lower than the cutoff frequency of the optical system.

Fig. 2 Illustration of MRFL design process and strategy

3.3 Optimization procedure

3.3.1 Objective Lens

The objective lens captures an 80° FOV and is shared by the wide-angle probe as well as the high-magnification probe. As stated in section 2, it requires a diffraction limited performance. A U.S. patent by Murayama [US 7,379,252 B2] was selected as the starting point, because it is a typical inverse telephoto lens. The F/# of this patent lens is larger than F/6.9, with a FOV of 140°. The throughput of the patent lens is calculated by equation (6).

$$A\Omega = \left(WD \times \tan\left(HFOV\right)\right)^2 \times \pi\left(\tan^{-1}\left(\frac{EPD}{2WD}\right)\right)^2 \tag{6}$$

Our goal is to design an objective lens of F/2.5, with a FOV of 80°. The patent lens has throughput of 0.0347, which is less than the required throughput of 0.3539 of our objective lens. After several initial optimization trials, it was found the lens form was inadequate in correcting spherical aberration and chromatic aberrations. Therefore we decided to add a lens before the stop and a doublet behind the stop. After further optimization, with the constraints on EFL, telecentricity in image space, lens diameter and image clearance, the performance was improved significantly. The lens layout and the polychromatic modulation transfer function (MTF) plots were shown in Fig. 3.

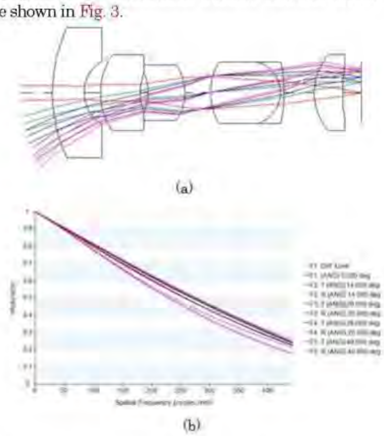

Fig. 3 Intermediate design: (a) layout; (b) MTF performance

One key problem of this objective design, however, is the large image distortion, which is about-24%. Distortion is a field-dependent magnification error, and our MRFL system needs to provide high resolution image of the entire FOV, we constrained the distortion to be less than -17%. Another limitation of this design is the large incident angle on the last lens, which could potentially increase the difficulty of assembling. Therefore, another lens was added to split the power of the last lens. The optimized objective lens is shown in Fig. 4. All the fields have good performance and the chief ray angle of each field on the image plane is less than 0.1°, which indicates the objective lens has great telecentricity in image space.

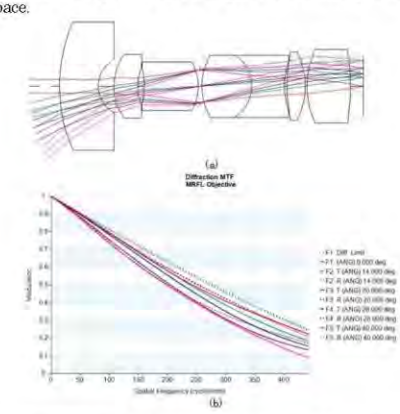

Fig. 4 Improved objective lens: (a) layout; (b) MTF performance

3.3.2 Relay Lens

As described in the design strategy, we chose the Peztval lens type for the half of the relay lens group. In order to increase the length of the relay lens, the doublets were optimized to a rod lens type. Optimization constraints were added on the lens diameter and telecentricity in image space. Fig. 5 shows an initial design of half of one relay group. The OPD plot indicates the main residual aberrations are coma and lateral colors, which will be naturally corrected in a symmetric system.

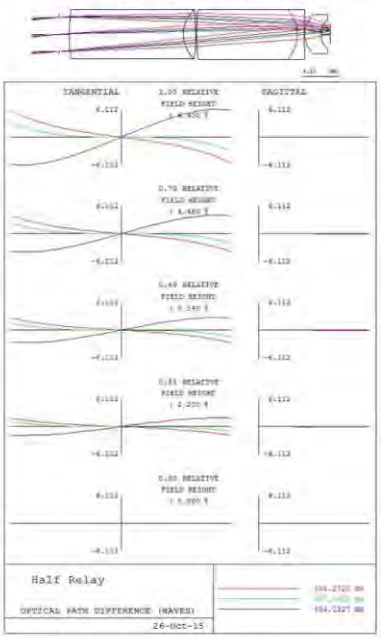

Fig. 5 Starting relay lens: (a) layout; (b) OPD plot

The optimized relay group achieved a diffraction limited performance, as shown in Fig. 6. The total length of the relay is 80mm, with outstanding telecentricity in image space. The angles of incidence of the chief rays of all five sampled fields are constraint to be less than 0.01°, which enables the flexibility of concatenating several groups of the same relay lens to create MRFL systems of different length profile. As shown in Fig. 7, there is no distortion due to the symmetry of the lens structure. The residual high order field curvature will be corrected when optimized together with the objective lens group [10].

One thing to be noted is that due to the long relay length, the refractive indices of all the lenses are larger than 1.58.The relay length can be increased by a factor of n, where n is the index of the rod lens [10,11]. The flint meniscus lenses at both ends are used to correct the field curvature and astigmatism. The indices of the first doublet are close to each other, thus the middle surface can correct the higher order spherical aberrations. The other doublet is a conventional doublet which is composed of a crown and a flint lenses to correct the axial chromatic aberration.

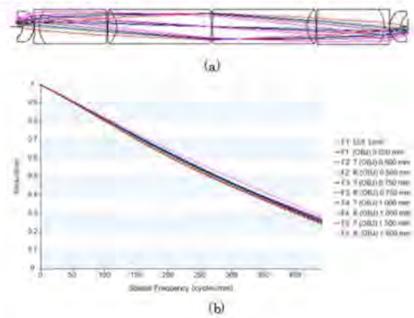

Fig. 6 Optimized relay lens: (a) layout; (b) MTF performance

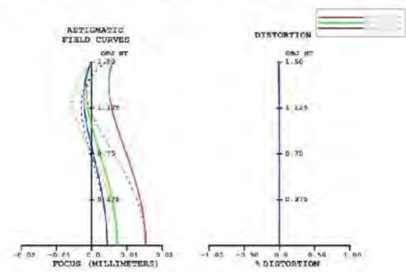

Fig. 7 Field curvature and distortion of the optimized relay lens

3.3 .3 Integration of the Objective and relay lenses

Following the separate design of the objective lens and relay lens with good performance, as suggested in Fig. 2, the objective lens together with the multiple relay lenses are integrated together for further optimization. One problem of the integrated system directly from the designs in Fig. 3 and Fig. 6 was that the accumulated axial chromatic aberration and spherical aberration degraded the performance significantly. As shown in Fig. 8, the MTF performance drops a significant amount, as the number of relay increases. By interpreting the OPD fans shown in Fig. 9, we identify the main residual aberrations are the axial color and sphero-chromatism.

Due to the low F/# and large FOV, it was difficult to compensate these accumulated aberrations from the multiple relay groups by overcorrecting the objective lens. Therefore, we planned to correct them by overcorrecting the scanning lens.

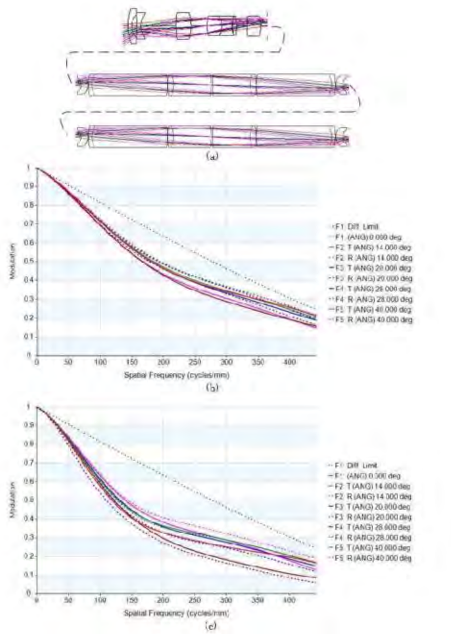

Fig. 8 Objective multiple sets of relays: (a) layout; (b) MTF performance 2 relay groups; (c) MTF performance 4 relay groups.

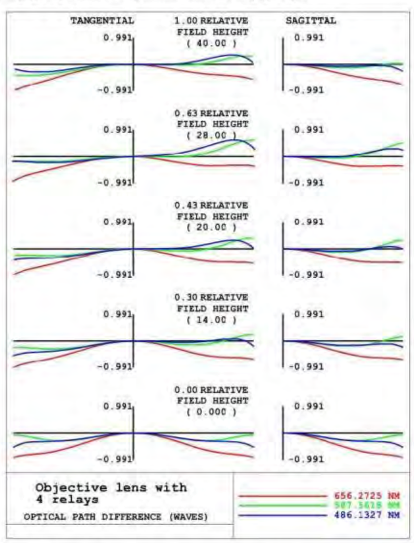

Fig.9 OPD fan of objective lens with 4 sets of relays

3.3.4 Scanning Lens

Two doublets were selected as the starting point for the scanning lens design. A perfect lens model with a focal length of 90mm was used to simulate the high-magnification probe. The initial result is shown in Fig. 10. The second doublet has an air gap which can effectively correct the higher order aberrations. During the optimization, constraints were added on the angle of incidence of the marginal rays to make the light beams well collimated at the stop location. The pupil clearance was also constrained so that a polarization beam splitter can be fit in. The MTF curve indicates its performance is nearly diffraction limited and this design form was chosen as the starting point for further design of the high-magnification probe.

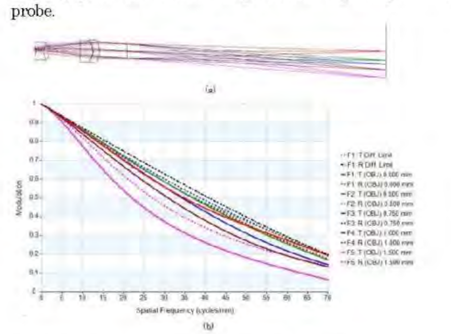

Fig. 10 Initial scanning lens: (a) layout; (b) MTF performance

3.3.5 High-magnification Probe

A triplet was selected for the high-magnification probe as shown in Fig. 11. It was optimized with the scanning lens. The MTF curves of the central FOV and the peripheral FOV show that the high-magnification probe has near diffraction limited performance over the scan range.

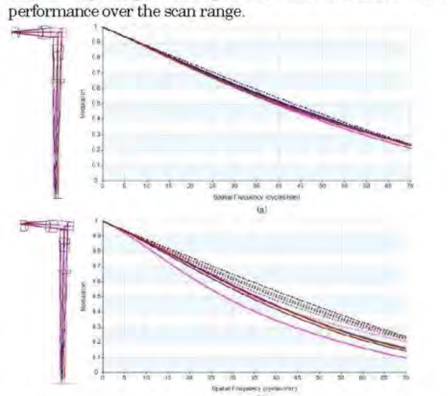

Fig. 11 (a) layout; and MTF performance of central FOV; (b) layout and MTF performance of peripheral FOV.

Although the performance of the high-magnification probe is near diffraction limited, when the objective lens and relay lens groups were added to the system, the performance dropped significantly. The MTF performances of the high-magnification probe with 4 sets of relay are shown in Fig. 12. It was difficult to compensate those residual aberrations by the scanning lens group, so we decided to use a plastic refractive-diffractive hybrid lens to correct them. The diffractive optical element (DOE) has opposite dispersion, and a plastic lens can be manufactured by diamond turning machine, we can take the advantage of aspheric surface to correct the residual aberrations [12].

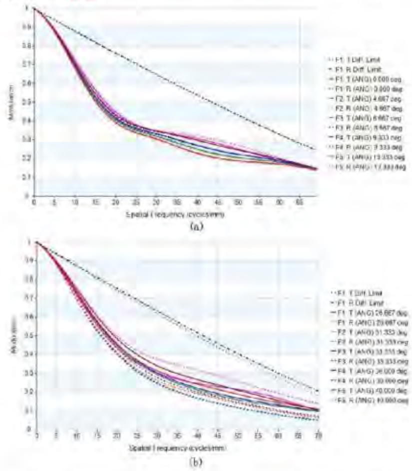

Fig. 12 MTF performance of high-magnification probe with 4 sets of relays: (a) central FOV; (b) peripheral FOV.

The optimized high-magnification probe of MRFL with 4 sets of relay groups is shown in figure 13. The MTF curves demonstrate the system has near diffraction limited performance and the image contrast at the spatial frequency of 60lp/mm is greater than 0.2 for the central FOV and 0.1 when the scanning mirror is steered toward the peripheral FOV

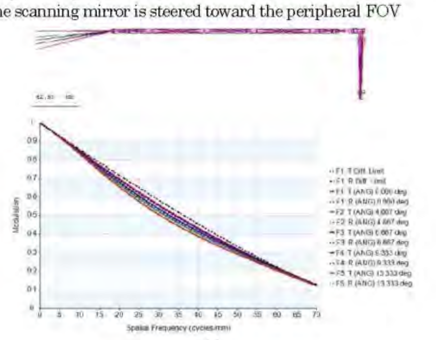

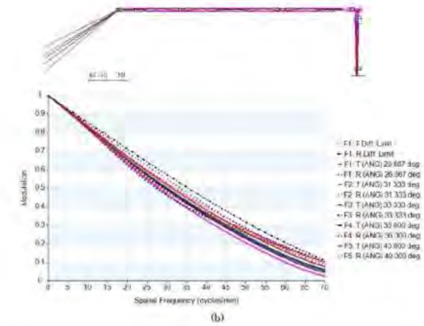

Fig. 13 High-magnification probe of MRFL with the hybrid lens: (a) central FOV; (b) peripheral FOV.

3.3.6 Wide-angle Probe

The design of the wide-angle probe is straightforward compared to the high-magnification probe, because the magnification of the wide-angel probe is smaller and it does not require a diffraction limited performance. As shown in figure 14, a doublet and a field lens can make the performance good enough. The MTF shows the contrast is greater than 0.3 at the frequency of 60lp/mm.

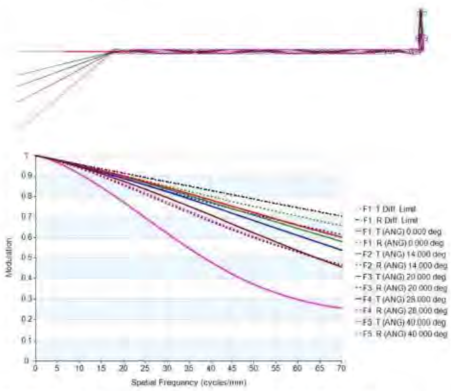

Fig. 14 Wide-angle probe of MRFL: (a) layout; (b) MTF performance.

4. Performance Analysis

The previous section shows the optimized design of the MRFL system can meet the performance requirements as stated in section 2. In this section, a detailed analysis of the MRFL is carried out to demonstrate the MRFL prototype would have the required as-built performance accounting for fabrication and assembly errors. First of all, the diffraction efficiency of the DOE versus the lens radius and wavelengths is shown. Secondly, the tolerance analysis is demonstrated. Finally, the stray light and ghost image analysis are performed by non-sequential ray tracing in LightTools ®.

4.1 DOE analysis

The diffractive lens has great advantage in correcting chromatic aberrations but the diffraction efficiency varies with the lens radius and the wavelength. A properly working DOE needs to have a good diffraction efficiency across the lens surface and the working spectral range.

In a kinoform diffractive optical element, the physical features become finer toward the lens edge, and the diffraction efficiency at the lens edge is typically lower than that of the lens center. Figure 15 shows the diffraction efficiency as a function of the radius of the diffractive surface at the designed wavelength 550nm. The overall efficiency varies from 98.7% to 98.5% when the physical feature reaches the maximum diffractive surface radius of 2.5mm.

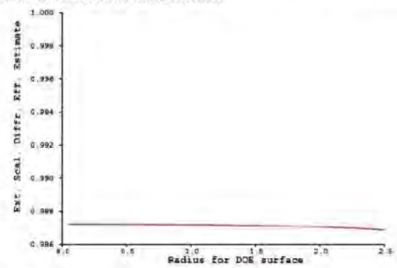

Fig. 15 Diffraction efficiency versus lens radius

On the other hand, the diffraction efficiency is also a function of wavelength as well as profile accuracy Figure 16 shows that the diffraction efficiency of the DOE varies from 80% to nearly 100% across the visible range and the DOE profile is approximated by a 16-level binary mask which yields a good approximation of the kinoform DOE manufactured by a diamond turning machine.

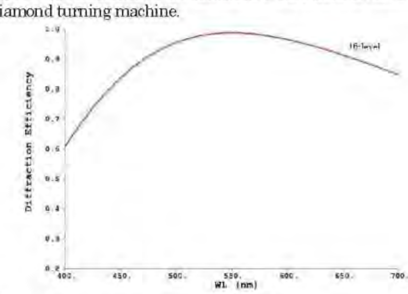

Fig. 16 Diffraction efficiency versus wavelengths

4.2 Tolerance Analysis

The tolerance analysis of the MRFL is complicated, since a standard length profile MRFL has more than 90 optical surfaces and a short length profile MRFL has more than 70 optical surfaces. Even when each surface has a small amount of error, these errors are accumulated through all the lenses and can degrade the final image quality significantly. Therefore the compensator strategy is very critical to achieve the required performance.

The manufacturing errors were set as shown in Table 2. These tolerances are based on the precision-level fabrication process by Optimax which fabricated all the lenses for the MRFL prototypes except the plastic DOE lens. In order to compensate the errors in glass materials, lens radii and center thicknesses, all intermediate image and the final image positions along optical axis were set as the compensators. To compensate those non-symmetrical errors, such as lens wedge and barrel tilt, the first meniscus lens of each relay lens group and the final image plane are allowed to tilt some amount. These meniscus lenses are close to the intermediate images, therefore it is more sensitive to those tilting errors.

The MTF performance was used as the merit function in the tolerance process [13]. Figures 17(a) and 17(b) demonstrate the cumulative probability plots of the MTF of 60lp/mm of the central FOV and the peripheral FOV, respectively. Figures 17(c) and 17(d) show the tolerance result of the MTF of 30lp/mm of the central and peripheral FOV. The MTF degradation of all the sampled fields are less than 0.05 at 99.7% (+/-3 sigma) probability for both frequencies of 30lp/mm and 60lp/mm. Therefore by properly adjusting those compensators, the assembled MRFL is expected to achieve the required as-built performance.

Table 2 Tolerance chart

Glass material (nd, vd)	+/-0.0005, +/- 0.5%
Diameter (mm)	+0.000/-0.025
Center thickness (mm)	+/-0.05
Radius	3 fringes
Irregularity	0.5 fringes
Wedge (ETD, mm)	0.01

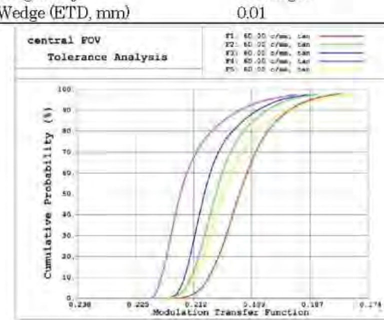

(a)

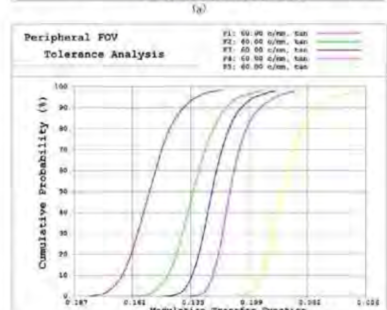

(b)

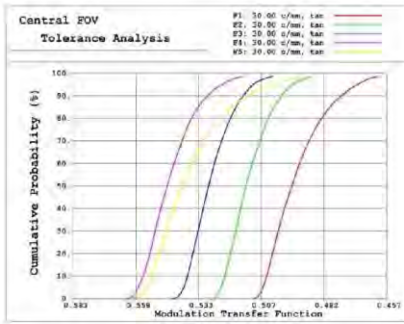

(c)

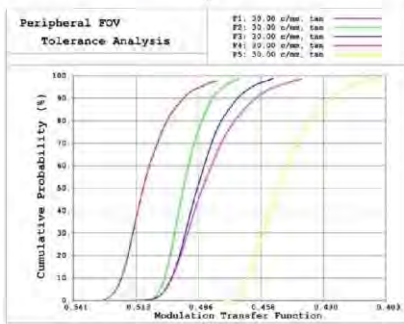

(d)

Fig. 17 tolerance analysis results: (a) and (b) Cumulative probability plot for MTF tolerance of 60lp/mm; (c) and (d) Cumulative probability plot for MTF tolerance of 30lp/mm

4.3 Stray light and ghost image analysis

Stray light and ghost image analysis is necessary for building an optical system, since these issues can degrade the performance of the real optical system. A non-sequential model of the MRFL with a standard length profile is built using LightTools. Stray light may come from the total internal reflection at the lens edge surface. Thus in the prototype, we blackened the edge surface of all the rod lens which may cause stray light. Ghost image always comes from the double reflection between lens surfaces. In the prototype, all the lens surfaces were coated with broad band anti-reflection (BBAR) coating with a transmission of 99.5% over the visible range.

In the LightTools model, all the lens surfaces were set with BBAR coating; the rod lens edge surfaces were set as absorber. Several point sources representing 0°, 13°, 26° and 40° are placed on the object pane targeting at the MRFL. 10,000 non-sequential rays were traced for each point source, the Ray Path Analyzer was used to filter the imaging light, stray light and the ghost light [14, 15]. Figure 18 and 19 are the non-sequential ray tracing result for the MRFL aiming at the center FOV. Figure 17 is the light distribution on the image plane with a point source at 0°. The simulation result does not show the stray light or ghost image problem. By using the ray path filter analysis of LightTools and deselect the imaging path, a ghost image point is shown. The ghost image is formed from the double reflection from the rod lens surface. Since the object point is on axis, the ghost image does not shift. However, Figure 18 shows a ghost image path of the 13° field, which is not coincident with the imaging path. Nevertheless, the relative power of the ghost image is less than 0.5% of the real image. Therefore we can conclude that the central FOV of the MRFL is free from stray light and ghost image. Figure 19 and figure 20 demonstrate the light distribution on the image plane with a light source at 26° and 40° respectively. In these two situations, the scanning mirror is tilted so that the image of the 26° field is at the center of the image sensor and that of the 40° is at the edge of the image sensor. Similar to the central FOV, the ghost paths exist, but the relative power of the ghost paths and stray light is less than 5% of the real image. Consequently, it can be concluded that the MRFL system is free of stray light and ghost image over the entire FOV.

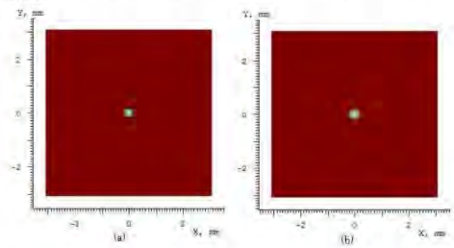

Fig. 18 light distribution of the 0° point source: (a) all ray paths; (b) stray light and ghost image ray path

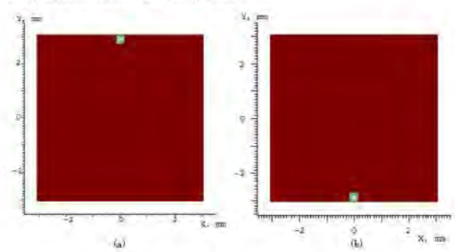

Fig. 18 light distribution of the 13° point source: (a) all ray paths; (b) stray light and ghost image ray path

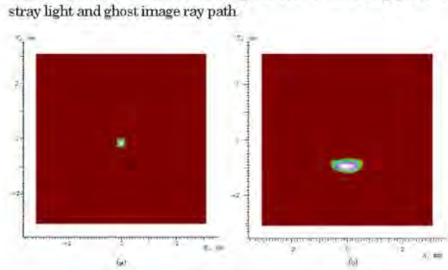

Fig. 19 light distribution of the 26° point source: (a) all ray paths; (b) stray light and ghost image ray path

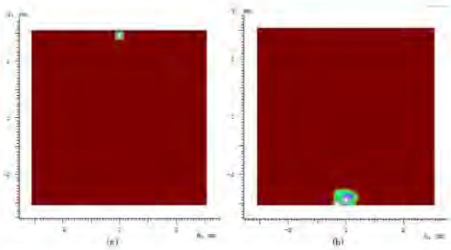

Fig. 20 light distribution of the 40° point source: (a) all ray paths; (b) stray light and ghost image ray path

5. MRFL prototype

The MRFL prototypes with a normal length profile and a short length profile were assembled. . The objective lens and the multiple sets of relay lenses were aligned and assembled on a v-groove, as shown in figure 21. All the tube lenses are blacked on the side surfaces to prevent stray light. A complete 3D model of the mechanical mounting is shown in figure 22. The laparoscope tube contains the objective lens and the relay lenses. The scanning lens and two imaging probes are mounted together with the 2D scanner in a mechanical housing. The laparoscope tube is secured in position by threads on the scanning lens mount. The mechanical housing has a volume of 73.5mm(W)×80mm(H)×100mm(L). The prototypes were demonstrated to have the required as-built performance. The detailed system characterization and in-vivo evaluation are described in the previous paper [7].

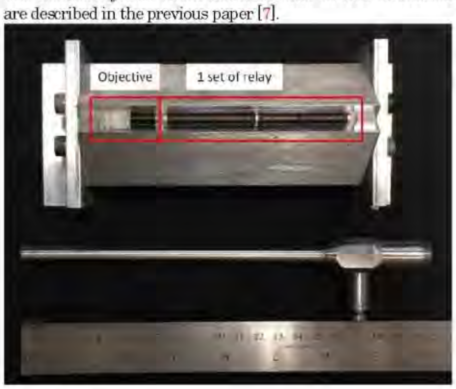

Fig. 21 MRFL assembly

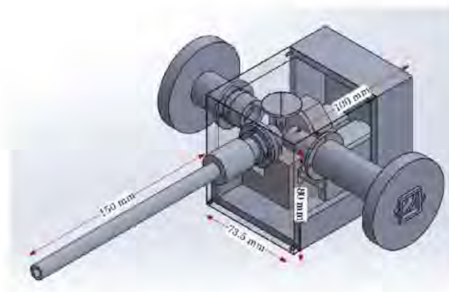

Fig. 22 MRFL 3D mechanical model

6. Summary and future work

In summary, this paper discusses the detailed design strategies and procedure of the multi-resolution foveated laparoscope. The system performances including the MTF performance, the diffraction efficiency of the DOE, tolerance analysis, stray light and ghost image analysis are demonstrated. In the end, the MRFL mechanical model and prototypes are shown.

In the future, we will test the MRFL in the laparoscopy training section and develop different display and control modes for this dual-view system to improve the performance and outcome of the laparoscopic surgery.

Acknowledgments and disclosure

This work is funded by NIH awards R21EB013370, R01EB18921 and TRIF imaging fellowship at the University of Arizona. The authors would like to acknowledge Dr. Xinda Hu for the help on the mechanical design and fabrication. Dr. Hong Hua has a disclosed financial interest in Magic Leap Inc.. This relationship has been properly disclosed to The University of Arizona and reviewed by the Institutional Review Committee in accordance with its conflict of interest policies.

References

1. J. Rassweiler, O. Seemann, M. Schulze, D. Teber, M. Hatzinger, and T. Frede, "Laparoscopic versus open radical prostatectomy: a comparative study at a single institution," J. Urol. 169(5), 1689–1693 (2003).
2. J. Heemskerk, R. Zandbergen, J. G. Maessen, J. W. M. Greve, and N. D. Bouvy, "Advantages of advanced laparoscopic systems," Surg. Endosc. 20(5), 730–733 (2006)
3. M. P. Wu, C. S. Ou, S. L. Chen, E. Y. Yen, and R. Rowbotham, "Complications and recommended practices for electrosurgery in laparoscopy," Am. J. Surg. 179(1), 67–73 (2000).
4. F. S. Tsai, D. Johnson, C. S. Francis, S. H. Cho, W. Qiao, A. Arianpour, Y. Mintz, S. Horgan, M. Talamini, and Y. H. Lo, "Fluidic lens laparoscopic zoom camera for minimally invasive surgery," J. Biomed. Opt. 15(3), 030504 (2010).
5. B. Tamadazte, G. Fiard, J. Long, P. Cinquin, and S. Voros, "Enhanced vision system for laparoscopic

surgery," in proceeding of IEEE conference on Engineering in Medicine and Biology Society (Osaka, Japan, 2013), pp. 5702–5705
6. Y. Qin, H. Hua, and M. Nguyen, "Multiresolution foveated laparoscope with high resolvability," Opt. Lett. 38(13), 2191–2193 (2013).
7. Y. Qin, H. Hua, and M. Nguyen, "Characterization and in-vivo evaluation of a multi-resolution foveated laparoscope for minimally invasive surgery," Biomed. Opt. Express 5(8), 2548–2562 (2014).
8. S. A. Pierre, M. N. Ferrandino, W. N. Simmons, C. Fernandez, P. Zhong, D. M. Albala, and G. M. Preminger, "High definition laparoscopy: objective assessment of performance characteristics and comparison with standard laparoscopy," J. Endourol. **23**(3), 523–528 (2009).
9. Laikin M., Lens Design, 4th ed. (Marcel Dekker, 2006).
10. R. Liang, Optical design for biomedical imaging (SPIE Press, 2010).
11. T. H. Tomkinson, J. L. Bentley, M. K. Crawford, C. J. Harkrider, D. T. Moore, and J. L. Rouke, "Rigid endoscopic relay systems: a comparative study," Appl. Opt. **35**, 6674-6683 (1996).
12. Malacara D., Handbook of Optical Design (Marcel Dekker, New York, 2004)
13. CODE V Reference Manuals, (Version 10.6). Synopsys OSG, 2014.
14. LightTools Reference Manuals, (Version 7.2). Synopsys OSG, (2013).
15. Breault R. P., "Control of stray light," in Handbook of Optics (McGraw-Hill, New York, 1995).

APPENDIX C: Characterization and in-vivo evaluation of a multi-resolution foveated laparoscope for minimally invasive surgery

Yi Qin, Hong Hua, and Mike Nguyen

This paper was published in Biomedical Optics Express, Vol. 5, Issue 8, pp. 2548-2562 (2014)

Characterization and in-vivo evaluation of a multi-resolution foveated laparoscope for minimally invasive surgery

Yi Qin,[1] Hong Hua,[1,*] and Mike Nguyen[2]

[1] *3D visualization and imaging system laboratory, College of Optical Sciences, University of Arizona, 1630 E University Blvd., Tucson, AZ, 85721, USA*

[2] *Institute of Urology, University of Southern California, Los Angeles, CA, 90089, USA*

*hhua@optics.arizona.edu

Abstract: The state-of-the-art laparoscope lacks the ability to capture high-magnification and wide-angle images simultaneously, which introduces challenges when both close- up views for details and wide-angle overviews for orientation are required in clinical practice. A multi-resolution foveated laparoscope (MRFL) which can provide the surgeon both high-magnification close-up and wide-angle images was proposed to address the limitations of the state-of-art surgical laparoscopes. In this paper, we present the overall system design from both clinical and optical system perspectives along with a set of experiments to characterize the optical performances of our prototype system and describe our preliminary in-vivo evaluation of the prototype with a pig model. The experimental results demonstrate that at the optimum working distance of 120mm, the high-magnification probe has a resolution of 6.35lp/mm and image a surgical area of 53 × 40mm^2; the wide-angle probe provides a surgical area coverage of 160 × 120mm^2 with a resolution of 2.83lp/mm. The in-vivo evaluation demonstrates that MRFL has great potential in clinical applications for improving the safety and efficiency of the laparoscopic surgery.

OCIS codes: (170.2150) Endoscopic imaging; (170.3880) Medical and biological imaging; (120.3890) Medical optics instrumentation; (170.0010) Imaging system; (220.0220) Optical design and fabrication.

References and links

1. J. Rassweiler, O. Seemann, M. Schulze, D. Teber, M. Hatzinger, and T. Frede, "Laparoscopic versus open radical prostatectomy: a comparative study at a single institution," J. Urol. **169**(5), 1689–1693 (2003).
2. J. Heemskerk, R. Zandbergen, J. G. Maessen, J. W. M. Greve, and N. D. Bouvy, "Advantages of advanced laparoscopic systems," Surg. Endosc. **20**(5), 730–733 (2006).
3. M. P. Wu, C. S. Ou, S. L. Chen, E. Y. Yen, and R. Rowbotham, "Complications and recommended practices for electrosurgery in laparoscopy," Am. J. Surg. **179**(1), 67–73 (2000).
4. C. R. Voyles and R. D. Tucker, "Education and engineering solutions for potential problems with laparoscopic monopolar electrosurgery," Am. J. Surg. **164**(1), 57–62 (1992).
5. D. Canes, M. M. Desai, M. Aron, G. P. Haber, R. K. Goel, R. J. Stein, J. H. Kaouk, and I. S. Gill, "Transumbilical single-port surgery: evolution and current status," Eur. Urol. **54**(5), 1020–1030 (2008).
6. J. Rassweiler, K. C. Safi, S. Subotic, D. Teber, and T. Frede, "Robotics and telesurgery - an update on their position in laparoscopic radical prostatectomy," Minim. Invasive Ther. Allied Technol. **14**(2), 109–122 (2005).
7. F. S. Tsai, D. Johnson, C. S. Francis, S. H. Cho, W. Qiao, A. Arianpour, Y. Mintz, S. Horgan, M. Talamini, and Y. H. Lo, "Fluidic lens laparoscopic zoom camera for minimally invasive surgery," J. Biomed. Opt. **15**(3), 030504 (2010).
8. S. Lee, M. Choi, E. Lee, K. D. Jung, J. H. Chang, and W. Kim, "Zoom lens design using liquid lens for laparoscope," Opt. Express **21**(2), 1751–1761 (2013).
9. B. S. Terry, Z. C. Mills, J. A. Schoen, and M. E. Rentschler, "Single-port-access surgery with a novel magnet camera system," IEEE Trans. Biomed. Eng. **59**(4), 1187–1193 (2012).

#210808 - $15.00 USD Received 24 Apr 2014; revised 22 Jun 2014; accepted 5 Jul 2014; published 10 Jul 2014
(C) 2014 OSA 1 August 2014 | Vol. 5, No. 8 | DOI:10.1364/BOE.5.002548 | BIOMEDICAL OPTICS EXPRESS 2548

10. B. Tamadazte, G. Fiard, J. Long, P. Cinguin, and S. Voros, "Enhanced vision system for laparoscopic surgery," in proceeding of IEEE conference on Engineering in Medicine and Biology Society (Osaka, Japan, **2013**), pp. 5702–5705.
11. Y. Yamauchi, J. Yamashita, Y. Fukui, K. Yokoyama, T. Sekiya, E. Ito, M. Kanai, T. Fukuyo, D. Hashimoto, and H. Iseki, "A dual-view endoscope with image shift," in proceedings of Computer assisted radiology and surgery (Paris, France, **2002**), pp. 183–187.
12. Y. Qin, H. Hua, and M. Nguyen, "Multiresolution foveated laparoscope with high resolvability," Opt. Lett. **38**(13), 2191–2193 (2013).
13. S. A. Pierre, M. N. Ferrandino, W. N. Simmons, C. Fernandez, P. Zhong, D. M. Albala, and G. M. Preminger, "High definition laparoscopy: objective assessment of performance characteristics and comparison with standard laparoscopy," J. Endourol. **23**(3), 523–528 (2009).

1. Introduction

Laparoscopy has been established as the most successful means of providing minimally invasive surgery (MIS) due to a number of well-recognized advantages compared to the conventional open surgery, such as reduced pain, shorter recovery time and low infection rate [1]. Statistics shows that 96% of 1.06 million cases of cholecystectomy and 75% of 359,000 cases of appendectomy were performed by MIS in the United States in 2011 [2]. It has become a standard clinical procedure for cholecystectomy, appendectomy, and splenectomy.

However, the state-of-the-art laparoscopic technology suffers from several significant limitations, one of which is a tradeoff of limited instantaneous field of view (FOV) for high spatial resolution versus wide FOV for situational awareness but with diminished resolution [2]. Standard laparoscopes (SL) lack the ability to acquire both wide-angle and high-resolution images simultaneously through a single scope. With a standard laparoscope, in order to see fine details of a surgical field, laparoscopic procedures must usually be carried out at a highly zoomed-in view, where the scope is moved in to operate at a short working distance (WD), typically less than 50mm. A highly zoomed-in view leads to the loss of peripheral vision and awareness of situations occurring outside the immediate focus area of the laparoscope. One example occurs when a non-insulated laparoscopic instrument is in inadvertent and unrecognized contact with an energized instrument resulting in spread of electric current being applied to unintended structures, a situation known as "direct coupling" [3]. Insulation failures in energized instruments themselves can also directly lead to injury to bowel, vascular, and other structures. Several other serious complications of the laparoscopic surgery may occur partially due to the loss of situational awareness, including bile duct injury, bile leaks, bleeding and bowel injury. These injuries often remain unrecognized if they occur on the part of the surgical instrument which is not within the keyhole field of view (FOV) of the laparoscope [4]. At present, this limitation is clinically addressed by manually moving the entire laparoscope in and out of the camera port to obtain either close-up or wide-angle views, respectively. In addition, all of this maneuvering to adjust the laparoscope's position requires a trained assistant to hold, move, and manipulate the laparoscope almost constantly.

The practice of frequently maneuvering the laparoscope by a trained assistant can lead to poor or awkward ergonomic scenarios; for example, having to work with hands in a cross-over position between the surgeon and the assistant holding the camera [5]. This type of ergonomic conflicts imposes inherent technical challenges to laparoscopic procedures, and it is further aggravated with the introduction of single port access (SPA) techniques to laparoscopic surgery. SPA uses one combined surgical port for all instruments instead of using multiple ports in the abdominal wall. The grouping of port access in SPA procedures, however, raises a number of challenges, including tunnel vision due to the in-line arrangement of instruments, poor triangulation of instruments, requiring crossing of instruments to obtain proper retraction, and increased risk of instrument collision due to the close proximity to other surgical devices. It has been suggested that varying the optical magnification and increasing the working distance of laparoscope can eliminate this limitation [6].

#210808 - $15.00 USD Received 24 Apr 2014; revised 22 Jun 2014; accepted 5 Jul 2014; published 10 Jul 2014
(C) 2014 OSA 1 August 2014 | Vol. 5, No. 8 | DOI:10.1364/BOE.5.002548 | BIOMEDICAL OPTICS EXPRESS 2549

Aiming to address these limitations, several different types of laparoscopic technologies have been developed to effectively change the FOV and magnification [7,8] or to control viewing direction. For instance, some of the latest commercial laparoscopes are equipped with optical zoom capability [www.stryker.com, www.karlstorz.com] or provide different viewing directions by offering a flexible tip end [medical.olympusamerica.com]. Alternatively, miniature cameras for laparoscopic surgery have been introduced for single-port-access surgery [9]. These laparoscopic systems, however, are not able to simultaneously capture the high-magnification view and the wide-angle view. The enhanced vision laparoscopic system by Tamadazte et al can concurrently provide different views, but the high-magnification view is fixed and thus maneuvering the laparoscope during the surgery is inevitably required [10]. The dual-view endoscope prototype demonstrated by Yamauchi et al provides the ability to capture a zoomed-in view and a wide-angle view simultaneously through an image-shifting prim, but the prototype is limited by its low resolution and low light throughput [11].

Recently, we reported the development of a multi-resolution foveated laparoscope (MRFL) to address the limitations of those existing technologies. A MRFL prototype was demonstrated with a large working distance and the ability to simultaneously capture both high-magnification and wide-angle images in real-time in a fully integrated system. Additionally, the high-magnification probe can be optically scanned toward and engaged at any subfield within the wide-angle field [12]. Following up our initial prototype demonstration in [12], in this paper the overall system design of a MRFL prototype system is presented from both clinical and optical system perspectives (Section 2). In addition, we will present two sets of experiments performed recently with the prototype. The first set of experiments aims to characterize the optical performances of our prototype system (Section 3) and the second set of experiments aims to validate the clinical use of the instrument through our preliminary in-vivo evaluation of the prototype with a live porcine model (Section 4).

2. MRFL system design

From a clinical application perspective, Fig. 1 shows the conceptual layout of a MRFL with low length profile in MIS surgery. The MRFL consists of two fully-integrated imaging probes in a single laparoscope, a wide-angle probe and a high-magnification probe. The wide-angle probe with relatively low magnification captures a wide-angle overview of the abdominal cavity for orientation and situational awareness, while concurrently the high-magnification probe with narrow but adequate FOV obtains images of a sub-region of the wide-angle field at much higher resolution for accurate surgical operation. The instrument therefore provides the ability to survey a large surgical field and to visualize a targeted area in high spatial resolvability for surgical treatment. Concurrent access to both imaging scales in real time offers un-compromised context and resolution, which is expected to offer improved situational awareness and therefore better patient safety and surgical outcome.

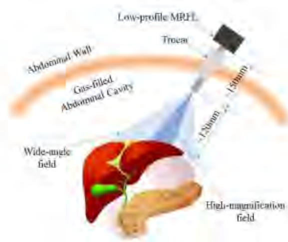

Fig. 1. Conceptual idea for operation of MRFL in laparoscopic surgery.

#210808 - $15.00 USD Received 24 Apr 2014; revised 22 Jun 2014; accepted 5 Jul 2014; published 10 Jul 2014
(C) 2014 OSA 1 August 2014 | Vol. 5, No. 8 | DOI:10.1364/BOE.5.002548 | BIOMEDICAL OPTICS EXPRESS 2550

Additionally, a two-dimensional optical scanner integrated within the system can steer and engage the high-magnification probe to any region of interest (ROI) within the wide-angle field. Therefore, the MRFL system can be secured at a fixed location on the abdominal wall and no physical advancing or withdrawing the MRFL scope is needed to obtain different views. Such arrangement will not only allow MIS procedures to be performed without requiring a dedicated camera assistant or robotic arm, but will also reduce physical interference with other surgical instrument and awkward ergonomic conflicts.

Thirdly, the foveated high-magnification scope provides much more improved spatial resolution than a standard laparoscope and enables highly resolvable visualization of tissues and thus enhances intro-operative surgical decision making. It is thus expected to enable enhanced surgical technique, accuracy, and potentially reduce operation time.

Finally, it is worth noting that the MRFL is optimized to maintain a much longer working distance and low-length profile than those of a standard laparoscope. As illustrated in Fig. 1, the designed WD of a MRFL is about 120mm or larger, while the typical WD of a standard laparoscope is about 50mm for operation. The length of a low-profile MRFL is about 150mm while a SL has a typical insertion length of more than 350mm. With a longer working distance, the surgical area captured by the MRFL can be effectively increased, and the instrument can be positioned at a further distance from the surgical site to mitigate physical interferences with other surgical instrument in the abdominal cavity. The low-length profile characteristics of the MRFL system further helps to reduce instrument crowdedness.

These features discussed above on an MRFL scope are highly desirable in the SPA procedures which suffer from severe instruments crowdedness though one single trocar and the keyhole tunnel vision. Since the MRFL is secured at a large distance away from the surgical area and no physical movement is needed, it reduces the interference between the laparoscope and other surgical instruments. In addition, the multi-resolution foveated capability eliminated the keyhole tunnel vision of the standard laparoscope used in the SPA procedure.

From an optical system design perspective, Fig. 2 illustrates the schematic layout of a low-length profile MRFL system, while Fig. 3 shows the optical layout of our MRFL prototype. The optical system consists of a shared objective lens group, two shared rod lens relay groups, a scanning lens group, a high-magnification imaging probe, a wide-angle imaging probe and a beamsplitter separating the paths of the two imaging probe. The objective lens captures the entire surgical area and forms an intermediate image at its back focal plane. The intermediate image is then relayed twice by the relay lens groups to the front focal plane of the scanning lens group. The scanning lens collimates the beams and relays the pupil onto a 2D scanning mirror. A polarization beam splitter (PBS) along with a quarter wave plate (QWP) is inserted between the scanning lens and the scanning mirror for splitting the light paths for the wide-angle and high-magnification probes. The PBS reflects s-polarized light toward the wide-angle image probe and transmits p-polarized light toward the QWP and scanning mirror. The fast axis of the QWP is oriented at a 45° angle with the p-polarization axis which allows the effective conversion of incident p-polarization into s-polarization following the double pass of the QWP. The PBS then reflects the converted s-polarized light toward the high-magnification imaging probe.

#210808 - $15.00 USD Received 24 Apr 2014; revised 22 Jun 2014; accepted 5 Jul 2014; published 10 Jul 2014

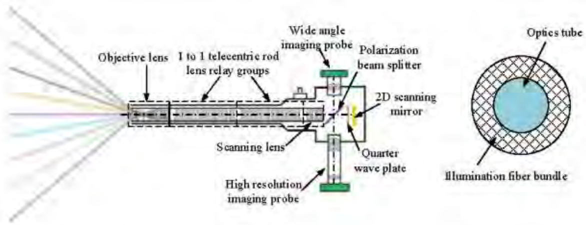

Fig. 2. Schematic layout of a dual-resolution, foveated laparoscope for minimally invasive surgery. The scope consists of a wide-angle imaging probe and a high-magnification probe. The two probes share the same objective lens, relay lens groups, and scanning lens groups.

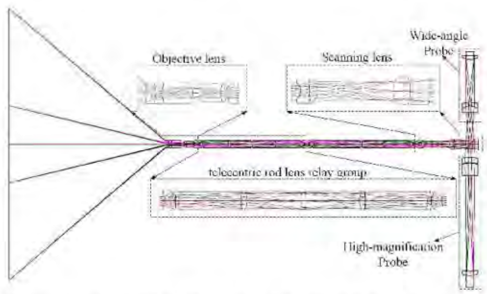

Fig. 3. Optical system layout of a MRFL prototype with a low-length profile, consisting of an objective lens group (a), 2 telecentric rod lens relay groups (b), a scanning lens group (c), a wide-angle probe (d), and a high-magnification probe (e).

Figure 4 demonstrates two integrated MRFL prototypes of different length profiles: a normal profile and a low profile, compared against a commercially available Karl Storz 26033AP standard laparoscope. The first-order optical design specifications of our MRFL prototype systems are summarized in Table 1. The overall optical system was optimized for a working distance of 120mm. The shared objective lens and relay lens groups were designed to capture an overall 80° FOV, with a 0.8mm entrance pupil diameter (EPD) and a 120mm working distance. The relay lens group has an optical magnification of −1. The wide-angle probe captures the entire 80° FOV imaged by the objective-relay groups, while the high-magnification probe captures a 26° FOV of interest. The ratio of the optical power of the two probes is 3 to achieve high-magnification for the foveated probe. In both imaging probes of the prototypes, a 1/3" CCD sensor (DR2-13S2C-CS by PointGrey), with 1280 × 960 pixels and pixel size of 3.75um, was utilized. A motorized 2D optical scanner (Zaber T-OMG series) was integrated to enable the ability to steer the FOV of high-magnification probe across the entire surgical field in less than 0.1 seconds in a positional accuracy of 0.1mm. The anticipated beamsplitting effect on light attenuation was partially compensated by the fact that the F/2.5 objective lens has nearly 5.76 times light collection capability as much as a typical F/6 objective lens in most SLs.

#210808 - $15.00 USD Received 24 Apr 2014; revised 22 Jun 2014; accepted 5 Jul 2014; published 10 Jul 2014

At a 120mm working distance, the wide-angle probe captures a surgical area of 160 × 120mm^2 which is over 9 times of the typical surgical area imaged by a standard laparoscope operating at a 50mm working distance, while it provides a spatial resolution limit of 240um or theoretical spatial frequency limit of 2.1 lp/mm which is equivalent to that of a standard laparoscope. At a 120mm working distance, the high-magnification probe captures a surgical area of 53 × 40mm^2 which is equivalent to the field coverage of a standard laparoscope operating at a 50mm working distance, but it provides a spatial resolution limit of 80um or theoretical spatial frequency limit of 6.25 lp/mm which is three-times as good as that of a standard laparoscope [13].

Two other aspects of the system specifications are that both the F/2.5 objective lens and the relay lens groups are required to be telecentric in the image space and the lens diameter needs to be smaller than 5mm such that they can be assembled in a standard 10mm diameter rigid laparoscope package. Adopting a standard packaging not only allows using the standard fiber illumination bundle and light sources for standard laparoscopes, but also offers the ability to assess our prototypes through a standard laparoscope trocar port and similar procedures. The telecentricity aspect further enables the ability to concatenate a flexible number of relay lens groups of limited diameter without causing noticeable image quality degradation in order to implement prototypes of different length profiles. For instance two groups of relays are needed to build the low-length profile prototype in Fig. 4 with a total insertion length of about 150mm while 4 groups of relays allow extending the insertion length to over 300mm for the normal-profile MRFL prototype in the same figure.

Table 1. First-order optical design specifications of a MRFL prototype system

Parameter		Value
Overall system specifications		
	Working distance	120mm
	Depth of field	80-180mm
	Field of view	80°
	Visual field size at 120mm working distance	
Shared objective and relay lenses		
	FOV	80°
	Entrance pupil diameter	0.8 mm
	F/#	2.5
	Lens diameter	< 6 mm
	Overall packaging diameter with illumination fiber bundle	10mm
High-magnification imaging probe		
	FOV	26°
	Visual field size at 120mm working distance	53 × 40 mm^2
	Spatial resolution in object space at 120mm working distance	80 um or 6.25lp/mm
	Imaging sensor	Point Grey Dragonfly II, 1/3", 1280 × 960 pixels
	2D scanner	Zaber T-OMG series, < 100ms scan across the entire field
Wide-angle imaging probe		
	FOV	80°
	Visual field size at 120mm working distance	160 × 120 mm^2
	Spatial resolution in object space at 120mm working distance	240 um or 2.1lp/mm
	Imaging sensor	Point Grey Dragonfly II, 1/3", 1280 × 960 pixels

#210808 - $15.00 USD Received 24 Apr 2014; revised 22 Jun 2014; accepted 5 Jul 2014; published 10 Jul 2014

1 August 2014 | Vol. 5, No. 8 | DOI:10.1364/BOE.5.002548 | BIOMEDICAL OPTICS EXPRESS 2553

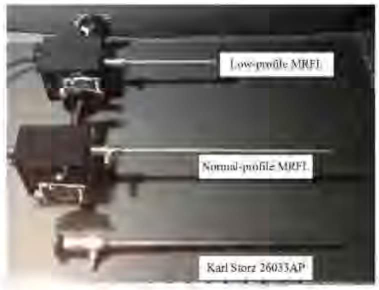

Fig. 4. MRFL prototypes in comparison with a commercially available standard laparoscope.

3. Characterization of optical performance

The optics of the MRFL prototypes was custom-designed and built and the optical system was assembled in our lab. It was optimized with a 120mm optimal WD and a working range of 80~180mm, within which the modulation transfer function (MTF) values of both the wide-angle and high-resolution probes are greater than 0.2 at the Nyquist frequency of the image sensors. This section will describe a set of experiments performed to characterize the optical performance of the prototypes, including the obtained resolution of both imaging probes at 120mm working distance (section 3.1 and section 3.2), the throughput analysis (Section 3.3), and the MTF (section 3.4). The results obtained through the experiments are summarized in Table 2.

Table 2. Optical performance characterization of a low-length profile MRFL prototype at 120mm working distance

	Wide-angle imaging probe		High-magnification imaging probe	
Field	Center	Corner	Center	Corner
Field of view (mm^2)	160 × 120		53 × 40	
Limiting resolution (um)	176.68	280.90	78.74	140.45
Limiting spatial frequency (lps/mm)	2.83	1.78	6.35	3.56
Throughput (mm^2sr)	0.3351		0.0372	

3.1 Resolution measurement of high-magnification probe at 120mm working distance

A 1951 USAF glass slide resolution target (Groups 0-3) was used to measure the limiting resolution of both the high-magnification probe and the wide-angle probe. A flat-panel LED source was used as the backlight to uniformly illuminate the target slide within a large area. A holographic diffuser with an 80° diffusing angle was placed behind the resolution target which enables the diffused light from the target across the entire field can fulfill the entrance pupil of the MRFL.

Figure 5(a) shows the captured image of the resolution target with the high-magnification probe at 120mm working distances orienting at the center field, along with the intensity profiles of three horizontal target bars in Group 2 (element 4 through 6). Figure 5(b) shows the intensity profiles of three horizontal bars in Group 2 (element 2 through 4). The contrasts of the group 2 bars in both horizontal and vertical directions are listed in Table 3. It demonstrates that when the high-magnification probe orients at the center field, the group 2 element 5 bar (6.35 lp/mm or 78.74um) can be resolved in the vertical direction, and the group 2 element 4 bar (5.66 lp/mm or 88.34um) is resolvable in the horizontal direction.

#210808 - $15.00 USD Received 24 Apr 2014; revised 22 Jun 2014; accepted 5 Jul 2014; published 10 Jul 2014
(C) 2014 OSA 1 August 2014 | Vol. 5, No. 8 | DOI:10.1364/BOE.5.002548 | BIOMEDICAL OPTICS EXPRESS 2554

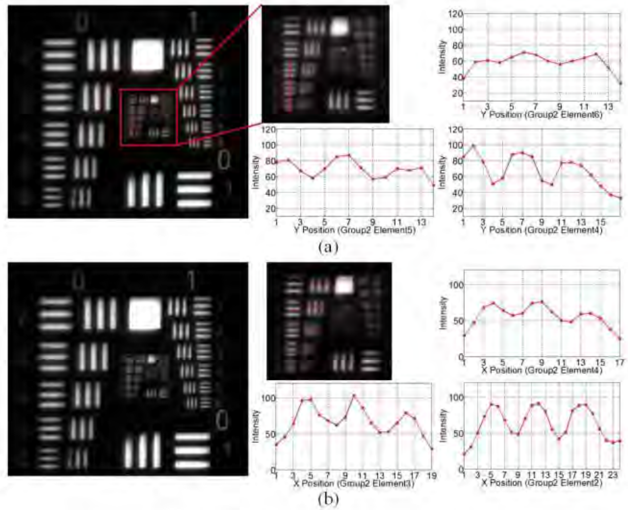

Fig. 5 Images and intensity profiles of the resolution target of the high-magnification probe at 120mm working distance orienting at the center field, (a) in vertical direction; (b) in horizontal direction.

Table 3. Image contrast of the high-magnification probe orienting at the center field

Contrast	G2 E6 (7.13 lp/mm)	G2 E5 (6.35 lp/mm)	G2 E4 (5.66 lp/mm)	G2 E3 (5.04 lp/mm)	G2 E2 (4.49 lp/mm)
Vertical	0.0806	0.1616	0.2760	0.3362	0.4530
Horizontal	0	0.1103	0.1429	0.24	0.3333

Figures 6(a) and 6(b) demonstrate the captured image and intensity profiles of the resolution target with the high-magnification probe at 120mm working distances orienting at the corner field in the vertical and horizontal directions, respectively. The contrasts of group 1 bars in both horizontal and vertical directions are listed in Table 4. It demonstrates that the high-magnification probe is able to resolve the group 1 element 6 bar (3.56 lp/mm or 140.45um) in both directions when it orients at the corner field.

Compared with the resolution of the high-magnification probe orienting at the center field, the resolution is lower when it orients at the corner field. One reason is that the MRFL is designed for a flat field, when the high-magnification probe orients at the corner field, the actual working distance is equivalent to 134mm, substantially larger than 120mm, and thus the spatial resolution is expected to decrease. Another reason is the distortion of the optical system, which is a magnification error related to field position. Alike a typical wide-field of view imaging system, the corner field of the MRFL optics is subject to a substantial amount of barrel distortion (15% at diagonal 80 degrees). Consequently, the actual magnification of the corner field is smaller than the center field, which leads to a lower spatial resolution. Off-axis aberrations such as astigmatism and lateral chromatic aberration can cause the performance drop as well. As shown in Fig. 5, the image contrast in the vertical direction is higher than that in the horizontal direction; and lateral color is somewhat noticeable in Fig. 6 as well.

#210808 - $15.00 USD Received 24 Apr 2014; revised 22 Jun 2014; accepted 5 Jul 2014; published 10 Jul 2014

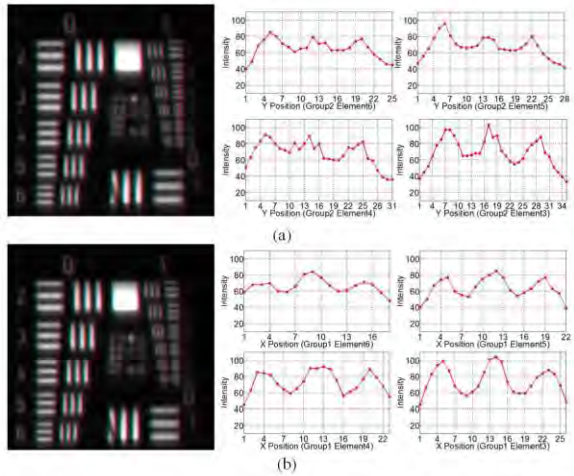

Fig. 6. Images and intensity profiles of the resolution target of the high-magnification probe at 120mm working distance orienting at the corner field, (a) in vertical direction; (b) in horizontal direction.

Table 4. Image contrast of the high-magnification probe orienting at the corner field.

Contrast	G1 E6 3.56 lp/mm	G1 E5 3.17 lp/mm	G1 E4 2.83 lp/mm	G1 E3 2.52 lp/mm	G1 E2 2.24 lp/mm	G1 E1 2.00 lp/mm
Vertical	0.1288	0.1371	0.1504	0.2308	0.2526	0.3666
Horizontal	0.1152	0.1965	0.2132	0.2557	0.2779	0.3424

3.2 Resolution measurement of wide-angle probe at 120mm working distance

Figure 7 shows the resolution of the center field of the wide-angle probe at 120mm working distances. In the center field, the group 1 element 4 bar can be resolved, which corresponds to a spatial frequency of 2.83lp/mm or a limiting resolution of 176um. The contrast of each resolution target is shown in Table 5.

Table 5. Image contrast of the center field of the wide-angle probe

Contrast	G1 E4 2.83 lp/mm	G1 E3 2.52 lp/mm	G1 E2 2.24 lp/mm	G1 E1 2.00 lp/mm
Vertical	0.3260	0.4637	0.5610	0.6014
Horizontal	0.1813	0.3035	0.4875	0.5935

Figure 8 demonstrates the resolution of the corner field of the wide-angle probe at 120mm working distance. It is shown that the group 0 element 5 can be resolved, which corresponds to a spatial frequency of 1.59lp/mm or a limiting resolution of 314um. The contrast of the bar target is listed in Table 6.

Table 6. Image contrast of the corner field of the wide-angle probe

Contrast	G0 E4 1.59 lp/mm	G0 E3 1.41 lp/mm	G0 E2 1.26 lp/mm	G0 E1 1.12 lp/mm
Vertical	0.1706	0.2693	0.2562	0.3869
Horizontal	0.1604	0.3059	0.4969	0.5951

#210808 - $15.00 USD Received 24 Apr 2014; revised 22 Jun 2014; accepted 5 Jul 2014; published 10 Jul 2014

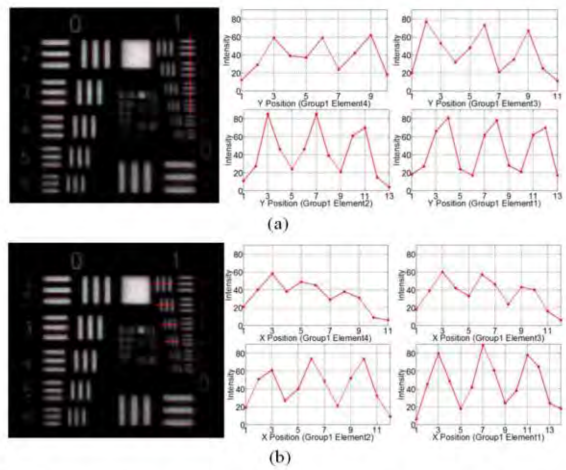

Fig. 7. Images and intensity profiles of the resolution target of the center field of the wide-angle probe at 120mm working distance, (a) in vertical direction; (b) in horizontal direction.

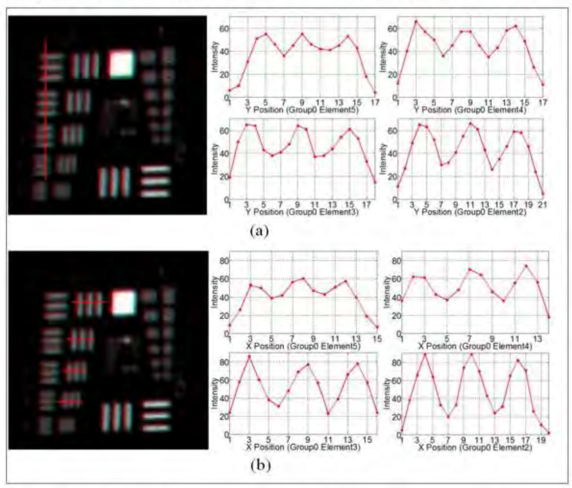

Fig. 8. Images and intensity profiles of the resolution target of the center field of the wide-angle probe at 120mm working distance, (a) in vertical direction; (b) in horizontal direction

Comparing Fig. 7 and Fig. 8, it can be found that in the corner field, certain amount of distortion and lateral color are observable. These aberrations degrade the performance of the corner field. However, it is still acceptable since the wide-angle probe is used for orientation

#210808 - $15.00 USD Received 24 Apr 2014; revised 22 Jun 2014; accepted 5 Jul 2014; published 10 Jul 2014

1 August 2014 | Vol. 5, No. 8 | DOI:10.1364/BOE.5.002548 | BIOMEDICAL OPTICS EXPRESS 2557

and situational awareness, the performance is not as critical as that of the high-magnification probe.

3.3 Throughput analysis

The throughput of an optical system determines the light collection capability. When a digital imaging sensor such as CCD or CMOS is used, the throughput will affect the frame rate and signal to noise ratio. If the throughput is insufficient, the signal to noise ratio will decrease, thus the image will appear noisy and the contrast will also be reduced. The throughput of an imaging probe in the MRFL system, is defined by

$$\Phi = \varepsilon A \Omega \tag{1}$$

where ε is the light transmission efficiency of the imaging probe, A is the area captured by the probe, and Ω is the solid angle of the entrance pupil. ε is mainly affected by the beamsplitting ratio between the wide-angle and high-magnification imaging paths and it is 50% for both imaging probes in our prototype implementation. The solid angle Ω can be calculated by $\Omega = 2\pi(1-\cos\theta_0)$ where θ_0 is defined as $\theta_0 = \tan^{-1}(EPD/2WD)$. The throughput of the wide-angle probe and the high-magnification probe at 120mm working distance is $0.3351 mm^2 sr$ and $0.0372 mm^2 sr$, respectively. Similarly, at 80mm working distance, the throughput of the wide-angle probe and high-magnification probe is 0.2945 $mm^2 sr$ and 0.0327 $mm^2 sr$, respectively. The throughput of the high-magnification probe is only 1/9 of the wide-angle probe.

When the surgical area is inadequately illuminated, the much lower throughput of the high-magnification probe inevitably leads to lower signal to noise ratio and lower image contrast of the its images than that of the wide-angle image. To balance the effects of throughput difference between the two imaging probes, we plan to implement a different beam splitting ratio along with an improved illumination source for future MRFL developments.

3.4 MTF measurement

To further verify the optical performance of the high-magnification probe, we adopted the slanted edge method to measure the MTF of the high-magnification probe orienting at the center field [Imatest LLC]. The MTF measurements in both horizontal and vertical directions are carried out. As shown in Fig. 9, the dashed black line is the diffraction limited MTF, the red curve is the MTF of the designed high-magnification probe, the solid blue curve is the measured MTF in horizontal direction, and the dashed blue curve is the MTF in vertical direction. In the horizontal direction, about 10% MTF drop was observed across the measured spatial frequency range (up to 70lps/mm), while in the vertical direction, about 20% MTF drop was observed. These performance drop may be attributed to lens manufacturing errors and system assembling errors.

#210808 - $15.00 USD Received 24 Apr 2014; revised 22 Jun 2014; accepted 5 Jul 2014; published 10 Jul 2014

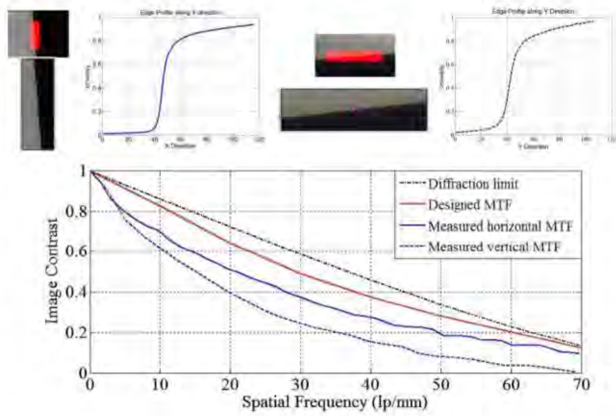

Fig. 9. MTF measurement

It shall be noted that the MTF curves in Fig. 11 were obtained in the image space. To better characterize the optical performance of the MRFL system, the MTF in the object space need to be calculated. This can be done by calculating the optical magnification of the high-magnification probe, which is given by

$$m_{high-mag} = \frac{f_{obj}}{WD} \times m_{relay}^{n} \frac{f_{high-mag}}{f_{scan}} \quad (2)$$

Where the focal length of the objective, scanning lens and high-magnification probe are 2mm, 14mm and 90mm, respectively, the magnification of each relay lens group, m_{relay}, −1, and n is the number of relay groups . In our current MRFL prototype, the magnification of the high-magnification probe is determined to 0.107 for a working distance of 120mm.

Driven by the limited dynamic range of the imaging sensor, hereby 15% was selected to be the threshold MTF value and based on Fig. 9 60lp/mm was determined to be the maximum resolvable spatial frequency in the image space. The corresponding spatial frequency ξ_{max} in the object space can be calculated by $\xi_{max} = 60 \times m_{high-mag} = 6.42 lp/mm$, which agrees with the limiting resolution measured in Section 3.1.

4. Biological model evaluation

Following the successful fabrication and optical performance characterization of the MRFL prototypes, the MRFL prototypes was evaluated on a live porcine model at the live animal lab in the Keck School of Medicine at the University of Southern California. The porcine was placed under general anesthesia with its abdomen incised with a CO_2-filled cavity. As shown in Fig. 10, three incisions were made on the abdominal wall of the pig with three standard trocars for laparoscopic procedures in place. During the test, one of the trocars was utilized for positioning a MRFL prototype while a standard laparoscope for comparison or a laparoscopic grabber or scissor may be inserted through the other trocars. Figure 10 demonstrated the setup with a normal-length MRFL prototype inserted through the bottom trocar. The images shown in Fig. 11 and Fig. 12 were captured with this setup where only about half of the normal-length tube was inserted into the trocar to ensure a working distance round 120mm.

#210808 - $15.00 USD Received 24 Apr 2014; revised 22 Jun 2014; accepted 5 Jul 2014; published 10 Jul 2014

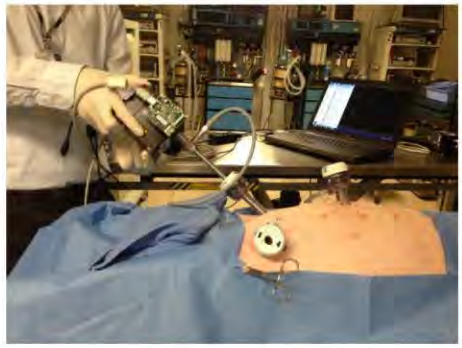

Fig. 10. In-vivo animal test

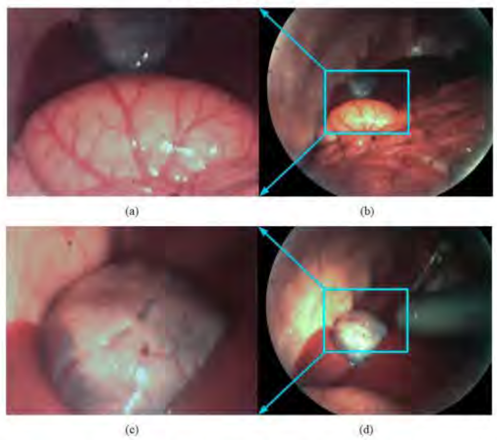

Fig. 11. MRFL in-vivo evaluation with a porcine model at an approximately 120mm working distance from the surgical cite: (a) high-magnification image of the spleen; (b) wide-angle image of the spleen; (c) high-magnification image of the gallbladder; (d) wide-angle image of the gallbladder. The high-magnification and wide-angle images were acquired simultaneously through the MRFL prototype.

Figures 11(a) and 11(b) demonstrate the high-magnification image and wide-angle image of the spleen captured simultaneously by the two imaging probes of the MRFL prototype, where the splenectomy was performed. Figures 11(c) and 11(d) demonstrate images of the gallbladder for cholecystectomy. The cyan-boxes in Figs. 11(b) and 11(d) marks the corresponding regions of interest captured the high-magnification foveated probe. The surgical areas displayed in Figs. 11(a) and 11(c) by the high-magnification probe are similar to those by the standard laparoscope used for comparison. These pictures further demonstrate that the high-magnification probe's capability of capturing the adequate fine structures of the spleen and the gallbladder for surgical procedures. Figures 11(b) and 11(d) demonstrate the

#210808 - $15.00 USD Received 24 Apr 2014; revised 22 Jun 2014; accepted 5 Jul 2014; published 10 Jul 2014

surgical fields of the wide-angle probe which is substantially larger than that by the standard laparoscope in comparison. The wide-angle views can guide the manipulation of other instruments without collision. In addition, Fig. 11(d) shows the position of a standard laparoscope used for comparison, which suggest that the working distance of the standard laparoscope is much smaller than that of the MRFL. In order to get the close-up view similar to that by the high-magnification probe of the MRFL system or wide-angle view similar to that by the wide-angle probe, the standard laparoscope needs to move forward or withdraw backward from the surgical site.

Figure 12 demonstrates the capabilities offered by an MRFL system in terms of maintaining situational awareness and preventing accidental contact of the instruments with unintended organs or structures. Along with the MRFL inserted through one of the three trocars, the surgeon grabbed the gallbladder with a surgical grabber on his left hand and inserted a surgical scissor through the third trocar with his right hand. As shown in Figs. 12(a) and 12(c), the high-magnification probe captured the needed details for surgical procedure, equivalent to the close-up view of a standard laparoscope, but failed to make aware of the path of the scissor and its close approach to the other organs. However, without the need of retracting the scope, the wide-angle probe of the MRFL system simultaneously captured the overview of the abdominal cavity shown in Fig. 12(b) and 12(d), which helped the surgeon fully aware of the insertion path of the scissor in the abdominal cavity and effectively prevented the accidental contact of the instruments with other organs. In the current MIS surgery, when a standard laparoscope is used at a zoomed-in view for surgical operation, the surgeon loses his or her vision outside the immediate focus of the laparoscope and thus loses awareness of any injuries occurring outside the close-up view, which can cause fatal problems in some extreme case such as massive hemorrhage. The capability of simultaneously capturing close-up and wide-angle views in a MRFL system can effectively address such limitation.

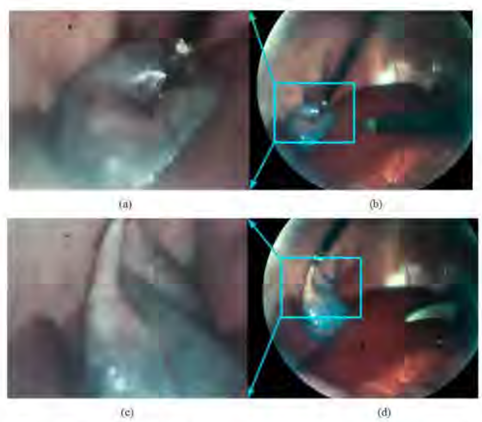

Fig. 12. Demonstration of situational awareness. (a) (c) high-magnification images of the gallbladder captured by the high-magnification probe of the MRFL system failed to show the insertion and close approach of another surgical instrument; (b) (d) wide-angle views, corresponding to (a) and (c), respectively, by the wide-angle probe shows the overview of the abdominal cavity with a clear visualization of the surgical instruments as well as their insertion path, preventing accidental collision or injuries.

#210808 - $15.00 USD Received 24 Apr 2014; revised 22 Jun 2014; accepted 5 Jul 2014; published 10 Jul 2014

5. Conclusion

In summary, this paper presented the overall system design of a MRFL prototype, described the optical performance of the prototype obtained through a set of characterization experiments, and validated the clinical use of the prototype through a preliminary evaluation with a live porcine model. The results demonstrated that the MRFL has the capability of capturing both high-magnification and wide-angle views simultaneously through an integrated system, providing adequate details for surgical procedures and large field coverage without the need of moving forward or withdrawing the laparoscope. The results further demonstrated that the MRFL system can provide surgeons superior situational awareness, and can effectively prevent accidental injuries on unintended structures and reduce the complications. Last but not the least, having a large working distance with the MRFL system can effectively reduce instruments collision inside the abdominal cavity, which is anticipated to improve the safety and efficiency of MIS procedures.

For the future work, we will focus on solving the throughput difference between the high-magnification probe and wide-angle probe to improve the image quality, and carrying out more clinical studies to evaluate the outcome of MIS surgery using the MRFL.

Acknowledgments

We would like to thank the Laparoscopic Surgery Training Lab in the Keck School of Medicine at the University of Southern California. This work is supported by NIH grants R21EB013370 and R01 EB18921-01.

#210808 - $15.00 USD Received 24 Apr 2014; revised 22 Jun 2014; accepted 5 Jul 2014; published 10 Jul 2014

APPENDIX D: A continuously zoomable multi-resolution foveated laparoscope with auto-focus capability

Yi Qin and Hong Hua

This paper will be submitted to Optics Express for review.

A continuously zoomable multi-resolution foveated laparoscope with auto-focus capability

Yi Qin and Hong Hua*

3D Visualization and Imaging Lab, College of Optical Sciences, University of Arizona, 1630 E University Blvd., Tucson, AZ, 85721, USA
*hhua@optics.arizona.edu

Abstract: In modern minimally invasive surgeries (MIS), standard laparoscopes suffer from the tradeoff between the spatial resolution and field of view (FOV). The inability of simultaneously acquiring high-resolution images for accurate operation and wide-angle overviews for situational awareness limits the efficiency and outcome of the MIS. A dual view multi-resolution foveated laparoscope (MRFL) which can simultaneously provide the surgeon with a high-resolution view as well as a wide-angle overview was proposed and demonstrated to have great potential for improving the MIS. Although experiment results demonstrated the high-magnification probe has an adequate magnification for viewing surgical details, the dual-view MRFL is limited to two fixed levels of magnifications. A fine adjustment of the magnification is highly desired for obtaining high resolution images with desired field coverage. In this paper, a high magnification probe with continuous zooming and auto-focus capabilities without mechanical moving parts is demonstrated. By taking the advantages of two electrically tunable lenses, one for optical zoom and the other for image focus compensation, the optical magnification of the high-magnification probe varies from 2× to 3× compared with that of the wide-angle probe, while the focused object position stays the same as the wide-angle probe. The optical design and the tunable lens analysis are presented, followed by prototype demonstration and performance evaluation.

OCIS codes: (170.2150) Endoscopic imaging; (170.3880) Medical and biological imaging; (120.3890) Medical optics instrumentation; (170.4580) Optical diagnostics for medicine; (170.0010) Imaging system; (220.0220) Optical design and fabrication.

References and links

1. J. Rassweiler, O. Seemann, M. Schulze, D. Teber, M. Hatzinger, and T. Frede, "Laparoscopic versus open radical prostatectomy: a comparative study at a single institution," J. Urol. 169(5), 1689–1693 (2003).
2. J. Heemskerk, R. Zandbergen, J. G. Maessen, J. W. M. Greve, and N. D. Bouvy, "Advantages of advanced laparoscopic systems," Surg. Endosc. 20(5), 730–733 (2006).
3. M. P. Wu, C. S. Ou, S. L. Chen, E. Y. Yen, and R. Rowbotham, "Complications and recommended practices for electrosurgery in laparoscopy," Am. J. Surg. 179(1), 67–73 (2000).
4. D. Cheng, Y. Wang, L. Yu and X. Liu, "Optical Design and Evaluation of a 4 mm Cost-Effective Ultra-High-Definition Arthroscope," Biomedical Optics Express 5(8), 2697–2714 (2014).
5. F. S. Tsai, D. Johnson, C. S. Francis, S. H. Cho, W. Qiao, A. Arianpour, Y. Mintz, S. Horgan, M. Talamini, and Y. H. Lo, "Fluidic lens laparoscopic zoom camera for minimally invasive surgery," J. Biomed. Opt. 15(3), 030504 (2010).
6. S. Lee, M. Choi, E. Lee, K. D. Jung, J. H. Chang, and W. Kim, "Zoom lens design using liquid lens for laparoscope," Opt. Express 21(2), 1751–1761 (2013).
7. B. Tamadazte, G. Fiard, J. Long, P. Cinquin, and S. Voros, "Enhanced vision system for laparoscopic surgery," in proceeding of IEEE conference on Engineering in Medicine and Biology Society (Osaka, Japan, 2013), pp. 5702–5705.

8. Y. Yamauchi, J. Yamashita, Y. Fukui, K. Yokoyama, T. Sekiya, E. Ito, M. Kanai, T. Fukuyo, D. Hashimoto, and H. Iseki, "A dual-view endoscope with image shift," in proceedings of Computer assisted radiology and surgery (Paris, France, 2002), pp. 183–187.
9. Y. Qin, H. Hua, and M. Nguyen, "Multiresolution foveated laparoscope with high resolvability," Opt. Lett. 38(13), 2191–2193 (2013).
10. Y. Qin, H. Hua, and M. Nguyen, "Characterization and in-vivo evaluation of a multi-resolution foveated laparoscope for minimally invasive surgery," Biomed. Opt. Express 5(8), 2548–2562 (2014).

1. Introduction

Laparoscope accelerates the development of modern medical surgeries. It has become a standard instrument to perform a wide range of minimally invasive surgery (MIS), such as cholecystectomy, appendectomy and hysterectomy [1]. The standard single-view laparoscope, however, suffers several limitations. One of the major limitations is the tradeoff between the limited field of view (FOV) for high spatial resolution versus the wide FOV for situational awareness but with diminished resolution [2]. Standard laparoscopes lack the ability to acquire both wide-angle and high-resolution images simultaneously through a single scope. This limitation introduces challenges when used in scenarios requiring both close-up views for details and wide-angle overviews for orientation and situational awareness during surgical maneuvers. Moreover, in the single port access (SPA) procedure, this limitation is more aggravated, since all the instruments are inserted through one shared trocar. The instruments conflict and tunnel vision make the SPA procedures quite challenging. It has been suggested that varying the optical magnification and making the laparoscope low profile can improve the efficiency and outcome of the SPA surgery [3].

In recent years, several advanced laparoscopic or endoscopic technologies have been developed to address those limitations. For example, the compact ultra-high-definition endoscope [4] can reduce the instrument conflict while remaining high resolution, the zoom laparoscope [5,6] or zoom camera head [Stryker 1488 HD] can effectively change the optical magnification, thus change the field coverage and resolution; variable viewing direction laparoscopes [7,8] can change their view by varying its viewing direction optically or mechanically. None of these existing solutions, however, are unable to simultaneously acquire both wide-angle images and high-resolution images.

We proposed a multi-resolution foveated laparoscope (MRFL), which is capable of providing the surgeon with both a wide-angle view and a high-resolution view simultaneously though an integrated system [9]. The MRFL consists of two fully integrated imaging probes, a wide-angle probe and a high-magnification probe (foveated probe), and the two probes share the same objective lens group, multiple rod lens relay groups and a scanning lens group. Compared with a standard laparoscope, the wide-angle probe, at a working distance about 120mm, captures about 8× surgical area with a similar spatial resolution; and the foveated probe acquires a similar field coverage but 3× spatial resolution. The dual-view capability of the MRFL effectively solves the FOV-resolution tradeoff of a standard laparoscope, which promises great potentials in improving the efficiency and safety of MIS.

Although the foveated probe was demonstrated to offer an adequate magnification for viewing surgical details through an in-vivo evaluation with a porcine model [10], the existing MRFL prototype is limited to two fixed levels of magnifications. The fixed level of magnification limits the flexibility of obtaining a foveated view at an adequate magnification without turning to a manual maneuver of the instrument. A fine adjustment of the optical magnification is highly desired for the foveated probe to obtain views with a desired size of field coverage and spatial detail resolvability. For instance, since the optical magnification of the foveated probe of the existing MRFL prototype is 3× as a standard laparoscope, it is sufficient to perform MIS procedures such as cholecystectomy and appendectomy. However, for surgeries like liver section and colon resection, larger field coverage may help the surgeon to perform the operation more efficiently.

In this paper, we present the design and prototype of a high-magnification probe with continuous zooming (2× ~ 3×) and auto-focusing capabilities is presented, while the wide-angle probe of the MRFL remains the same as the existing prototype. The foveated zoom probe is able to adjust its optical magnification and keep focused on the same object without any mechanically moving part. This is achieved by utilizing two electronically controlled tunable lenses. The optical approach and the design challenges of the high-magnification zoom probe are presented in detail in Section 2, followed by the optical design and prototype demonstration in Section 3 and a preliminary evaluation of the optical performance and zooming capability in Section 4.

2. Optical approach

The key requirement of the zoomable MRFL is the ability to continuously vary the optical magnification and spatial resolution of the foveated probe without affecting the wide-angle view and to maintain the same focusing distance in the object space for different zoom positions. It is anticipated that the focusing distance of the wide-angle and foveated probes will remain the same and fixed once the scope is positioned at its desired working distance. This requirement imposes a major challenge because varying the optical power for zoom inevitably causes a change of object-image conjugate planes, which results in a change of focusing distance in the object space or a change of the detector plane position in the image space. If not appropriately compensated, varying the optical power of the foveated probe alone may cause severe mismatch of focused object between the wide-angle and foveated probes and cause image blurry during zooming.

The schematic layout of the foveated probe with continuous optical zooming and auto-focusing capabilities is shown in Fig. 1, in which both the focusing distance in the object space and the detector plane maintain fixed with no mechanically moving parts. It consists of two electrically-controlled tunable lens groups and an imaging lens. The two tunable lens groups form a Keplerian telescope. By properly adjusting the focal lengths of these two tunable lens groups, making the sum of the focal lengths equal to a constant, the optical magnification can be tuned without changing the object distance or imaging distance. The rays in solid lines in Fig. 1 illustrate a lower optical magnification than those rays in dashed lines.

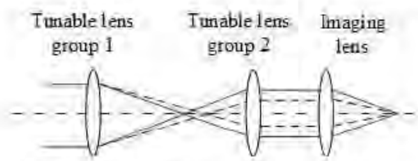

Fig. 1 Schematic layout of the zoom probe design in MRFL system

The equivalent focal length of the zoom probe is calculated by Eq. (1), where f_{TL1} and f_{TL2} are the focal lengths of the first and second tunable lens group, respectively; and f_{img} is the focal length of the imaging lens.

$$f_{zoom} = \frac{f_{TL1}}{f_{TL2}} \times f_{img} \tag{1}$$

The overall zoom ratio of the foveated probe is defined by the ratio between the focal length of the zoom probe and that of the wide-angle probe. Given that the desired zoom ratio is 2× ~ 3× and the focal length of the wide-angle probe is 30mm in our existing MRFL prototype [9], the focal length of the zoom probe varies from 60mm to 90mm, corresponding to the 2× and 3× zoon ratio, respectively. In order to make the probe compact, the focal length of the imaging lens is specified to be 15mm. Therefore the magnification of the Keplerian telescope, which can be simply calculated by $m = -f_{TL2}/f_{TL1}$, should vary from -1/4 to -1/6.

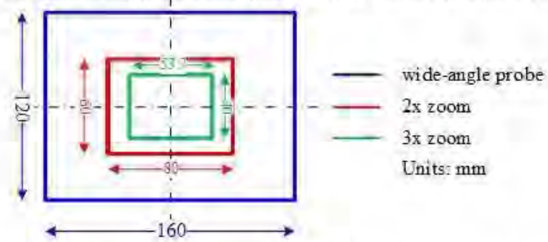

Fig. 2 Field coverage of zoomable foveated probe at two different zoom ratios in comparison to the field coverage of the wide-angle probe.

The corresponding field coverage of the two extreme magnifications, i.e. 2× and 3×, is shown in Fig. 2. The blue rectangle shows a field coverage of 160×120mm^2, which is field coverage of the wide-angle probe at a 120mm working distance. The red rectangle and the green rectangle indicate the field coverage of the zoom probe of 2× and 3× zoom ratio, respectively. At the 2× zoom ratio, the field coverage is about 80×60mm^2, which is about 1/4 of the wide-angle probe. At 3× zoom ratio, the field coverage is about 53.7×40mm^2, which is about 1/9 of the wide-angle probe.

The tunable lenses used are Optotune EL-10-30-LD., which has a focal range of 40mm to 120mm. In order to achieve the magnification from -1/6 to -1/4, offset lenses are added to each tunable lens, therefore the focal range of each tunable lens group can be adjust based on the focal lengths of the offset lenses. Figure 3(a) and 3(b) show the focal range of the tunable lens groups as a function of the focal length of the offset lenses for the first and second tunable lens groups, respectively. The calculation is based on Gaussian optics and assuming the offset lens is assumed to be in contact with the tunable lens.

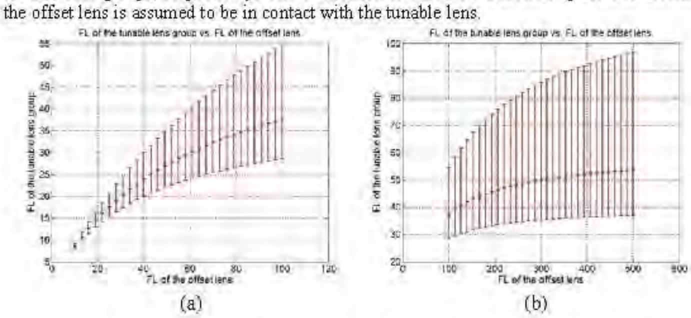

Fig. 3 The focal range of the tunable lens groups as a function of the focal length of the offset lens: (a) focal length of the offset lens 10mm-100mm; (b) focal length of the offset lens 100mm-500mm

As indicated in Fig.3, the shorter the focal length of the tunable lens group, the smaller the focal range is. Since the spacing between the tunable lens groups is a constant, the change of focal length of each tunable lens group is the same but with different signs. In addition, since the magnification of the telescope varies from -1/6 to -1/4, the second tunable group requires a smaller focal length. We first specified the focal length of the second tunable lens group to be 15mm for the zoom ratio of 2×, and then determined the focal length of the first tunable lens group to be 60mm. As a result, the spacing between the two tunable lens groups is 75mm. For the zoom ratio of 3x, the focal lengths of the second and first tunable lens groups needed to be 13.57mm and 81.43mm, respectively. As shown in Fig. 3, an offset lens with a focal length of 20mm can be used in the second tunable group to achieve the required focal range. For the first tunable group, the offset lens choice is quite flexible, because it does not make use of the full focal range of the tunable lens.

3. Optical design and system prototype

The most challenging aspect of the zoom probe design is the aberration correction across the zoom range while fixing the object or image distance. In addition, since the zoom probe can be scanned and registered within the wide-angle view, it needs to correct the aberrations of those peripheral fields as well. In order to cut the budget and reduce the delivery time, we decided to design the zoom probe by using off-the-shelf lenses, which raised another challenge. Although lens venders such as Edmund Optics, Ross Optical and Thorlabs have plenty choices for off-the-shelf lenses, the lens shapes are limited to plano-convex, plano-concave, double convex and double concave. Additionally, the glass choices are quite narrow. Most singlets are made from BK7, and some lenses with large optical power are made from flint glasses such as SF4 or SF5. Moreover, the doublet choices are limited. Therefore it is quite challenging to achieve design with a near-diffraction limited performance.

The foveated imaging probe of the MRFL system with the optimized zoom probe is shown in Fig. 4. As discussed in the previous section, the two tunable lens groups form a Keplerian telescope which is capable of continuous zooming and autofocusing. Besides the tunable lenses, all other lenses in the zoom probe are off-the-shelf lenses from Edmund Optics and Ross Optical. In the first tunable group, a plano-convex lens is inserted between the tunable lens and the beam splitter to reduce the beam diameter such that the converging beam diameter is smaller than the 10-mm clear aperture of the tunable lens. The plano-concave lens behind the tunable lens adds the adequate optical power to the first tunable group and corrects the spherical aberration to some extent. In the second tunable group, a doublet with a strongly curved middle surface is placed near the relayed pupil location, in order to correct the chromatic aberration and sphero-chromatism. In the imaging lens group, a plano-concave lens and a plano-convex lens were used to correct the field curvature and astigmatism.

The MTF performance of the zoom probe is demonstrated in Fig.5. Figure5 (a) shows the polychromatic MTF at the 3× zoom ratio for sampled fields of 0°, 4.4° 6.3°,9.3°,13°, when the foveated probe is aimed at the central 26° FOV, corresponding to a 0° scanning angle. Figure 5(b) summarizes the MTF performance across the zoom range (2× ~ 3×) for both the 0° and the maximum 26.6° scanning angle. Each curve is the average MTF of a specific zoom ratio and scan angle and is averaged across the 5 sampled field angles in both tangential and sagittal directions. For instance, the curve for the 3× peripheral FOV corresponds to the average MTF within a 26° FOV with the scanner steered toward the 26° and the tunable lenses set for 3× optical zoom. As indicated by the figure, all the fields and zooms have a similar near-diffraction limited performance.

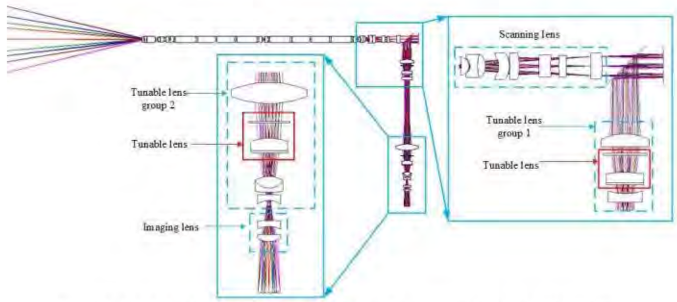

Fig. 4 Optical design layout of the high-magnification foveated imaging probe of the MRFL system with the newly designed zoom probe

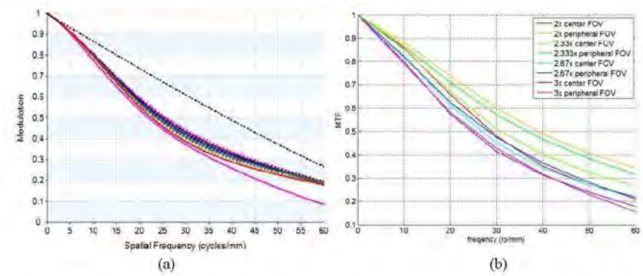

Fig. 5 MTF performance of the high-magnification zoom probe: (a) the polychromatic MTF of the central 26° FOV with 3x zoom (on the plot, you should have legends to show the sampled field angles as well as the wavelength weighting); (b) The average polychromatic MTF of central and peripheral FOVs for the zoom ratio of 2x, 2.33x, 2.67x and 3x (can you add markers to each curve to easily differentiate them??).

The 3D model of the zoom MRFL is shown in Fig.6. The zoom probe is mounted by the cage system from Edmund Optics, and all the lens mounts are 3D printed by QuickParts using the stereolithography. The lenses are UV cured with the 3D printed lens mounts. The total cost of the zoom probe alone is less than $1500, because all the components including the optics are off-the-shelf-components. For comparison, we quoted another design with all customized lenses, and it costed about $10,000 and the delivery time was more than 1 month. In the next section, the performance of the zoom probe will be demonstrated. Moreover it also demonstrates the capability of off-the-shelf lenses to build high quality optical system.

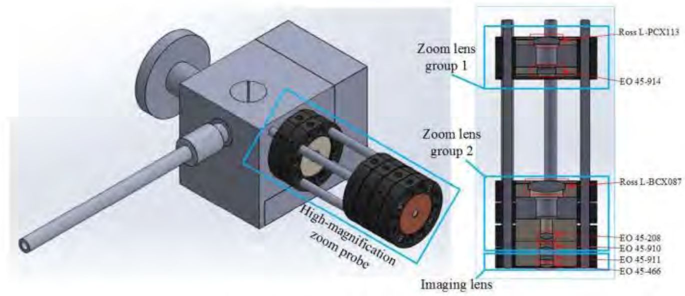

Figure 6 3D model of the zoom MRFL

4. Performance evaluation

A US1951 resolution target was used to test the resolution of the zoom probe. The resolution target is located at optimized 120mm working distance. Figures 7 (a) through 7(d) demonstrate the resolution of the zoom probe of four different zoom ratios from 2× to 3×. As shown in the figures, the best resolvable bar images vary from element 3 group 2 (5.04lp/mm) for the 2× zoom to element 2 group 3 (8.98lp/mm for the 3x zoom ratio.

Figures 8(a) through 8(d) demonstrate the field of view coverage corresponding to four different zoom ratios from 2× to 3×. A bladder model was used as the object, and was placed at 120mm working distance. To be noted, as the field coverage changes due to the action of varying the optical magnification of the zoom probe, the bladder model is always in focus which demonstrates the auto-focus capability of the probe.

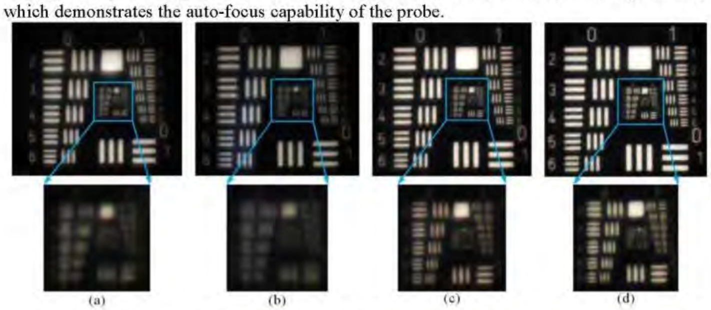

Fig. 7 USAF 1951 resolution target images at different zoom ratios: (a) 2× zoom; (b) 2.33× zoom; (c) 2.67× zoom (d) 3× zoom

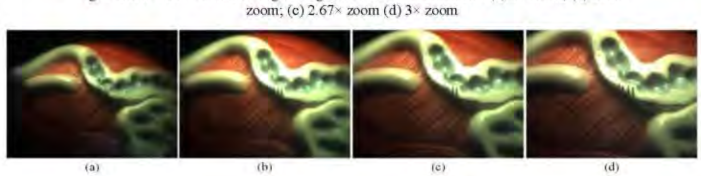

Fig. 8 Images of a bladder model of at different zoom ratios: (a) (a) 2× zoom; (b) 2.33× zoom; (c) 2.67× zoom (d) 3× zoom

5. Conclusion

In conclusion, we have developed a high-magnification zoom probe for the multi-resolution foveated laparoscope, which can effectively change the optical magnification and field coverage of the high-resolution view, while maintaining a fixed imaging distance. Two commercially available tunable lenses were implemented in the design, so that no mechanical moving parts are needed to achieve the zooming and auto-focusing functions. The zoom ratio of this probe varies from 2× to 3×. The corresponding field coverage varies from 80×60mm² to 53.7×40mm², and the maximum resolution varies between 5.04lp/mm and 8.98lp/mm in object space at a 120mm working distance. The zoom and auto-focusing capabilities will further improve the maneuverability of the dual-view multi-resolution foveated laparoscope, and make it adaptable to more types of minimally invasive surgeries.

Acknowledgement
This work is supported by NIH grant R01 EB18921 and TRIF imaging fellowship, University of Arizona. Dr. Hong Hua has a disclosed financial interest in Magic Leap Inc. that had no involvement in the work reported here. The terms of this arrangement have been properly disclosed to The University of Arizona and reviewed by the Institutional Review Committee in accordance with its conflict of interest policies.